



# C14-Laves phase high entropy alloys for hydrogen storage: a review

Cite this: DOI: 10.1039/d5mh01719j

Badr El Aalami, <sup>ab</sup> Hosni Idrissi<sup>b</sup> and Vera Trabadelo <sup>\*a</sup>

Recently, solid-state hydrogen storage materials have attracted significant research attention within the hydrogen energy community owing to their higher hydrogen storage density and affordable safety compared to conventional systems (*i.e.*, gaseous and liquid storage systems). Among these materials, high entropy alloys (HEAs) possessing C14-Laves single-phase structures have emerged as promising candidates for this application, attributed to their unique structural properties and superior performance. Unlike traditional alloys, the complex composition and high configurational entropy of C14-Laves phase HEAs reveal a new balanced design strategy for hydrogen storage that stabilizes single phase structures, encourages reversible hydrides, and provides exceptional cycling stability. Numerous remarkable studies have already demonstrated the potential of C14-Laves phase alloys, typically for stationary hydrogen storage applications. In this review, first, the definition and concept of HEAs as well as the evaluation of the compositional design strategies for the formation of a favorable C14-Laves single solid-solution phase are highlighted. Moreover, the thermodynamic modeling of the hydrogenation properties, manufacturing processes, and hydrogen storage properties in the latest state-of-the-art C14-Laves phase structured HEAs are presented and discussed. Finally, possible applications, potential challenges, and perspectives are outlined.

Received 9th September 2025,  
Accepted 25th November 2025

DOI: 10.1039/d5mh01719j

rsc.li/materials-horizons

## Wider impact

Hydrogen is a key vector toward a reliable and sustainable energy supply. However, hydrogen storage is one of the most challenging aspects in hydrogen technology. Metal hydride-based solid-state hydrogen storage has gained considerable attention owing to its higher volumetric densities and safety compared to traditional gaseous and liquid storage systems. Yet, most reported metal hydrides remain far from commercialization, mainly due to limited hydrogen storage capacity or lack of reversibility under practical conditions. In this context, high entropy alloys (HEAs) have emerged as a novel class of alloys with great potential for hydrogen storage. Among the different HEA compositions, those featuring a single C14-Laves phase have shown excellent hydrogen-related properties, such as room temperature reversibility, rapid kinetics, easy activation, and good cyclability as demonstrated by several studies supporting their future in hydrogen storage applications. Furthermore, a key advantage of HEAs is their vast compositional formulations, offering numerous possibilities to fine tune the desired microstructures and, hence, properties of hydrides. Therefore, achieving optimal hydrogen performance will largely depend on effective design strategies to predict the formation of the C14-Laves phase and appropriate processing methods. This review focuses on recent progress on C14-Laves phase HEAs for hydrogen storage, highlighting all the previous aspects.

## 1. Introduction

The world's reliance on energy continues to grow daily.<sup>1</sup> This results in massive consumption of fossil fuels and the depletion of certain key natural resources, like coal and petroleum.<sup>2,3</sup> Consequently, some problems arise, *i.e.*, economic challenges,

diplomatic conflicts, and, most critically, climate disorder due to the excessive release of carbon emissions into the atmosphere.<sup>4,5</sup> Additionally, increased demand will be placed on sustainable energy sources such as solar, wind, and hydrothermal to meet energy needs.<sup>3</sup> However, the latter also face significant challenges, including intermittency, high initial costs, complex technologies, and regular maintenance requirements.<sup>6,7</sup> Given these circumstances, a global trend towards finding alternative sources for energy as well as clean gaseous fuels, *e.g.*, H<sub>2</sub> and CH<sub>4</sub>, appears quite promising.<sup>8</sup> These alternatives are expected to be sufficiently efficient and environmentally friendly to address future energy demands.<sup>9</sup> Hydrogen, for instance, is an ideal and clean energy carrier that satisfies the

<sup>a</sup> High Throughput Multidisciplinary Research Laboratory (HTMR), College of Chemical Sciences and Engineering (CCSE), Mohammed VI Polytechnic University (UM6P), Lot 660, Hay Moulay Rachid, Benguerir 43150, Morocco.  
E-mail: vera.trabadelo@um6p.ma

<sup>b</sup> Institute of Mechanics, Materials and Civil Engineering, IMAP Division, UCLowain, Place Sainte Barbe, 2, B-1348, Lowain-la-Neuve, Belgium



above criteria.<sup>10</sup> It can be produced through various methods, among others electrolysis using renewable energies, and it only generates electricity and water as a secondary product when used in fuel cells.<sup>11</sup> Due to its high calorific density, which is over twice that of gasoline,<sup>12</sup> and zero-carbon footprint when combusted,<sup>13</sup> hydrogen is an outstanding energy vector that shows great potential as well as an attractive road map worldwide across various fields, including industrial processes, fuel production, and energy generation.<sup>10,14</sup> Hence, the growth of the hydrogen energy sector has become a key strategy for communities to promote energy transition and ensure a reliable and sustainable energy supply.<sup>15,16</sup> In general, hydrogen technology involves production, storage, transportation, and application.<sup>17</sup> As the most abundant<sup>8</sup> and lightest element on

earth,<sup>18</sup> hydrogen can be cost-effective to produce but challenging to store.<sup>19</sup> Nevertheless, its high flammability and explosive nature as a gas pose significant risks, especially when temperatures rise or its concentration in the air exceeds safety limits.<sup>20</sup> Moreover, in comparison to fossil fuels, hydrogen has a lower volumetric energy density.<sup>21</sup> Therefore, safety comes first when handling hydrogen, and long-term hydrogen storage systems that have the potential for higher energy density are the most concerning aspects of hydrogen technology.<sup>15</sup> Currently, hydrogen storage methods are divided into two categories as given in Fig. 1:<sup>15,21,22</sup> physical storage as a gas or liquid and chemical storage. The gas form of hydrogen storage often requires high-pressure tanks ( $\sim 700$  bar) and large volume systems are typically used.<sup>23</sup> Although this method is the most commercially adopted on the market, it still represents constant safety hazards.<sup>24,25</sup> Liquid hydrogen, despite its high energy density, involves consistent cryogenic temperatures since hydrogen boils at  $-252.8$  °C under standard atmospheric pressure, which implies high levels of maintenance.<sup>26</sup>

While chemical-based storage is comparatively safer and offers a more flexible means to store hydrogen than physical-based methods, notable issues persist in certain systems. For instance, liquid-organic carriers, regardless of their high volumetric density and ease of transportation, involve specific reactor configurations and noble metal catalysts (*i.e.*, Pt, Pd) to overcome the endothermic nature of the dehydrogenation reaction, production of likely CO/HC side-products during H release, and mostly the limited lifecycle of catalysts upon degradation.<sup>27–29</sup> Physisorption methods using adsorbents such as MOFs, COFs, and zeolites appear advantageous as they are fully reversible and demonstrate fast kinetics; however, the marked temperature dependence of these materials implies cryogenic conditions or high pressures to maintain high hydrogen uptake in addition to the structural instability of the adsorbents.<sup>30–32</sup> Given these current technical issues, solid-



**Badr El Aalami**

*Badr El Aalami received his MS degree in Materials Science and Nano-Engineering from the Mohammed VI Polytechnic University (UM6P), Morocco in 2023. He is currently pursuing his PhD jointly at the High Throughput Multidisciplinary Research Laboratory (HTMR) at UM6P, Morocco, and the Materials and Processes Engineering (IMAP) division of the Institute of Mechanics, Materials and Civil Engineering (IMMC) at UCLouvain, Belgium. His current research activities include the design, synthesis, and characterization of high-entropy alloys towards hydrogen storage applications and the microstructural stability of single phase HEAs.*

*Badr El Aalami received his MS degree in Materials Science and Nano-Engineering from the Mohammed VI Polytechnic University (UM6P), Morocco in 2023. He is currently pursuing his PhD jointly at the High Throughput Multidisciplinary Research Laboratory (HTMR) at UM6P, Morocco, and the Materials and Processes Engineering (IMAP) division of the Institute of Mechanics, Materials and Civil Engineering (IMMC) at UCLouvain, Belgium. His current research activities include the design, synthesis, and characterization of high-entropy alloys towards hydrogen storage applications and the microstructural stability of single phase HEAs.*



**Hosni Idrissi**

*Hosni Idrissi is a Professor at the Institute of Mechanics, Materials, and Civil Engineering (IMMC) at UCLouvain in Belgium. He is mandated by the Belgian National Fund for Scientific Research (FSR-FNRS). The research of Pr. H. Idrissi focuses on the investigation of the elementary mechanisms controlling the processing and deformation of inorganic materials using transmission electron microscopy (TEM). In this context, conventional and advanced ex situ and in situ techniques are used to characterize crystalline materials with micro-nanostructures dominated by internal interfaces such as nanocrystalline metallic thin films and advanced steels and alloys exhibiting twin and phase boundaries, nanoprecipitates and nanocracks.*

*Hosni Idrissi is a Professor at the Institute of Mechanics, Materials, and Civil Engineering (IMMC) at UCLouvain in Belgium. He is mandated by the Belgian National Fund for Scientific Research (FSR-FNRS). The research of Pr. H. Idrissi focuses on the investigation of the elementary mechanisms controlling the processing and deformation of inorganic materials using transmission electron microscopy (TEM). In this context, conventional and advanced ex situ and in situ techniques are used to characterize crystalline materials with micro-nanostructures dominated by internal interfaces such as nanocrystalline metallic thin films and advanced steels and alloys exhibiting twin and phase boundaries, nanoprecipitates and nanocracks.*



**Vera Trabadelo**

*Prof. Vera Trabadelo completed her PhD in Materials Science (Metallurgy) at the University of Navarra (Spain) in 2006 for the development of high-speed steels for tribological applications. After working as a scientist in Empa (Switzerland), she joined UM6P in 2017 as a postdoctoral researcher and in 2019 she was appointed as Assistant Professor; in May 2023 she received her Habilitation to Direct Research (HDR). She is currently the coordinator of the research line in Metallurgy at HTMR. Her research is focused on the design (by Computational Thermodynamics) and development of novel alloys with different targeted applications.*

*Prof. Vera Trabadelo completed her PhD in Materials Science (Metallurgy) at the University of Navarra (Spain) in 2006 for the development of high-speed steels for tribological applications. After working as a scientist in Empa (Switzerland), she joined UM6P in 2017 as a postdoctoral researcher and in 2019 she was appointed as Assistant Professor; in May 2023 she received her Habilitation to Direct Research (HDR). She is currently the coordinator of the research line in Metallurgy at HTMR. Her research is focused on the design (by Computational Thermodynamics) and development of novel alloys with different targeted applications.*



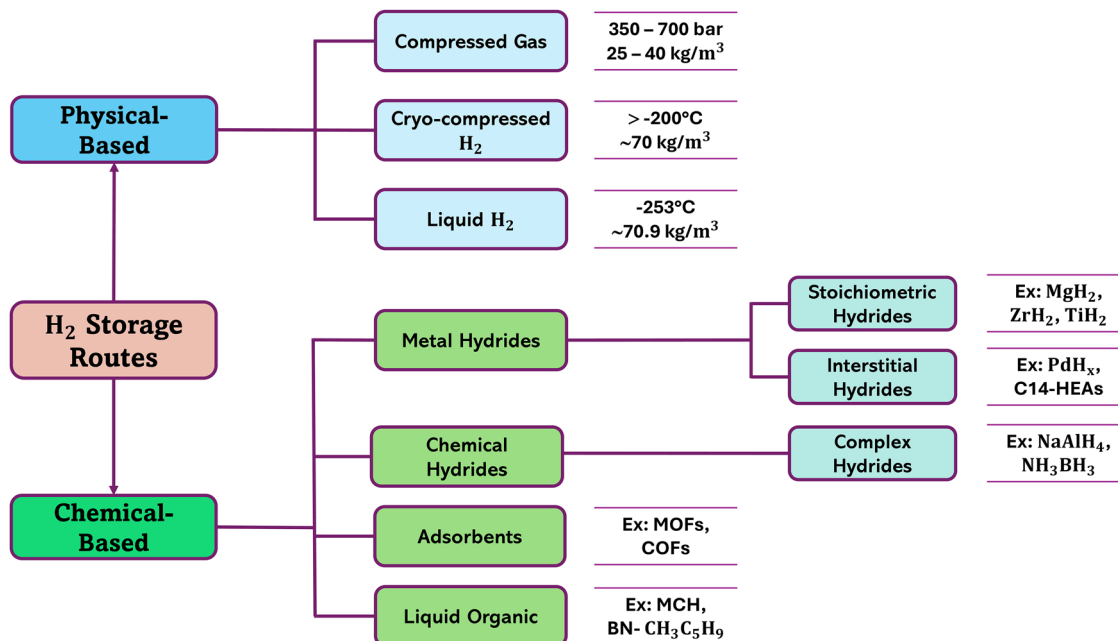


Fig. 1 Available hydrogen storage technologies.<sup>15,21,22</sup> This figure was made based on the illustrations reported in ref. 15, 21 and 22.

state hydrogen storage in the form of metal/alloy-hydrides appears to be a promising alternative, offering high volumetric hydrogen density, low pressure and temperature operation conditions, and enhanced security.<sup>22,33–36</sup>

The main challenge for solid-state hydrogen storage is finding a material that, at the same time, meets key criteria of high storage capacity, reversible hydrogen absorption/desorption at room or low temperatures, fast kinetics, easy activation, long-term stability and cyclability, operation near atmospheric pressure, and high gravimetric density.<sup>33,37–39</sup> Clearly, a hydride that meets all of these conditions simultaneously would be ideal, even for commercial applications. However, most solid-state hydrogen storage researchers focus on developing materials with improved capacity and reversibility at room temperature.<sup>10,40–43</sup> To achieve a better balance of the previously described hydrogenation properties, numerous candidates with various stoichiometries (elemental, binary, ternary, *etc.*) have been investigated over the past few decades.<sup>44,45</sup> Magnesium hydride, MgH<sub>2</sub>, is the most popular and extensively studied hydride owing to its unique advantages of a substantial hydrogen storage capacity (7.6 wt%), affordability, and widespread abundance.<sup>46</sup> However, its high activation energy required for hydrogenation/dehydrogenation processes, along with poor thermodynamic and kinetic properties, stand as a barrier for the market scalability of Mg-based hydrides and their derivatives of Mg-based alloys.<sup>46–48</sup> To reach optimal reversibility, LaNi<sub>5</sub> hydride has been studied for over six decades.<sup>49</sup> Although it has a very low hydrogen capacity compared to MgH<sub>2</sub>,<sup>50</sup> it has the ability to store hydrogen reversibly at room temperature with excellent absorption/desorption properties and long-term cyclability and stability.<sup>51,52</sup> However, lanthanum (La) is a rare-earth element and

highly sensitive to air.<sup>53</sup> Subsequently, TiFe materials have gained researchers' attention as binary transition metal absorbers due to their moderate cost and low hydrogenation/dehydrogenation temperatures. However, they are often difficult to activate and exhibit low resistance to contamination.<sup>54–56</sup>

From simple to more complex hydrides, tremendous efforts and investigations have been dedicated to developing efficient hydrogen storage systems. Nevertheless, all existing metal hydrides still face several limitations.<sup>57</sup> It is noteworthy to address that a viable hydrogen storage system must be low-cost, compact, and efficient to meet targeted goals. Recently, research has shifted towards using alloy-hydrides with sub- and metastable structures for hydrogen storage.<sup>58</sup> Among this emerging class of alloys are multi-principal alloys, commonly called high entropy alloys (HEAs).<sup>59,60</sup> HEAs are conventionally defined as multi-component alloys made up of five or more main constituent elements, each of which has an atomic ratio between 5 and 35 at%.<sup>37</sup> Since 2004,<sup>61,62</sup> this new family of alloys has gained significant attention thanks to their exceptional structural and functional properties.<sup>63,64</sup> HEAs began their exploration for hydrogen storage properties in 2010 with the first publication on CoFeMnTi<sub>x</sub>V<sub>y</sub>Zr<sub>z</sub> high-entropy hydrides.<sup>65</sup> Since then, research in this area has grown significantly.<sup>20</sup>

Most HEAs are typically monophasic structures, such as face-centered cubic (FCC), body-centered cubic (BCC), hexagonal (C14-Laves), or, occasionally, a dominant phase with minor traces of a secondary phase.<sup>66–69</sup> This review shows a distinct ordered methodology for designing C14-Laves phase HEAs where chemical composition controls the type of hydrogen sites and their occupancies with the objective of tailoring the thermodynamic properties, including plateau pressure and desorption enthalpy, exploring the role of high configurational



entropy in stabilizing complex intermetallics, and providing a more accurate prediction of phase diagrams and site energies through coupling CALPHAD and DFT approaches. This level of precise design has not been achieved in the case of BCC alloys.<sup>70</sup> As a result, C14-Laves phase HEAs reveal a new conceptual advance for hydrogen storage design that mitigates the conventional trade-off between high absorption capacity and poor reversibility and kinetics seen in traditional alloys (*i.e.*, MgH<sub>2</sub>, BCC alloys, *etc.*), which allows for the achievement, at the same time, of moderate/high capacity, rapid kinetics, and excellent reversibility.<sup>43,71–73</sup>

In 2023, Kong *et al.*<sup>37</sup> conducted a comprehensive review on BCC-structured HEAs, showing that BCC-based alloys present high potential for developing hydrogen storage materials. In the past two years, more than ten extensive reviews have been published on HEAs,<sup>20,74–76</sup> highlighting the current state of research and future prospects of HEAs for hydrogen storage applications. That said, despite the publication of over 40 articles on HEAs with C14-Laves phase structure since their emergence,<sup>77–80</sup> there is still a notable absence of an exhaustive survey specifically focusing on C14-Laves phase hydrogen storage alloys.

The present review summarizes the state-of-the-art and recent scientific findings on HEAs featuring C14-Laves phase structures for hydrogen storage. It evaluates the theory and compositional design driven by the interaction of hydrogen atoms with alloy elements and provides a critical theoretical guideline for predicting the constituent phase(s) of these alloys. The CALPHAD approach, DFT computations, and the thermodynamic modeling of hydrogenation properties of these alloys are also reviewed, and the manufacturing methods are examined. Finally, the study details multiple dimensions of hydrogen storage properties, including absorption capacity, activation energy, kinetics, and cyclability, and concludes with a discussion on possible applications, potential challenges, and perspectives.

## 2. High entropy alloys

### 2.1. Brief history

Historically speaking, HEAs were first discovered in the late 18th century by the German scientist Franz Karl Achard and his colleagues.<sup>60</sup> By synthesizing a series of equimass multicomponent alloys made up of 5 to 7 elements, they led the way in cutting-edge research. Despite this remarkable achievement, it attracted no attention from the global metallurgical community.<sup>81,82</sup> It was only in 2004 that Cantor *et al.*<sup>61</sup> and Yeh *et al.*<sup>62</sup> officially introduced the notion of multicomponent alloys, generally known today as HEAs. While initially developed for metallic alloys to enhance their mechanical properties, this new class of materials has rapidly expanded to cover all material categories.<sup>74,83</sup> As illustrated in Fig. 2a, the number of publications per year has grown exponentially across various application areas in the last two decades, including high-entropy ceramics,<sup>84</sup> high-entropy amorphous alloys,<sup>85</sup>

intermetallic HEAs,<sup>86</sup> lightweight HEAs,<sup>87</sup> and nanostructured HEAs.<sup>88</sup> This growth is driven by the exceptional physicochemical, magnetic, catalytic, functional, and structural properties of these materials.<sup>89–91</sup> Among the functional properties of HEAs, hydrogen storage stands out as one of the most interesting and it has been gaining significant interest since 2010 when Kao *et al.*<sup>65</sup> published the first paper on HEAs for hydrogen storage featuring the CoFeMnTi<sub>x</sub>V<sub>y</sub>Zr<sub>z</sub> system. Over the past few years, this area has witnessed a marked rise in scientific production, as shown in Fig. 2b.

### 2.2. Definition and concept

Since their discovery, there has not been a universal definition for HEAs.<sup>20</sup> However, unlike traditional alloys, HEAs are not made up of just one or two principal elements.<sup>93</sup> Hence, this emerging class of alloys has been given various designations, including high entropy alloys (HEAs),<sup>20,94,95</sup> multi-principal element alloys (MPEAs),<sup>96,97</sup> multi-component alloys (MCAs),<sup>72,98,99</sup> or complex concentrated alloys (CCAs).<sup>100</sup> Following these terms, two definitions are most widely recognized.<sup>101,102</sup> The first definition, proposed in 2004, is based on composition. It defines a HEA as an alloy made up of five or more main constituent elements, each of which has an atomic ratio between 5 and 35 at%.<sup>37,61,93,103</sup> The alloys can be further designed with equimolar or non-equimolar compositions.<sup>92</sup> Fig. 2c shows a ternary phase diagram comparing the distribution of primary components in conventional alloys and HEAs. Additionally, some authors also allow for the inclusion of minor elements (*e.g.*, magnesium (Mg), aluminum (Al), *etc.*) with concentrations below 5 at%.<sup>89,104</sup> The second definition is entropy-based, describing a HEA as a random solid-solution with a mixing entropy larger than 1.5*R*, where *R* represents the gas constant (*R* = 8.31 J K<sup>-1</sup>·mol<sup>-1</sup>).<sup>75</sup> Most HEAs reported in the past 20 years demonstrate both definitions as they consist of a minimum number of five major elements within the previously mentioned atomic range, which naturally leads to a large number of configurational states and, consequently, a higher mixing entropy. Generally, the more elements involved, the greater the mixing entropy.<sup>105</sup> As a result, both definitions often coexist and are validated in practice.

From a microstructural point of view, HEAs can be classified as single-phase alloys (such as FCC, BCC, or hexagonal closed packing (HCP) HEAs) or multiphase alloys (such as ternary and quaternary alloys),<sup>60,106</sup> depending on the relative free energies involved, according to the following equations:<sup>93</sup>

$$\text{(Solid solution): } \Delta G_{\text{mix}} = \Delta H_{\text{mix}} - T\Delta S_{\text{mix}} \quad (1)$$

$$\text{(Intermetallics): } \Delta G_{\text{f}} = \Delta H_{\text{f}} - T\Delta S_{\text{f}} \quad (2)$$

where,  $\Delta G_{\text{mix}}$ ,  $\Delta H_{\text{mix}}$ , and  $\Delta S_{\text{mix}}$  are the Gibbs free energy, enthalpy, and entropy of mixing multiple elements, respectively.  $\Delta G_{\text{f}}$ ,  $\Delta H_{\text{f}}$ , and  $\Delta S_{\text{f}}$  correspond to the Gibbs free energy, enthalpy, and entropy for formation of intermetallic compounds, respectively. *T* denotes the absolute temperature. Single-phase HEAs are ideal candidates for solid-state hydrogen storage owing to their controlled chemical composition and relatively easy understanding of the hydrogen storage mechanism compared to multi-phase based HEAs.<sup>67,107,108</sup> Moreover, the formation of multiple phases



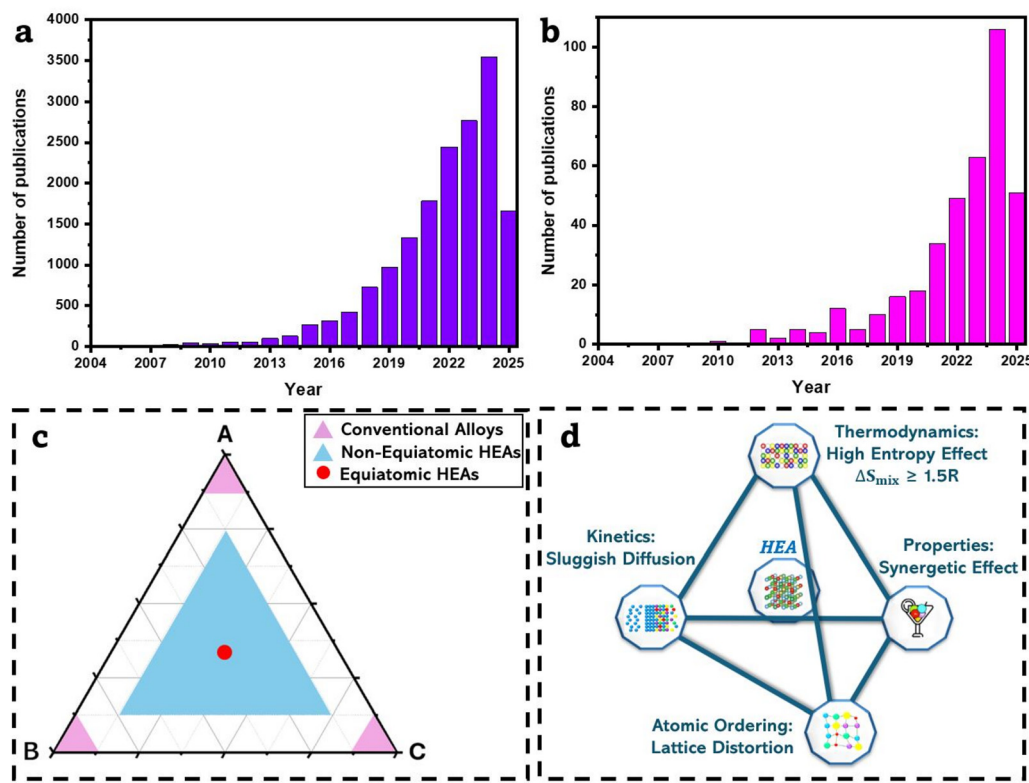


**Fig. 2** (a) Number of publications between 2004 and 2025 containing the terms “high entropy alloy(s)”, “multi-component alloy(s)”, “multi-principal element alloy(s)”, or “complex concentrated alloy(s)”. (b) Number of published articles from 2004 to 2025 with “high entropy alloy(s)”, “multi-component alloy(s)”, “multi-principal element alloy(s)”, or “complex concentrated alloy(s)” for “hydrogen storage” in the title, keywords, and abstract. *Source: Scopus database.* (c) Ternary phase diagram showing the compositional distribution of principal elements in conventional alloys versus HEAs.<sup>92</sup> (d) Schematic illustration of the “four core effects” of HEAs.<sup>75,90</sup> This figure was made based on the illustrations reported in ref. 75 and 90.

and intermetallics in the microstructure often results in significant challenges in achieving higher hydrogen capacities.<sup>109</sup> Therefore, maintaining high mixing entropy at high temperatures plays a key role in counteracting the formation of intermetallic compounds, leading to a thermodynamically stable solid-solution structure where  $\Delta G_{\text{mix}}$  is more negative (eqn (1)). However, single-phase HEAs exhibit certain limitations from a mechanical perspective.<sup>93</sup> For instance, certain single-phase alloys, including FCC and BCC, exhibit a trade-off between ductility and strength.<sup>110</sup> In addition, due to the lack of strengthening mechanisms, such as precipitates or secondary phases, single-phase HEAs may have lower creep resistance compared to multiphase alloys.<sup>111</sup> As a result, multi-phase HEAs, such as eutectic HEAs<sup>112</sup> and transformation induced plasticity (TRIP)-HEAs,<sup>113</sup> are preferred for improving mechanical properties. These alloys can increase ductility through transformation-induced plasticity in metastable phases and enhance hardness through interface strengthening in dual-phase alloys.<sup>114</sup>

### 2.3. Four core effects

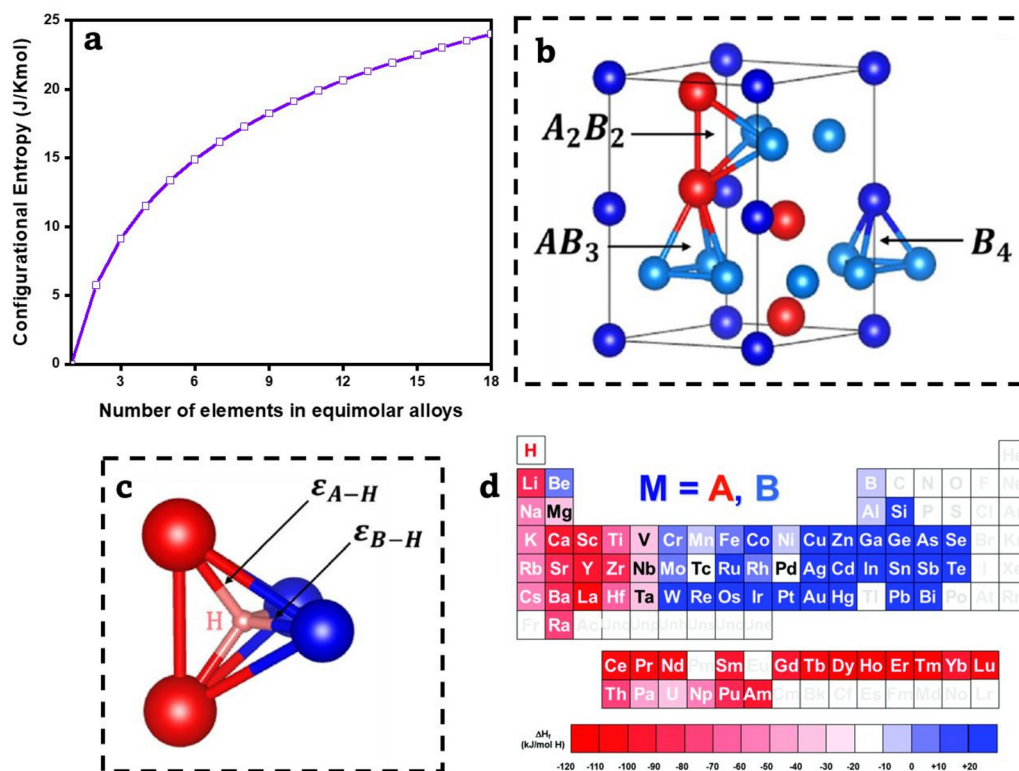
As previously mentioned, HEAs differ significantly from conventional alloys, leading to distinct microstructures and properties. In 2006, Yeh *et al.*<sup>115</sup> identified the source of these distinctions by introducing the four fundamental effects of HEAs that govern their behavior and properties. As shown in

Fig. 2d, these effects are high entropy effect, sluggish-diffusion effect, lattice-distortion effect, and the cocktail or synergetic effect.<sup>75,90</sup> The first three effects are relatively natural and can be theoretically and experimentally demonstrated. However, the cocktail effect remains difficult to predict to a certain extent, as it arises from the complex interaction of the other effects.

**2.3.1. High entropy effect.** One reason why HEAs initially received little attention was the belief that alloys with more than one or two principal elements would lead to inclusions, intermetallic compounds, and/or complex microstructures (Section 2.1). However, this assumption was proven incorrect, as HEAs often exhibit simple microstructures, predominantly, single-phase structures.<sup>116</sup> This simplicity results from the presence of multiple components in near-equal or equimolar proportions, which increases the mixing entropy and thereby stabilizes the HEA system thermodynamically.<sup>115</sup> As noted earlier (Section 2.2), a higher number of constituents, ideally in equimolar ratios, increases the configurational entropy, promoting the formation of a single-phase structure (eqn (1)). Fig. 3a shows the evolution of the configurational entropy as a function of the number of elements in equimolar HEAs, which is predicted by Boltzmann’s equation (eqn (3)).<sup>117</sup>

$$\Delta S_{\text{mix}} = R \ln(n) \quad (3)$$





**Fig. 3** (a) Correlation between the mixing entropy and the equimolar number of elements.<sup>117</sup> This figure was made based on eqn (3) reported in ref. 117. (b) Unit cell of the hexagonal C14-Laves phase (MgZn<sub>2</sub>-type) with three types of tetrahedral interstices available:  $A_2B_2$ ,  $AB_3$ , and  $B_4$ .<sup>72</sup> Reproduced with permission from ref. 72. Copyright © 2022, Elsevier Ltd. (c)  $A_2B_2$  sites formed by a tetrahedron having 2 bonds with energy  $\epsilon_{A-H}$  and 2 bonds with energy  $\epsilon_{B-H}$ .<sup>72</sup> Reproduced with permission from ref. 72. Copyright ©, 2022 Elsevier Ltd. (d) A periodic table showing the division of elements into hydride-forming (red) and non-hydride-forming (blue) based on the enthalpy of M–H metal hydride formation.<sup>145</sup> Reproduced from ref. 145 under the CC BY-NC 3.0 license with permission from the Royal Society of Chemistry. Copyright © 2021.

where  $n$  is the number of equimolar elements. The combination of eqn (1) and (3) demonstrates the direct transition from an elemental system to a thermodynamically favorable random solid solution. Furthermore, the high entropy effect goes further by lowering the electronegativity differences between the alloy's components, which helps prevent phase separation and/or the formation of some ordered intermetallic compounds within the alloy.<sup>60</sup> Indirectly, the high entropy effect was found to improve the HEA's hydrogen storage performance through the stabilization of a single-phase solid-solution (*i.e.*, C14-Laves or BCC), resulting in the contribution of a large number of interstitial sites to accommodate more hydrogen atoms within the lattice and thereby achieving higher absorption capacity. Besides, the high entropy effect also causes the lattice strain and distortion to increase, which eventually improves the kinetics and reversibility of the alloy.<sup>20,57</sup>

**2.3.2. Sluggish-diffusion effect.** Likewise, the sluggish-diffusion effect arises from the random distribution of five or more principal elements in HEAs, leading to significantly slower atomic diffusion kinetics and making diffusion processes more difficult to occur within these systems.<sup>75</sup> This second effect can be explained in various ways. From an energetic standpoint, the presence of multiple principal elements in HEAs leads to important fluctuations in the lattice

potential energy across different lattice sites, caused by variations in size, geometry, and coordination of these sites.<sup>118</sup> Moreover, as the number of elements in the alloy increases, the sluggish-diffusion effect becomes more pronounced as well.<sup>59</sup> As a result, atoms in HEAs encounter greater lattice potential energy barriers for diffusion, resulting in lower diffusion coefficients compared to those in conventional alloys.<sup>119</sup> From another point of view, some studies have examined the manufacturing process of HEAs and found that the sluggish-diffusion effect is primarily caused by the formation of nanocrystals and amorphous structures during solidification.<sup>62,90,120,121</sup> Besides, diffusion can lead to the formation of secondary phases within HEAs, emphasizing the crucial role of the high entropy effect (Section 2.3.1) in preventing such behavior and reinforcing the sluggish-diffusion effect. In terms of hydrogen storage behavior, Luo *et al.*<sup>20</sup> stated that the sluggish effect enhances the de/hydrogenation kinetics by preventing grain coarsening and, thereby reducing the alloy's grain size which leads to an increase in the density of grain boundaries that serve as effective diffusion channels for hydrogen. This microstructural feature improvement caused by the sluggish effect was also reported in several investigations to be important for achieving excellent hydrogen storage properties.<sup>57,122</sup>



**2.3.3. Lattice-distortion effect.** The coexistence of multiple elements within the same solid-solution induces severe lattice-distortion in HEAs, caused by variations in atomic sizes (size mismatch) and electronic distributions.<sup>123</sup> Therefore, each atom is displaced from its equilibrium position within the lattice, which significantly alters the overall energy and properties of the system.<sup>124</sup> Owen *et al.*<sup>125</sup> identified various types of strain that can arise from the lattice-distortion effect. They suggested that, if the size mismatch between atoms is sufficiently large, the distorted system could potentially transform its crystalline structure into an amorphous one. Consequently, the mechanical, electrical, thermal, magnetic, and chemical properties of HEAs are significantly influenced. For instance, Tandoc *et al.*<sup>126</sup> conducted computational modeling on the lattice distortion effect in refractory high entropy alloys, concluding a strong correlation between lattice distortion and room-temperature yield strength. Their findings indicate that lattice distortion positively influences both strength and ductility. Other researchers<sup>127–129</sup> have also emphasized that severe lattice distortion plays a crucial role in generating a high number of extended defects, such as dislocations, stacking faults, and twinning, which contribute to enhancing the mechanical properties of HEAs. Some studies<sup>33,130</sup> have reported that dislocations, induced by lattice distortion effects, can act as active sites for hydrogen insertion. According to Sahlberg *et al.*,<sup>131</sup> large lattice strain helps to make interstitial and octahedral sites more favorable to absorb significant amounts of hydrogen and hence increases the hydrogen storage capacity of the alloy. Therefore, the lattice distortion effect has proven to affect positively the properties of HEAs, particularly hydrogen storage performance.

**2.3.4. Cocktail effect.** Unlike the previous three effects, there has been no evidenced study, either theoretical or experimental, that deeply explores the mechanism of the cocktail effect.<sup>132,133</sup> However, it is consistently present and emerges from the synergistic interaction of all the properties of HEAs, thereby contributing to the achievement of the desired properties, such as mechanical strength, corrosion resistance, and hydrogen storage performance.<sup>75</sup> Ranganathan<sup>134</sup> was the first to introduce the concept of the cocktail effect, comparing multi-component alloys at the atomic level to a cocktail made of different types of alcohol “atoms”. Nonetheless, this synergistic effect has been explicitly demonstrated in some studies. For instance, Tong *et al.*<sup>135</sup> investigated the synergistic effect of adding aluminum to the  $Al_xCoCrCuFeNi$  ( $x = 0$  to 0.3) system.

The strong bonding between Al and the other components promoted the formation of a stable BCC phase, which in turn enhanced the strength of the alloys. Regarding hydrogen storage performance, Ma *et al.*<sup>136</sup> substituted Al by Fe in the  $ZrTiVAl_{1-x}Fe_x$  alloy system and found that the Fe substitution led to improved hydrogenation kinetics and capacities. Furthermore, with Fe replacing Al, the phase fraction of the C14 Laves phase increased, and Fe exhibited a strong catalytic effect in lowering the hydrogen desorption temperature of the  $ZrTiVAl$  alloy. Such characteristics are believed to be a consequence of the cocktail effect arising from modifications of the main HEA composition through doping or substitution of some elements. However, a comprehensive study is still needed to fully understand the concept and behavior of HEAs as well as the origins of the cocktail effect.

### 3. C14-Laves phase

Laves phases are among the most popular intermetallic phases valued for their mechanical and functional properties.<sup>137,138</sup> Laves phases are categorized into three crystal structures: cubic C15 (MgCu<sub>2</sub>-type),<sup>139</sup> hexagonal C14 (MgZn<sub>2</sub>-type),<sup>140</sup> and hexagonal C36 (MgNi<sub>2</sub>-type).<sup>141</sup> The C14-Laves phase is known for its excellent hydrogen storage properties compared to other Laves phase derivatives.<sup>72,140</sup> The optimum hydrogen storage properties of the C14-Laves phase are achieved through the stoichiometry of AB<sub>2</sub> systems, in which A are the elements that have high affinity to hydrogen; hence, they can easily form hydrides, while B are the non-hydride forming elements with very low affinity to hydrogen.<sup>142,143</sup> The crystallographic information of the AB<sub>2</sub> C14-Laves phase is summarized in Table 1. The AB<sub>2</sub> C14-Laves phase features a hexagonal structure (MgZn<sub>2</sub>-type) with space group  $P6_3/mmc$  (194) and includes three types of tetrahedral interstitial sites: A<sub>2</sub>B<sub>2</sub>, AB<sub>3</sub>, and B<sub>4</sub>, as shown in Fig. 3b. Each AB<sub>2</sub> formula unit contains 12 equivalent A<sub>2</sub>B<sub>2</sub> sites, 4 equivalent AB<sub>3</sub> sites, and 1 B<sub>4</sub> site.<sup>72</sup>

The theoretical maximum hydrogen storage capacity, AB<sub>2</sub>H<sub>17</sub>, could be achieved if all interstitial sites were fully occupied by hydrogen atoms.<sup>137</sup> However, this ideal situation is never attained because hydrogen cannot simultaneously occupy all available sites. This limitation is due to factors such as the varying size and geometry of the sites (not all sites are equally accessible), energy stability (hydrogen atoms prefer to occupy the lowest energy sites), and the influence of electronic

**Table 1** Crystallographic information of the AB<sub>2</sub> C14-Laves phase and atomic positions of the A and B elements.<sup>137</sup> This table is reproduced from ref. 137 with modifications under the CC BY 4.0 license with permission from Springer Nature. Copyright © 2020

Pearson symbol	Space group	Atom	Wyckoff site	Wyckoff positions			Atoms in the coordination polyhedron			
				x	y	z	CN	A	B1	B2
Hexagonal C14, MgZn <sub>2</sub> -type	$P6_3/mmc$ (194)	A	4f	1/3	2/3	z	16	4	9	3
		B1	6h	x	2x	1/4	12	6	4	2
		B2	2a	0	0	0	12	6	6	—

CN = coordination number.



interactions and repulsive forces. Merlino *et al.*<sup>144</sup> conducted a DFT study on hydrogen storage in the Zr(Cr<sub>0.5</sub>Ni<sub>0.5</sub>)<sub>2</sub> C14-Laves phase intermetallic, revealing that atomic hydrogen primarily prefers the A<sub>2</sub>B<sub>2</sub> sites, see Fig. 3c, with a Zr–Zr–Cr–Cr composition, followed by AB<sub>3</sub> sites. In contrast, B<sub>4</sub> sites were found to be unfavorable for hydrogen occupation. Furthermore, to the best of our knowledge, no detailed experimental study has been carried out to clarify the hydrogen absorption mechanism and determine its preferred sites within the lattice. Therefore, understanding and optimizing the behavior of the C14-Laves phase in HEAs can lead to more efficient and long-lasting hydrogen storage.

## 4. Design strategies of single C14-Laves phase structured HEAs for hydrogen storage

The properties of HEAs depend on their phase structure, which is influenced by the choice of elements and their concentrations. Therefore, a preliminary design is crucial to guide and optimize the experimental process.<sup>116</sup> Before designing such an alloy, selecting the appropriate elements comes first. For effective hydrogen storage in HEAs, it is important to combine hydrogen-absorbing elements (which have a lower hydride formation enthalpy and higher hydrogen affinity) with non-hydrogen-absorbing elements (which have a higher hydride formation enthalpy and lower hydrogen affinity) as illustrated in Fig. 3d.<sup>145</sup> In this context, alloy design occurs in two stages prior to manufacturing. The first stage focuses on predicting the alloy's phase structure and stability. Then, the second stage involves modeling the alloy's hydrogen storage properties to understand its behavior during hydrogen interaction and assessing pressure–composition–temperature (PCT) isotherms (Section 5). In this scope, empirical methods, computational thermodynamics, and density functional theory (DFT) calculations are used to design multicomponent alloys featuring a single C14-Laves phase for hydrogen storage.

### 4.1. Parametric approaches

Parametric calculations refer to theoretical methods employed during the early stages of composition design. These empirical models form the basic foundation for predicting solid-solution phases and are governed by the “Hume–Rothery” criteria, which researchers have extended and adapted to high-entropy alloys and are broadly applicable to all types of single-phase alloys, including C14-Laves phase HEAs.<sup>146</sup> These parameters encompass atomic size mismatch ( $\delta$ ), valence electron concentration (VEC), atomic radii ratio ( $r_A/r_B$ ), mixing entropy and enthalpy ( $\Delta S_{\text{mix}}/\Delta H_{\text{mix}}$ ), electronegativity difference ( $\Delta\chi$ ), and other factors to assess the formation and stability of solid-solution phases within the alloy.<sup>57</sup> In line with the fundamental concept of HEAs, the initial parameters that naturally come to mind are mixing entropy and enthalpy. These parameters provide an initial energetic perspective of such a system and

are defined in the following equations:<sup>147,148</sup>

$$\Delta S_{\text{mix}} = -R \sum_{i=1}^N c_i \ln c_i \quad (4)$$

$$\Delta H_{\text{mix}} = \sum_{i=1,ij}^N 4\Delta H_{ij}^{\text{mix}} c_i c_j \quad (5)$$

where  $c_i$  is the atomic fraction of the  $i$ -th component and  $\Delta H_{ij}^{\text{mix}}$  represents the enthalpy of mixing between the  $i$ -th and  $j$ -th elements in the liquid solid-solution of the alloy at equimolar concentration. The values of  $\Delta H_{ij}^{\text{mix}}$  have been also calculated and approximated for sub-regular solutions by Takeuchi and Inoue through Miedema's model.<sup>149</sup>

A higher mixing enthalpy reduces the free energy of solid-solution phases, promoting their formation, particularly at elevated temperatures.<sup>146</sup> As per eqn (1), when  $T_{\text{mix}}\Delta S_{\text{mix}} > |\Delta H_{\text{mix}}|$ , the total free energy of the alloy becomes negative, making the formation of a single-phase structure energetically preferred due to the high entropy effect (Section 2.3.1). More negative enthalpy promotes homogeneous solid-solution formation, uniform solidification, and faster kinetics. In contrast, a positive enthalpy leads to inhomogeneous microstructures and slower solidification.<sup>66</sup> Thus, formation enthalpy serves as a key parameter for optimizing alloy composition prior to synthesis.<sup>76</sup> To provide guidance during the design of C14-Laves structured HEAs, it was reported that a solid-solution phase is more likely to form when  $\Delta S_{\text{mix}} \geq 13 \text{ J K}^{-1} \text{ mol}^{-1}$  and  $-22 \text{ kJ mol}^{-1} \leq \Delta H_{\text{mix}} \leq 7 \text{ kJ mol}^{-1}$ .<sup>70,76,150,151</sup>

By combining the terms of  $T_{\text{mix}}\Delta S_{\text{mix}}$  and  $|\Delta H_{\text{mix}}|$  into one single term, Yang<sup>152</sup> introduced the  $\Omega$  parameter to predict phase formation in multicomponent alloys.  $\Omega$  represents the ratio of the entropic contribution to the Gibbs free energy at high temperatures relative to the enthalpic part and is determined using eqn (6):

$$\Omega = \frac{T_{\text{mix}}\Delta S_{\text{mix}}}{|\Delta H_{\text{mix}}|} \quad (6)$$

where  $T_{\text{mix}} = \sum_{i=1}^N c_i(T_m)_i$  is the weighted average melting point of a mixture containing  $N$  components and  $(T_m)_i$ <sup>153</sup> is the melting point of the  $i$ -th component.

The latter author suggested that when  $\Omega \geq 1.1$ , the entropic contribution prevails over the enthalpic part, resulting in a negative Gibbs free energy and a higher probability of forming a single-phase disordered solid solution structure. Conversely, when  $\Omega < 1$ , the mixing enthalpy becomes the dominant factor, increasing the Gibbs free energy and favoring the stabilization of multiple phases, intermetallic compounds, and ordered structures.<sup>37,70,152</sup>

The key factor influencing the phase stability of the alloy is the valence electron concentration (VEC), which is calculated using eqn (7):

$$\text{VEC} = \sum_{i=1}^N c_i(\text{VEC}_i) \quad (7)$$



Table 2 Physical properties and hydrogen solution enthalpy at infinite dilution for elements type A and B

Type	Element	Radius <sup>154</sup> [Å]	VEC <sub>i</sub> <sup>154</sup>	Melting point <sup>153</sup> [°C]	χ <sub>Allen<sub>i</sub></sub> <sup>153</sup>	ΔH <sub>i</sub> <sup>∞148</sup> [kJ mol <sup>-1</sup> H <sup>-1</sup> ]
A	Ti	1.462	4	1668	1.38	-52
	Zr	1.603	4	1855	1.32	-52
	V	1.316	5	1910	1.53	-26
	Nb	1.429	5	2477	1.41	-35
B	Cr	1.249	6	1907	1.65	28
	Mn	1.350	7	1246	1.75	1
	Fe	1.241	8	1538	1.80	29
	Co	1.251	9	1495	1.84	21
	Ni	1.246	10	1455	1.88	10
	Cu	1.278	11	1084.62	1.85	46
	Mo	1.363	6	2623	1.47	—
	Al	1.432	3	660.32	1.61	—

where VEC<sub>i</sub> is the valence electron concentration of the *i*-th element, corresponding to the total number of electrons in its outer shell. Table 2 summarizes the VEC<sub>i</sub><sup>154</sup> values for some of the most commonly used elements in multi-component alloys. The VEC is an essential parameter for predicting the crystal structure of HEAs.<sup>39,90,150</sup> According to Gorban *et al.*,<sup>155</sup> C14-Laves alloys in HEAs typically form within the VEC range of 4.4 to 8.1. Subsequent studies have confirmed through theoretical design that the calculated VEC values consistently fall within this range.<sup>136,151,156</sup> Furthermore, other researchers highlight that a pure single C14-Laves phase is more likely to form within a narrower VEC range of 6.4 to 6.7.<sup>42,154,157</sup> In addition to predicting phase structure, the VEC has been shown to affect hydrogen properties. According to Nygård *et al.*<sup>154</sup> the hydrogen desorption process can take place at room temperature when the total VEC in HEAs is 6.4. In another study, the authors found that with a VEC of 6.4, the alloy showed fast kinetics, a hydrogen capacity of 1.7 wt%, and full reversibility at room temperature, without requiring any activation process.<sup>42</sup> These results may reflect another aspect of the VEC's impact on hydrogen storage performance, but these observations appear to be valid mainly for the specific composition in the latter study.

The atomic size difference ( $\delta$ ) is another critical parameter that induces lattice distortion (Section 2.3.3) and impacts phase formation. It is determined by the differences in atomic radii among the alloy's components, as expressed in eqn (8):<sup>147</sup>

$$\delta = \sqrt{\sum_{i=1}^N c_i \left(1 - \frac{r_i}{\bar{r}}\right)^2} \times 100\% \quad (8)$$

where *N* is the number of elements, *c<sub>i</sub>* is the concentration of the component *i*, *r<sub>i</sub>*<sup>155</sup> is the atomic radius of component *i*, and  $\bar{r} = \sum_{i=1}^N c_i r_i$  is the average atomic size of the *N* components in the alloy.

Significant differences in atomic sizes result in considerable distortion of the alloy's lattice. This lattice distortion can adversely impact the physical properties of HEAs, such as thermal and electrical conductivity.<sup>90</sup> However, this effect can be advantageous for hydrogen storage properties in C14-Laves HEAs as highlighted by Mishra *et al.*<sup>151</sup> In their study of a series

of multi-component alloys they reported higher  $\delta$  values for these alloys compared to those observed in counterpart phases such as BCC and FCC.<sup>37,90</sup> Moreover, Miracle *et al.*<sup>59</sup> and Yurchenko *et al.*,<sup>70</sup> have also stated that the formation of Laves phases in HEAs occurs when  $\delta > 5\%$ .

The C14-Laves phase, being an intermetallic phase, consists of two types of atoms: A-type and B-type (Section 3). Guo *et al.*<sup>158</sup> proposed an additional criterion based on the atomic radii ratio, *r<sub>A</sub>/r<sub>B</sub>*, which is calculated using eqn (9):

$$\frac{r_A}{r_B} = \frac{\sum_i c_i^A r_i}{\sum_i c_i^B r_i} \quad (9)$$

where *c<sub>i</sub><sup>A</sup>* and *c<sub>i</sub><sup>B</sup>* are the atomic concentration of the *i*-th component in the sublattices A and B, respectively (*i.e.*,  $\sum_i c_i^A = \sum_i c_i^B = 1$ ).

Table 2 provides a summary of the atomic radii of common elements used in the design of multi-principal element alloys. An empirical criterion indicates that the C14-Laves phase can form when the atomic radius ratio (*r<sub>A</sub>/r<sub>B</sub>*) falls between 1.04 and 1.68.<sup>70,140,155,158</sup> This range also sets an upper limit for size mismatch, emphasizing the direct interconnection between these parameters and highlighting the importance of selecting appropriate elements. In another work, Ponsoni *et al.*<sup>72</sup> used the empirical approach to design their alloys and found that over 1200 compositions contained the C14-Laves phase when the atomic radius ratio was  $1.1233 < r_A/r_B < 1.223$ ,  $\delta > 5\%$ , and  $5.8 < \text{VEC} < 7.0$ . The fluctuation in several parameter ranges between studies shows that the parametric approach alone is not entirely dependable for HEA design.

The electronegativity mismatch is another parameter investigated for phase selection criteria.<sup>76,146</sup> Besides the formation and stability of solid solution structures, it also influences the topology of the final phase, especially for C14-Laves phase structured alloys.<sup>151</sup> Based on the electronegativities of the alloy components, the electronegativity mismatch ( $\Delta\chi$ ) can be calculated using eqn (10):<sup>76</sup>

$$\Delta\chi = \sqrt{\sum_{i=1}^N c_i (\chi_i - \bar{\chi})^2} \times 100\% \quad (10)$$



where  $\chi_i^{153}$  is the electronegativity of the  $i$ -th element and  $\bar{\chi} = \frac{1}{N} \sum_{i=1}^N c_i \chi_i$  is the average electronegativity of the  $N$  components in the alloy.

Two widely used scales for electronegativity difference are the Pauling and Allen scales.<sup>90</sup> Pauling electronegativity ( $\Delta\chi_{\text{Pauling}}$ ) measures an atom's ability to attract electrons in a molecule.<sup>153</sup> According to Somo *et al.*,<sup>76</sup> the average Pauling electronegativity mismatch ranges for solid-solution phases and intermetallic phases are 2–30% and 3–20%, respectively. Allen electronegativity ( $\Delta\chi_{\text{Allen}}$ ) is defined as the average one-electron energy of the valence shell electrons in ground-state free atoms.<sup>159</sup> Similar to the Pauling scale, there are two distinct ranges for Allen electronegativity mismatch: 8–38% for solid solutions and 10–25% for intermetallic compounds.<sup>76</sup>

Allen electronegativity is the most commonly used parameter for designing C14-Laves phase HEAs.<sup>151</sup> The criterion was set for  $\Delta\chi_{\text{Allen}} > 7\%$  in order to form the intermetallic Laves phases. This condition was also suggested by other researchers before.<sup>59,160</sup> Alternatively, Dong *et al.*<sup>161</sup> proposed a different value for the  $\Delta\chi_{\text{Allen}}$  parameter, suggesting that intermetallic Laves phases form when  $\Delta\chi_{\text{Allen}} > 20\%$ , which differs from the previous value. This result suggests that empirical methods have some limitations, as parameters may behave unpredictably and uncorrelated to each other within the same composition. Therefore, careful consideration is needed when using these methods for composition design.

For an effective design, all empirical parameters should be evaluated as each of them gives information about a distinct aspect of alloy behavior. In practice, it is less reliable to prioritize one single parameter over the others as such systems can sometimes fulfil one criterion and may not satisfy another. For instance, some alloys possess low values of  $\delta$  that favor solid-solution stability, while their  $\Delta H_{\text{mix}}$  is negatively large, which may promote the formation of intermetallics (eqn (1)).<sup>95</sup> In the case of C14-Laves phase HEAs, researchers have succeeded in resolving this issue by combining the empirical approach with the CALPHAD method to assess thermodynamic properties and stability.<sup>157,162,163</sup> Therefore, the empirical method suggests a collective evaluation of these parameters. Nevertheless, for the sake of efficiency, most studies have limited their empirical design to VEC,  $\delta$ ,  $\Delta\chi$ , and  $\Delta H_{\text{mix}}$ .<sup>43,77,164</sup> In terms of formation and stability of the single C14-Laves phase, both VEC and  $\delta$  are prioritized and should respect their averages as demonstrated in Table 3. For the hydrogen storage properties,  $\Delta H_{\text{mix}}$  and VEC are the best parameters to refer to, as they inform about chemical reactivity and the operation conditions of temperature and pressure.<sup>42,43</sup>

Besides the previous parameters discussed in this review, there are other factors that contribute to complementary

properties, some of which are purely thermodynamic.<sup>20,76,90,146</sup> The parameters mentioned here are the main empirical criteria used by researchers to, theoretically, guide the design of HEAs with C14-Laves phases. It is worth noting that these empirical conditions directly influence the microstructure and properties of these alloys, including their hydrogen sorption performance.<sup>76</sup> Table 3 lists these parameters and their specific ranges, providing a simple tool for predicting C14-Laves phase multi-principal alloys, particularly for hydrogen storage.<sup>70,151</sup> A common aspect between all these factors is the concentration of the  $i$ -th element ( $c_i$ ), highlighting the importance of selecting the right elements and their atomic fractions. This helps minimize variations in the thermo-physical properties of the alloy's components, leading to a more disordered solid solution with a well-defined structure.

Empirical models are a quick and basic way to predict whether a multicomponent alloy can form a stable solid-solution phase.<sup>146</sup> However, they are not all the time reliable due to the lack of phase diagrams.<sup>72</sup> These theoretical models work well when the alloy forms a single-phase structure that is uniform throughout the solid-solution, but this is not always the case in experiments. Moreover, in the parametric method, the critical values or ranges of the parameters only serve as an indication of the boundaries between forming single phase solid-solutions or multi-phase structures and intermetallics, which can sometimes appear arbitrary.<sup>89,93,150</sup> Often, additional phases coexist with the main phase, or the alloy may have two competing C14-Laves phases under certain thermodynamic conditions. In such cases, the parametric approach treats all the phases as a single-phase, leading to overlaps in regions of interfaces or multiphase solutions.<sup>146</sup> This results in the main limitation of this approach that it does not account for or compare the formation enthalpies of different possible phases, reducing its ability to consider all competing phases.<sup>93</sup> To improve the accuracy of the prediction, it is better to combine empirical models with a more robust method, such as the CALPHAD method.<sup>20</sup>

#### 4.2. Computational thermodynamics: the CALPHAD method

The CALculation of PHASE Diagrams (CALPHAD) method is another approach for guiding the design of multicomponent alloys.<sup>165</sup> CALPHAD uses computational tools to calculate phase diagrams of alloys at thermodynamic equilibrium.<sup>93</sup> Starting from pure elements, binary, and ternary systems, CALPHAD uses extrapolation to predict the properties of more complex and higher-order alloys.<sup>166,167</sup> Over the last few decades, calculating phase diagrams has become a powerful and reliable tool for predicting phase formation and stability, helping in the development of many practical engineering materials.<sup>137</sup> A key advantage of the CALPHAD method is its use of specific databases for each class of materials, based on

Table 3 The empirical parameters for C14-Laves phase's selection of multi-component alloys

Parameter	$\Delta S_{\text{mix}}^{70,151}$	$\Delta H_{\text{mix}}^{70,151}$	$\Omega^{37,70}$	VEC <sup>59,151</sup>	$\delta^{140,151}$	$r_A/r_B^{70,140}$	$\Delta\chi_{\text{Allen}}^{140,151}$
Range	$\Delta S_{\text{mix}} \geq 13 \text{ J K}^{-1} \text{ mol}^{-1}$	$-22 \text{ kJ mol}^{-1} \leq \Delta H_{\text{mix}} \leq 7 \text{ kJ mol}^{-1}$	$\Omega \geq 1.1$	$4.4 \leq \text{VEC} \leq 8.1$	$\delta > 5\%$	$1.04 \leq r_A/r_B \leq 1.68$	$\Delta\chi_{\text{Allen}} > 7\%$



solid experimental or calculated data (*i.e.*; *ab initio*), making it more trustworthy. As a result, and unlike the parametric approach, it accurately predicts all possible competing phases by analyzing their Gibbs–Helmholtz free energy.<sup>166,168</sup>

Since its first appearance, researchers and engineers have continuously worked to improve the CALPHAD method, making it more efficient and consistent. With recent advances in powerful computers and specialized software like ThermoCalc,<sup>169</sup> a strong correlation between predictions and experimental results has been reported. Ponsoni *et al.*<sup>43</sup> employed the CALPHAD method to guide the design of their HEA systems for hydrogen storage. As one of the intended compositions, the  $(\text{Ti}_{0.5}\text{Zr}_{0.5})_1(\text{Mn}_{0.5}\text{Cr}_{0.5})_2$  HEA was found to solidify primarily as the C14-Laves phase, as shown in Fig. 4a. The formation of a C15-Laves phase and other minor fractions of cubic phases during the last cooling stage are also depicted in the phase diagram. However, the XRD patterns in Fig. 4b revealed that the alloy only features a single C14-Laves phase and no reflections were observed from any other secondary phases due to the synthesis process. Similarly, in another study performed by the same author,<sup>156</sup> CALPHAD calculations predicted that the  $(\text{Ti}_{0.5}\text{Zr}_{0.5})_1(\text{Fe}_{0.33}\text{Mn}_{0.33}\text{Cr}_{0.33})_2$  alloy would solidify as a single C14-Laves phase. The phase diagram shows C14-Laves as the

main phase, but also indicates the presence of minor phases (see Fig. 4c). The XRD analysis in Fig. 4d of the as-cast alloy confirmed the presence of a purely single C14-Laves phase structure, but without visible reflections from secondary phases. The same results have been seen and confirmed by other investigations,<sup>77,78</sup> highlighting the robustness of the CALPHAD method in guiding thermodynamically the prediction of the microstructure of HEAs. Besides, depending on the processing technique, the alloy can display all the predicted phases shown in its phase diagram calculated by the CALPHAD approach.<sup>42,157,162,163</sup>

The CALPHAD method is now becoming a powerful tool for predicting phase stability and thermodynamic properties of materials, including multi-principal element alloys.<sup>170</sup> It is noteworthy to emphasize the strong ability of this method to extrapolate the properties to higher-order systems after defining the appropriate systems.<sup>168</sup> However, it is difficult to ignore some limitations. Since CALPHAD is largely an equilibrium-based method, it struggles to anticipate amorphous or metastable phases.<sup>171</sup> Furthermore, the synthesis method has a major impact on the alloy's microstructure and kinetics plays as important a role as thermodynamics.<sup>172</sup> As a result, the CALPHAD method is unable to assess the diffusion kinetics or

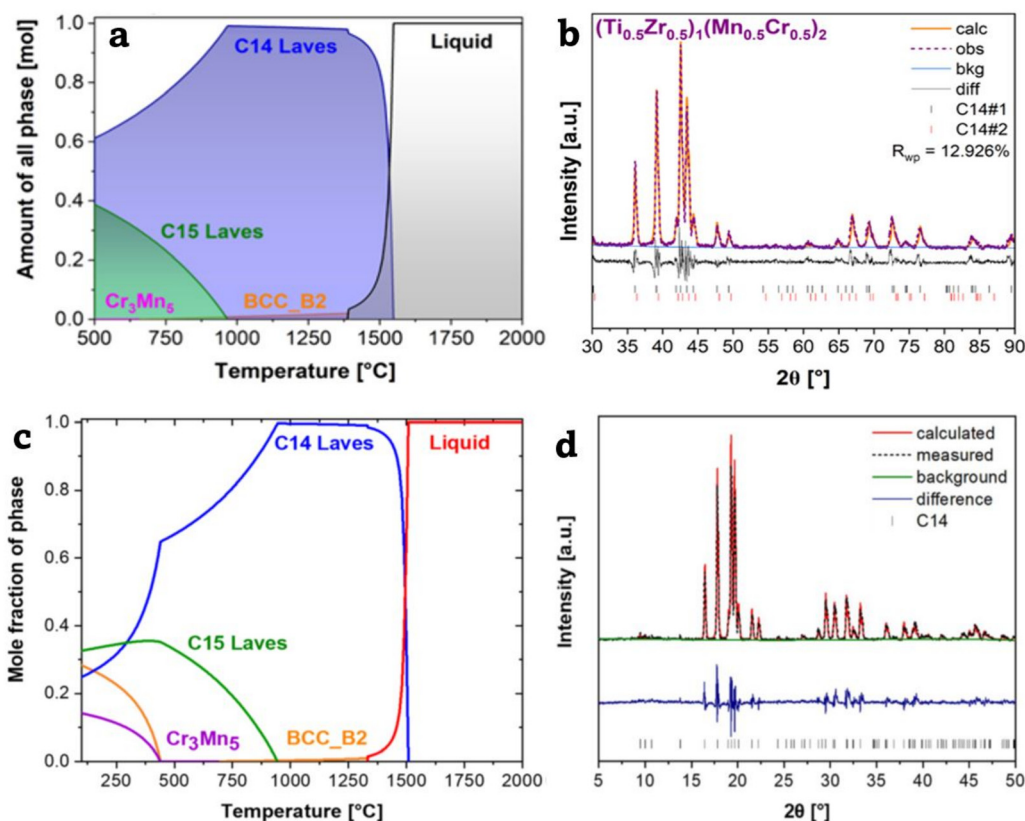


Fig. 4 (a) The calculated amount of equilibrium phases as a function of temperature using the CALPHAD method<sup>43</sup> and (b) the XRD patterns of the  $(\text{Ti}_{0.5}\text{Zr}_{0.5})_1(\text{Mn}_{0.5}\text{Cr}_{0.5})_2$  alloy.<sup>43</sup> Both figures are reproduced from ref. 43 under the CC BY 4.0 license with permission from the American Chemical Society. Copyright © 2025. (c) The phase diagram, represented by the mole fraction of equilibrium phases, of the  $(\text{Ti}_{0.5}\text{Zr}_{0.5})_1(\text{Fe}_{0.33}\text{Mn}_{0.33}\text{Cr}_{0.33})_2$  alloy<sup>156</sup> and (d) its corresponding XRD patterns.<sup>156</sup> Both alloys were synthesized using the arc melting technique. (c) and (d) are reproduced from ref. 156 under the CC BY 3.0 license with permission from the Royal Society of Chemistry. Copyright © 2023.



phase transformation pathways during preparation, and the final microstructure of a HEA may differ significantly from CALPHAD predictions.

To address these issues and overcome the limited database accuracy of the CALPHAD method, highly sophisticated and accurate techniques, such as machine learning (ML),<sup>173</sup> are now being used by researchers.<sup>174</sup> By combining ML with CALPHAD, prediction of the HEAs' structure phase becomes more precise, quicker, and of lower computational cost.<sup>41</sup> This hybrid approach enhances both thermodynamic modeling and microstructure evolution predictions, leading to more efficient alloy design.<sup>172,175</sup>

### 4.3. DFT computations

Aside from the empirical approach and the CALPHAD technique, computational methods such as density functional theory (DFT) are crucial for predicting hydrogen storage properties in HEAs by offering insights into the interaction of hydrogen at the atomic level and helping understand the hydrogen absorption and diffusion kinetics within the targeted system.<sup>176</sup> From this perspective, Merlino *et al.*<sup>144</sup> employed DFT to conduct a theoretical study on the hydrogen interaction mechanism within the Zr(Cr<sub>0.5</sub>Ni<sub>0.5</sub>)<sub>2</sub> C14-Laves phase alloy. The electronic structure, bonding energy, and total energy of hydrogen inside the various interstitial sites of the alloy lattice were calculated. The authors concluded that atomic hydrogen mostly favors the A<sub>2</sub>B<sub>2</sub> interstitial sites (Section 3), with the Zr–Zr–Cr–Cr composition. They also noted that, upon the increment of hydrogen content, an increase in the cell volume and magnetic moment was detected, highlighting the effect of hydrogen on the structural properties of the alloy. In addition, Mohammadi *et al.*<sup>177</sup> combined first-principles calculations with experiments to investigate the hydrogen storage performance of their C14-Laves alloys. They found an excellent correlation between the predicted calculations and experiments. The authors emphasized the robustness of computational methods in quickly designing new compositions with high hydrogen performance.

In the same context, another study<sup>178</sup> was carried out using first-principles calculations based on DFT computations to investigate the hydrogen absorption behavior in the TiZrV–MoNb system. The maximum hydrogen storage capacity, the minimum required hydrogen content for phase transition, the site occupation of hydrogen atoms, and phase transformation caused by hydrogen absorption were all determined. According to the calculations, a phase transition occurs from BCC to FCC when the hydrogen capacity reaches 1.5 wt%. In the BCC and FCC phases, hydrogen typically occupies octahedral and tetrahedral positions, respectively. Furthermore, calculations of enthalpy and binding energy indicate that the presence of hydrogen at tetrahedral positions enhances the FCC HEA's thermal stability. In terms of H desorption, Kurko *et al.*<sup>179</sup> investigated the dehydrogenation mechanisms of MgH<sub>2</sub> by studying how the surface and nearby surface layers affect the hydrogen desorption kinetics using DFT and the pseudopotential method. They discovered that the energy needed to desorb hydrogen becomes lower when fewer hydrogen atoms remained

on the surface. They also found that hydrogen diffusion from the bulk to the surface is strongly affected by the interatomic interactions, which has a big impact on the desorption process. These results suggest that one of the main factors limiting the dehydrogenation process is the surface tendency to keep hydrogen in a stable form, making it harder for hydrogen atoms to leave the material. From a crystallographic point of view, the H diffusion from bulk to surface could be more complex for HEAs due to the distortion effect of the lattice structure.<sup>130</sup> In brief, DFT computations represent a promising tool for designing hydrogen storage materials, particularly when combined with experimental research and other computational techniques such as Pressure–Composition–Temperature models (Section 5). As a result, high-performance HEAs with enhanced capacity, stability, and efficiency can be created for hydrogen storage.

While the compositional design is based on empirical factors like VEC and atomic mismatch, it shows drawbacks due to the vast number of possible HEAs for hydrogen storage. Calculating parameters for an infinite number of compositions and stoichiometries is time-consuming, and finding effective compositions is further limited by the complex and lengthy experimental validation process. The CALPHAD approach could be the perfect alternative to simulate and predict the thermodynamic properties of alloys and offers the advantage of quickly screening the phase diagrams of a large number of element combinations based on the target properties, which will save time and simplify the validation process. These predictions using thermodynamic calculations can be further refined by incorporating advanced computational models such as the DFT method for hydrogen storage properties. This approach enhances design accuracy and significantly saves experimental costs.

Overall, designing adequate compositions is a general procedure that must be conducted before experiments. In order to achieve the desired phase structure and properties, such compositions should be designed using the aforementioned techniques as illustrated in Fig. 5. The compositional design of C14-Laves phase structured HEAs for hydrogen storage will progressively rely on computational methods such as CALPHAD and DFT computations. It is also critical to ensure that the designed compositions include cost-effective and non-toxic elements, making them environmentally friendly and appropriate for marketable hydrogen storage applications.

## 5. PCT modeling for hydrogen storage of C14-Laves phase structured HEAs

Although it is essential, identifying suitable HEAs with optimized selection of components to achieve the predicted phase (*i.e.*, C14-Laves phase) through established design methods is still insufficient. The alloy must exhibit excellent hydrogen storage behavior. Therefore, being able to model the hydrogen storage properties of these alloys will provide valuable insights into their behavior during interactions with hydrogen gas molecules. Furthermore, it offers the opportunity to reoptimize



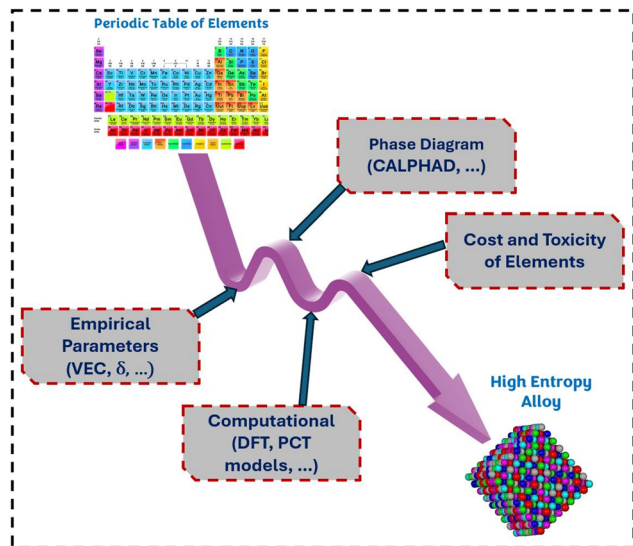


Fig. 5 Scheme showing the different compositional design strategies for multi-principal element alloys prior to manufacturing.

and fine-tune the chemical composition of the alloys to improve their reactivity with hydrogen.

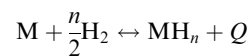
In these regards, PCT isotherms are graphical curves that depict the relationship between the hydrogen gas pressure, the amount of hydrogen absorbed or desorbed by the material (usually expressed as the hydrogen-to-metal ratio, H/M), and the temperature at which the system is maintained during the measurement process.<sup>180</sup> Likewise, PCT isotherms provide direct experimental validation of hydrogen storage properties in comparison with DFT simulations (Section 4.3), which offer fundamental insights into hydrogen interactions at the atomic level. Thus, effective material design and performance evaluation for hydrogen storage in HEAs are ensured by combining the two approaches.

Before moving to the mathematical modeling of PCT curves for hydrogen storage in C14-Laves phase structured HEAs, it is important to first understand the fundamentals of hydrogen absorption and how metal hydrides are formed.

### 5.1. Basics of hydrogen storage in metal hydrides

Metal hydrides provide an efficient and safe way to store large quantities of hydrogen compactly, especially when using transition metals and their alloys.<sup>8</sup> Remarkably,  $\text{Mg}_2\text{FeH}_6$ <sup>181</sup> and  $\text{Al}(\text{BH}_4)_3$ <sup>182</sup> have the highest reported volumetric hydrogen

densities, reaching up to  $150 \text{ kg m}^{-3}$ . Several intermetallic compounds among these metal hydrides, as shown in Table 4,<sup>22</sup> are composed of elements A (high affinity for hydrogen) and elements B (low affinity), as depicted in Fig. 3d, making them ideal candidates for hydrogen storage because of their exceptionally high volumetric hydrogen density in the host lattice.<sup>183</sup> Hydrogen reacts with various transition metals at room or elevated temperatures to form hydrides under a determined pressure.<sup>184</sup> The chemical-based hydrogen storage, known as the absorption process, is a type of solid-state storage that involves a reversible chemical reaction between metallic components and hydrogen to form metal hydrides. At equilibrium, this reaction is represented as follows:<sup>8,185</sup>



Here, M represents a metal,  $\text{MH}_n$  denotes the resulting hydride, and Q is the reaction heat. This equation shows that 1 mole of metal reacts with  $n$  moles of hydrogen atoms to form the corresponding hydride, “ $\text{MH}_n$ ”. The reaction mentioned above is typically exothermic, as the entropy of the hydride is generally lower than that of the metal and dihydrogen gas.<sup>22</sup> Consequently, at room or higher temperature, hydride formation is an exothermic process, while the reverse reaction of dehydrogenation is endothermic.<sup>186</sup> This means that most metal or alloy hydrides require the input of heat to release the absorbed hydrogen. For hydrogen storage, metals or alloys can be charged with hydrogen in two ways: by using molecular hydrogen gas ( $\text{H}_2$ ) or individual hydrogen atoms from an electrolyte.

The gaseous form is the most common and effective method for charging host materials. This process involves several reaction stages between hydrogen and the metal to form the hydride, as illustrated in Fig. 6. The initial step in hydride formation is the physisorption of hydrogen molecules, resulting from the attractive interaction between the hydrogen molecules and the metal surface *via* van der Waals forces (Fig. 6a and b).<sup>22,187,188</sup> Since this interaction includes both attractive and repulsive forces, which are directly dependent on the distance between the gas molecules and surface atoms, the hydrogen molecules interact with multiple surface atoms until their potential energy reaches a minimum, allowing complete physisorption. Typically, the physisorption energy is around  $4\text{--}6 \text{ kJ mol}^{-1}$  of  $\text{H}_2$ .<sup>187</sup> Once the  $\text{H}_2$  molecule is physisorbed onto the metal surface, the dissociation and chemisorption stage

Table 4 The prototype and structure of the most significant families of intermetallic compounds that form hydrides.<sup>22</sup> This table is reproduced from ref. 22 under the CC BY 4.0 license with permission from Wiley. Copyright © 2025

Intermetallic compound	Prototype	Hydride	Crystal structure
$\text{AB}_5$	$\text{LaNi}_5$	$\text{LaNi}_5\text{H}_6$	Haucke phases, hexagonal
$\text{AB}_2$	$\text{ZrV}_2, \text{ZrMn}_2, \text{TiMn}_2$	$\text{ZrV}_2\text{H}_{5.5}$	Laves phase, hexagonal, or cubic
$\text{AB}_3$	$\text{CeNi}_3, \text{YFe}_3$	$\text{CeNi}_3\text{H}_4$	Hexagonal, $\text{PuNi}_3$ -type
$\text{A}_2\text{B}_7$	$\text{Y}_2\text{Ni}_7, \text{Th}_2\text{Fe}_7$	$\text{Y}_2\text{Ni}_7\text{H}_3$	Hexagonal, $\text{Ce}_2\text{Ni}_7$ -type
$\text{A}_6\text{B}_{23}$	$\text{Ho}_6\text{Fe}_{23}$	$\text{Ho}_6\text{Fe}_{23}\text{H}_{12}$	Cubic, $\text{Th}_6\text{Mn}_{23}$ -type
AB	TiFe, ZrNi	TiFeH <sub>2</sub>	Cubic, CsCl or CrB-type
$\text{A}_2\text{B}$	$\text{Mg}_2\text{Ni}, \text{Ti}_2\text{Ni}$	$\text{Mg}_2\text{NiH}_4$	Cubic, $\text{Ti}_2\text{Ni}$ or $\text{MoSi}_2$ -type



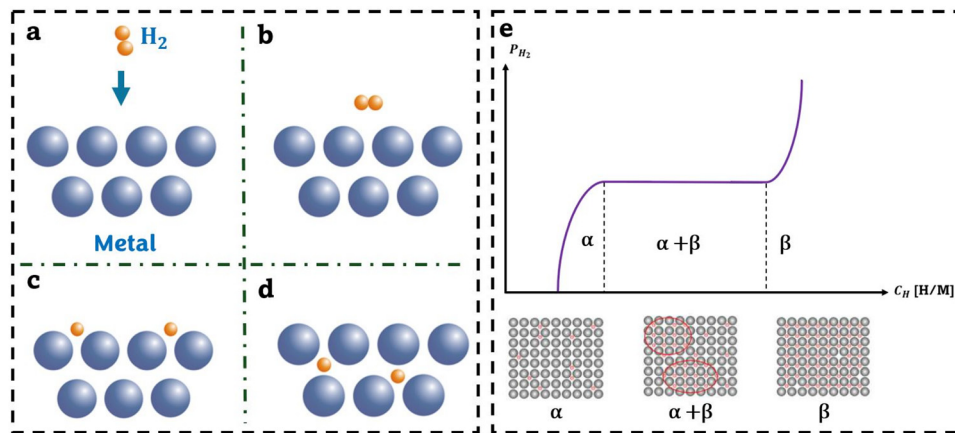


**Fig. 6** The reaction of  $\text{H}_2$  molecules with a host metal: (a) the  $\text{H}_2$  molecule approaches the metal's surface.<sup>187</sup> (b) Physisorption of the  $\text{H}_2$  molecule takes place through van der Waals forces.<sup>187</sup> (c) Chemisorption follows, where hydrogen atoms bind to the surface after dissociation.<sup>187</sup> (d) Hydrogen atoms then occupy subsurface sites and diffuse into interstitial sites within the bulk lattice.<sup>187</sup> (e) Typical PCT diagram of a metal hydride formation.<sup>187</sup> This figure was made based on the illustrations reported in ref. 187.

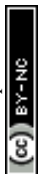
follows. Each hydrogen atom must overcome an activation energy barrier to dissociate the  $\text{H}_2$  molecule and form bonds with the metal atoms (Fig. 6c).<sup>189</sup> The typical chemisorption energy ranges from 20 to 150  $\text{kJ mol}^{-1}$  of  $\text{H}_2$ , which is significantly higher than that of physisorption. As a result, one drawback of chemisorption compared to physisorption for hydrogen storage is the need for higher operating pressures.<sup>183</sup> In the final stage, following dissociation on the metal surface, hydrogen atoms diffuse into the bulk, forming a solid solution called the  $\alpha$ -phase (Fig. 6d). The  $\alpha$ -phase begins to form at a specific temperature (usually room temperature for some C14-Laves alloys if the surface of the solid is clean), and the amount of hydrogen absorbed in the solid solution increases with hydrogen pressure. In the typical PCT diagram shown in Fig. 6e, this step is represented by the sharp rise in equilibrium pressure corresponding to the  $\alpha$ -phase. When the hydrogen content in the metal solid-solution ( $\alpha$ -phase) reaches a certain level, represented by the plateau region at constant pressure in the PCT curve where the two phases,  $\alpha$  and  $\beta$ , coexist, part of the material transforms into a metal hydride ( $\beta$ -phase) as described by the above reaction. This indicates that hydrogen atoms start to occupy the interstitial sites.<sup>185</sup> Therefore, hydrides form as hydrogen atoms occupy interstitial sites, typically tetrahedral or octahedral, within the metal lattice.<sup>190</sup> As more hydrogen is introduced, the reaction progresses within the plateau region, and the proportion of metal hydride in the solid solution increases (Fig. 6e). At this intermediate equilibrium stage, the hydrogen pressure is referred to as the equilibrium dissociation pressure ( $P_d$ ).<sup>140</sup> After the metal has fully converted into hydride, any additional hydrogen starts dissolving again into the metal hydride ( $\beta$ -phase), leading to a rise in hydrogen pressure, as indicated by the sharp increase following the plateau region in the PCT diagram.<sup>185</sup> Thus, it is important to note that, in addition to the influence of thermodynamic factors like temperature and hydrogen pressure, the maximum hydrogen capacity in the hydride phase is

determined by the number of available interstitial sites in the intermetallic lattice and their energy stability for hydrogen.<sup>183</sup> For instance, in Zr-based C14-Laves intermetallics, tetrahedral sites are preferred due to the high stability of hydrogen in these sites.<sup>144</sup>

The type of formed hydrides is influenced by a series of factors including the hydrogen content introduced to the alloy's structure, heat treatment, alloying additions, and stress states.<sup>191</sup> Thus, each hydride-forming component can form different hydrides during hydrogenation. Zirconium is one of the well-known elements that easily forms hydrides at low temperatures.<sup>192,193</sup> Fig. 7 displays the phase diagram, chemical formulas, and structures of the hydrides that are present in the Zr-H system.<sup>194,195</sup> According to Lumley *et al.*<sup>194</sup> Zr-metal can react with hydrogen to form four different hydrides, known as the  $\zeta$  ( $\text{Zr}_2\text{H}$ ),  $\gamma$  ( $\text{ZrH}$ ),  $\delta$  ( $\text{ZrH}_{1.5}$ ), and  $\epsilon$  ( $\text{ZrH}_2$ ) phases, besides the solid-solution  $\alpha$ -Zr.<sup>195</sup>

It was reported that the  $\gamma$ -hydride is considered to be a metastable phase with a tetragonal structure, as it is less frequently observed in Zr-metal or Zr-based alloys.<sup>196</sup> Other researchers, however, have found the  $\gamma$ -hydride to be formed under various cooling regimes<sup>197,198</sup> and at room temperature.<sup>199</sup> Unlike the  $\gamma$ -hydride, the  $\delta$ -hydride has a FCC structure and is reported as the most commonly observed and simulated phase in the literature in addition to its stability at moderate hydrogen concentrations.<sup>200</sup> In this phase, H atoms are dispersed randomly over all tetrahedral sites, including the black positions depicted in Fig. 7.<sup>192,194</sup>  $\zeta$ -ZrH arises during early hydrogenation stages. It is also a metastable hydride phase that is less commonly observed and sometimes denoted as  $\zeta$ -ZrH<sub>0.25</sub>.<sup>201</sup> The fourth Zr-hydride is represented by the tetragonal structure of the  $\epsilon$ -ZrH<sub>2</sub> phase and is described as a stable and dense hydride that forms at high hydrogen concentrations as shown in the Zr-H phase diagram.<sup>198</sup>

Generally, A-type elements (*i.e.*, Zr as seen in Fig. 7) experience phase transitions upon hydrogenation. BCC alloys also have the same behavior as they transform from a BCC solid-



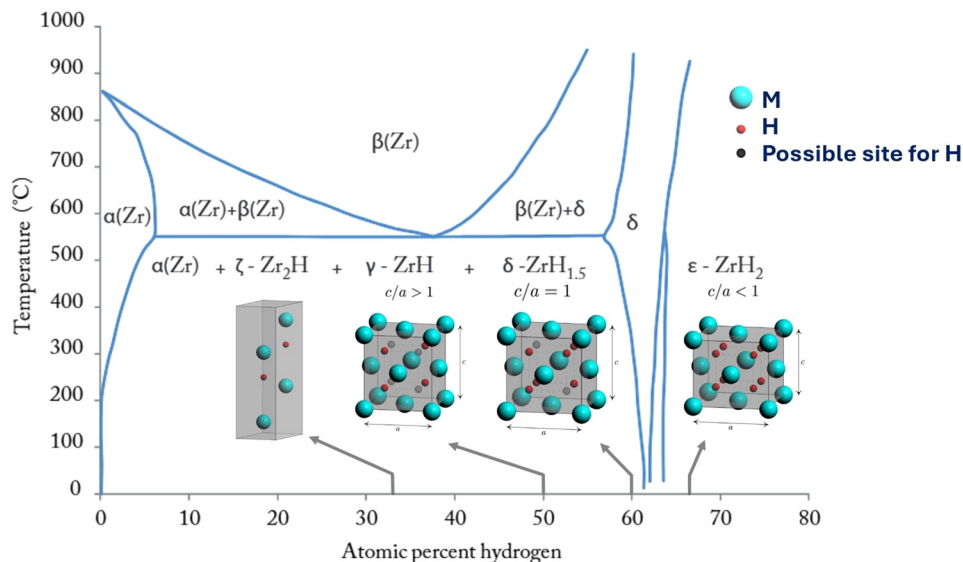


Fig. 7 Zr–H phase diagram and typical crystal structures of Zr based Hydrides.<sup>194,195</sup> Reproduced with permission from ref. 194 with modifications. Copyright © 2014, Elsevier Ltd. Reproduced from ref. 195 under the CC BY 4.0 license. Copyright © 2024, Elsevier B.V.

solution before hydrogenation to an FCC solid-solution after hydrogenation.<sup>68,98,202</sup> However, C14-Laves phase HEAs preserve their phase structure during H absorption. The obtained C14-hydride remains in the same original structure with only the expansion of the volume, which is caused by the dissolution of hydrogen atoms within the lattice.<sup>42,65,162</sup> In some situations, where the alloy is not well homogenized or contains several segregations of A-type elements or fractions of secondary BCC phase, some local ordered hydrides with different structures can occur depending on the hydrogenation conditions.<sup>65,203–205</sup> Nevertheless, exceptions to the fact that hydrogenation induces lattice expansion can occur. For example, certain rare earth metal dihydride phases exhibit a contraction during hydrogen loading due to structure transformations<sup>206</sup> or electronic factors.<sup>207,208</sup> Since the chemical reaction of hydrogenation is reversible, supplying the appropriate heat energy can initiate the dehydrogenation process, following the van't Hoff equation (eqn (16)) to obtain the PCT diagrams for the reverse process. Conducting multiple cycles of de/hydrogenation is crucial, as both cyclability and long-term stability are critical requirements for hydrogen storage systems.

## 5.2. Thermodynamic model for PCT diagram calculation

Understanding an alloy's hydrogen storage behavior depends on its PCT diagram. Measuring PCT isotherms is time-consuming, especially with numerous compositions, and often impractical. Thus, predicting an alloy's PCT diagram based on its chemical composition could greatly accelerate the search for alloys with optimized hydrogen storage properties.<sup>209</sup> Zepon *et al.*<sup>210</sup> were the first to propose a thermodynamic model for calculating PCT diagrams of BCC multi-principal element alloys. They made a series of approximations and assumptions to estimate the enthalpy and entropy of hydrogen solution, ultimately developing a mathematical model capable of

plotting PCT diagrams for each composition. Ponsoni *et al.*<sup>72</sup> adapted the same model to calculate PCT curves for C14-Laves phase-based HEAs and tested it for over 400 compositions.

As an initial approximation, this model is only applicable under an equilibrium condition known as *para-equilibrium* (PE).<sup>140</sup> PE is a thermodynamic equilibrium typically seen in conventional room and low-temperature hydrogen storage systems, where host material atoms are nearly immobile, with only hydrogen atoms being mobile. In these conditions, equilibrium is reached when the chemical potentials of hydrogen in the gas phase and in the metal are equal, as represented in eqn (11), leading to a minimum in the overall Gibbs free energy.<sup>211</sup>

$$\frac{1}{2}\mu_{\text{H}}^{\text{gas}} = \mu_{\text{H}}^{\text{metal}} \quad (11)$$

As mentioned in Section 3, the AB<sub>2</sub> C14-Laves phase features a hexagonal crystal structure with space group *P6<sub>3</sub>/mmc* (see Table 1). The C14 structure contains three types of tetrahedral interstitial sites: A<sub>2</sub>B<sub>2</sub>, AB<sub>3</sub>, and B<sub>4</sub> (see Fig. 3). Ponsoni *et al.*<sup>72</sup> considered that A-type elements (*e.g.*, Ti, Zr) occupy the 4f (A1) Wyckoff positions, while B-type elements (*e.g.*, Cr, Mn, Ni, Fe) occupy the 2a (B1) and 6h (B2) positions. This consideration is valid for both equiatomic and non-equiatomic HEAs, with the primary difference being that in non-equiatomic alloys, A-type elements can partially occupy B-type sites, and *vice versa*.<sup>212</sup> In addition, this model assumes no equilibrium between two solid phases, like the coexistence of a solid-solution and a hydride.<sup>210</sup> Experimentally, this condition cannot be ignored and often leads to a distinct plateau on PCT curves, indicating phase separation or transition during hydride formation, as reported by several studies.<sup>80,164,213</sup> As a result, the model does not consider these phase transitions when calculating PCT diagrams for C14-Laves phase alloys, meaning that the PCT plots will display the H solid-solution ( $\alpha$ -phase) followed directly by



the hydride metal ( $\beta$ -phase). Since  $A_2B_2$  sites are the most energetically stable interstitial sites for hosting hydrogen atoms in the  $AB_2$  C14-Laves phase, as demonstrated by DFT calculations in Merlino *et al.*'s work,<sup>144</sup> this model, as a second approximation, assumes that only  $A_2B_2$  sites participate in the solid-solution to form hydrides.

The model assumes thermodynamic equilibrium for the metal-hydrogen system, with the C14 Laves phase without hydrogen and  $H_2$  gas at 1 atm as the reference state. By combining all these approximations and hypotheses, the explicit equations for the terms  $\mu_H^{\text{metal}}$  and  $\mu_H^{\text{gas}}$  in eqn (11) can be derived in eqn (12) and eqn (13):

$$\mu_H^{\text{gas}} = \frac{1}{2}RT \ln\left(\frac{P_{H_2}}{P^0}\right) \quad (12)$$

$$\mu_H^{\text{metal}} = \frac{dG_{\text{mix}}}{dc_H} \quad (13)$$

where  $R$  is the ideal gas constant,  $T$  is the absolute temperature,  $P^0$  ( $P^0 = 1$  atm) is the reference state, and  $P_{H_2}$  is the given hydrogen pressure.  $c_H$  represents the amount of hydrogen in the phase and is determined by eqn (14) as:

$$c_H = \frac{n_H}{n_M} \quad (14)$$

Here,  $n_H$  and  $n_M$  indicate the number of moles of hydrogen and metal atoms in the phase, respectively. The final term in eqn (13) is  $\Delta G_{\text{mix}}$  and it refers to the change in the Gibbs free energy of mixing, eqn (15), between the C14 Laves phase with composition of the H solid-solution ( $c_H$ ) and the reference state. Under *para*-equilibrium (PE) conditions, the Gibbs free energy depends solely on  $c_H$ , as there is no change in the chemical composition of the C14-Laves phase components during hydrogenation.

$$\Delta G_{\text{mix}}(c_H) = \Delta H_{\text{mix}}(c_H) - T\Delta S_{\text{mix}}(c_H) \quad (15)$$

From eqn (11)–(13) and (15), the PCT diagram model for  $AB_2$  C14-Laves phase alloys can be calculated using eqn (16) (frequently called the Van't Hoff equation):<sup>187</sup>

$$\ln\left(\frac{P_{H_2}}{P^0}\right) = \frac{2}{RT}(\Delta H_{\text{mix}}(c_H) - T\Delta S_{\text{mix}}(c_H)) \quad (16)$$

For a more detailed explanation of the intermediate equations and parameters not shown here, readers should refer to the works of Ponsoni *et al.*<sup>72</sup> and Dornheim.<sup>187</sup> Fig. 8 compares the calculated PCT diagrams, derived from the thermodynamic model (eqn (16)), with the experimental PCT curves for six HEAs that primarily exhibit the C14-Laves phase.<sup>72</sup> The calculated PCT diagrams display relatively similar trends and are closely aligned with the experimental ones, with particularly strong agreement observed for the alloy  $(Ti_{0.5}Zr_{0.5})_1(V_{0.25}Ni_{0.55}Mn_{0.1}Fe_{0.1})_2$  at 305 K.<sup>214</sup> However, a notable difference in the shape of the curves between the model predictions and the experimental results is observed, particularly the absence of a well-defined plateau pressure as well as the difference in the pressure magnitudes compared to the experimental curves. This suggests that hydrogen absorption in these alloys occurs mainly through interstitial solid solution, as assumed in the model's development. This behavior is also observed in many experimental works where the authors reported that the fact of the absence of a well-defined plateau pressure is an indication that the hydrogen absorption probably occurred only by the interstitial solid-solution mechanism in the framework of the C14-structures.<sup>78,157,215</sup> In the other scenario where the PCT curves represent a well-defined plateau pressure (ideally, a horizontal plateau as seen in the typical PCT curve of the Fig. 6e), the hydrogen is stored in the form of hydrides, which demand most of the time heating to evacuate H due to the stability of this hydrides after formation.<sup>216,217</sup>

Nevertheless, the model efficiently estimated the equilibrium pressure for the PCT curves of the six alloys, offering a

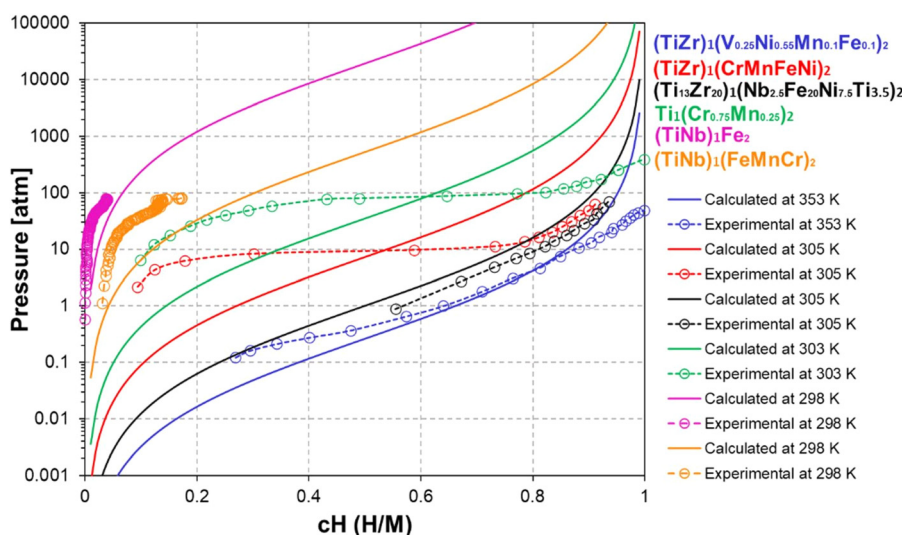


Fig. 8 The experimental absorption PCT diagram trends for six different alloys are compared with the calculated PCT plots, generated using the thermodynamic model proposed in Ponsoni *et al.*'s study.<sup>72</sup> This figure is reproduced with permission from ref. 72. Copyright © 2022, Elsevier Ltd.



good prediction of their operating pressure and temperature trends. Its simplicity allows for easy implementation in high-throughput calculations to generate PCT diagrams, helping to determine optimal pressure–temperature conditions for hydrogen storage alloys and screening a wide range of chemical compositions without the need for any complex or lengthy experimental trails. To enhance the model's predictability and accuracy regarding the shape of the PCT curves, further considerations should include a detailed investigation of hydrogen occupancy in various interstitial sites for each specific alloy, rather than focusing solely on  $A_2B_2$  tetrahedral sites. Additionally, assumptions related to thermodynamics may need refinement. In the future, this model could be significantly improved by integrating advanced tools such as *ab initio* calculations, molecular dynamics, neutron diffraction, and *in situ* XRD analyses.

## 6. Fabrication of C14-Laves phase-structured HEAs

The synthesis of multi-principal alloys involves diverse techniques, which depend on the intended properties, application, and whether the alloy is in bulk or used as a coating.<sup>218</sup> When dealing with bulk HEAs, the common methods are liquid forming and powder metallurgy, whereas vapor deposition is used for HEA coatings.<sup>219</sup> Liquid forming or liquid-state processing methods involve melting and casting processes, in which vacuum arc melting (VAM),<sup>205,220,221</sup> vacuum induction melting (VIM),<sup>222,223</sup> radio-frequency (RF) melting,<sup>224</sup> and laser cladding (LC)<sup>225</sup> are the most widely utilized manufacturing routes.<sup>226</sup> Powder metallurgy is primarily relying on mechanical alloying.<sup>37,117,227</sup> This process comprises the use of ball milling (BM), also known as high-energy ball milling technology (HEBM), to achieve nanocrystalline or amorphous particles with a uniform structure and evenly distributed components.<sup>228</sup> Vapor deposition is a surface modification technology, predominantly reliant on magnetron sputtering for the production of HEA thin films.<sup>229</sup> These coatings are deposited onto a substrate to alter its surface properties, aiming to meet the particular requirements of a given application.

All the aforementioned methods resemble the processes for conventional alloys, with the key distinction lying in the incorporation of specific features to guarantee the single-phase structure characteristic of HEAs. However, only a limited number of these techniques have been documented in the literature for manufacturing HEAs as hydrogen storage materials, and even fewer are specifically dedicated to the preparation of C14-Laves phase structured HEAs up to the present day.<sup>39,90</sup> Based on current research and experience, the primary method for synthesizing C14-Laves phase structured HEAs is through arc melting (AM).<sup>72,89,188,230</sup> Other researchers also succeeded in synthesizing HEAs featuring C14-Laves phase structures using Laser Engineered Net Shaping (LENS).<sup>215</sup> Even though other methods, such as ultra-severe plastic deformation (USPD),<sup>42,231</sup> induction melting (IM),<sup>223</sup> and radio-frequency

(RF) induction melting + melt spinning<sup>213,224</sup> have been proposed to synthesize Laves intermetallics for hydrogen storage, arc melting is still the preferred method to manufacture C14-Laves phase HEAs, followed by the LENS method. Both methods will be covered in detail in this review.

### 6.1. Arc melting (AM)

Arc melting is a metallurgical technique in which a metal or alloy is melted in a vacuum or inert atmosphere by an electric arc. This method is used to produce high-quality and refined materials with precise control over composition. It is widely recognized as the most common processing method for manufacturing HEAs intended for hydrogen storage applications in the existing literature.<sup>37,39,42,89,130</sup> The elevated melting temperature, reaching up to 3000 °C, allows for the melting of most alloying elements, which is practically beneficial for alloys containing refractory elements, such as Zr, V or Mo, and also aiding in the removal of volatile impurities and certain gases.<sup>232</sup> The key benefits of the arc melting process include reduced energy consumption, time efficiency, and lower porosity of the final product.<sup>233</sup> Consequently, scientists and researchers have directed their attention towards using the AM process, particularly for energy storage applications, in the manufacturing of HEAs. Additionally, the potential for rapid cooling immediately after melting is advantageous in ensuring the formation of single-phase HEAs.<sup>234,235</sup>

Initially, in a standard procedure, pure raw metals in the form of solid pieces such as foils, pellets, rods, or sheets are prepared in accordance with their specified weight. The weighted elements are then placed in a water-cooled copper crucible.<sup>236</sup> Subsequently, the chamber is evacuated, and argon gas is introduced, after which arc discharge melting takes place.<sup>237</sup> A simple scheme of the arc melting method is shown in Fig. 9a. The raw materials undergo melting and solidification to produce the final ingot. Occasionally, electromagnetic stirring is employed to ensure uniform mixing of the liquid metal during the melting process.<sup>238</sup> The melting process is often repeated multiple times (at least 3 times) to guarantee the chemical homogenization of the alloys.<sup>42,67,130,239,240</sup> Notably, metallic powders are not recommended for use as raw materials inside the AM chamber because of the substantial material loss caused by the extreme heat and plasma of arc melting, which causes the powder to evaporate or blow away.<sup>232</sup>

Edalati *et al.*<sup>42</sup> synthesized the TiZrCrMnFeNi high entropy alloy through arc melting, where the mixture was rotated and remelted six times to make sure the composition was homogenous. The resulting material primarily consisted of 95 wt% of the C14-Laves phase, with a minor amount of the cubic phase as confirmed by the XRD patterns. These findings were found to be basically consistent with the thermodynamic calculations conducted using the CALPHAD approach to forecast the alloy's final structure, showing the effectiveness of the arc melting technique in achieving correlated results. Similarly, Floriano *et al.*<sup>157</sup> conducted the synthesis of new equiatomic (TiZrNbFeNi) and non-equiatomic (Ti<sub>20</sub>Zr<sub>20</sub>Nb<sub>5</sub>Fe<sub>40</sub>Ni<sub>15</sub>) HEAs using



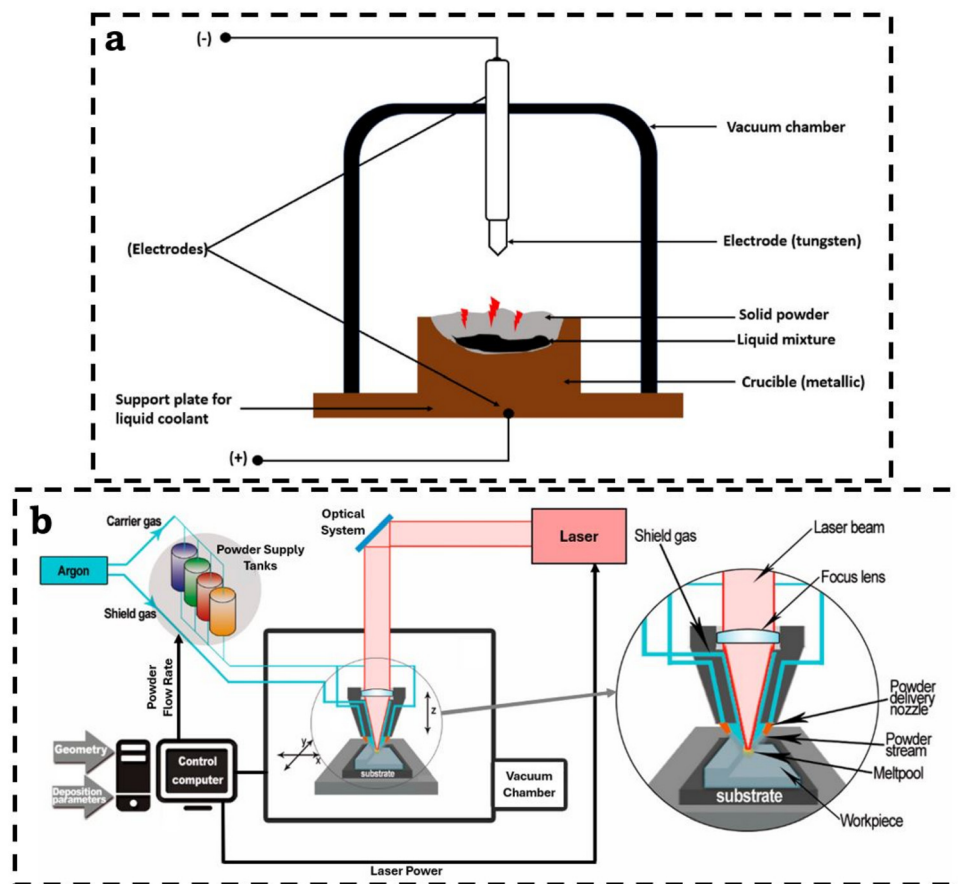


Fig. 9 (a) Schematic diagram of the arc melting method.<sup>237</sup> Reproduced from ref. 237 under the CC BY-NC-ND 4.0 license. Copyright © 2023, Elsevier B.V. (b) Typical scheme of the laser engineered net shaping technique.<sup>241</sup> Reproduced from ref. 241 under the CC BY license. Copyright © 2019, MDPI.

the arc melting method. Their results aligned with the thermodynamic calculations performed through the CALPHAD method, indicating a tendency to form a single C14-Laves phase. These outcomes further affirm the compatibility of the arc melting method with the predetermined alloy design.

Furthermore, the AM method has been performed in various studies to prepare alloys that maintain a good single-phase structure or dual-phase HEAs, with the predominant phase being the C14-Laves phase. Dangwal *et al.*<sup>130</sup> succeeded in producing both single-phase  $\text{TiV}_{1.5}\text{Zr}_{1.5}\text{CrMnFeNi}$  alloy and dual-phase  $\text{TiV}_{1.5}\text{ZrCr}_{0.5}\text{MnFeNi}$  alloy with interphase boundaries of C14 and 4 vol% BCC phases, using arc melting. This was achieved to explore the role of interphase boundaries in enhancing the hydrogen storage performance. In order to achieve homogeneous compositions, each alloy underwent rotation and remelting seven times. Moreover, in an interesting study, Chen *et al.*<sup>242</sup> successfully prepared a hexanary  $\text{TiZr-FeMnCrV}$  HEA with a single C14-Laves phase using arc melting. The study concluded that the alloy exhibits a substantial hydrogen capacity, particularly when the product was subjected to mild conditions of hydrogenation at 30 °C after the melting process.

Due to the aforementioned benefits, arc melting has emerged as the preferred method for synthesizing HEAs for hydrogen

storage, particularly those featuring single C14-Laves phase. On a different note, arc melting is also widely employed for producing HEAs with a Body-Centered Cubic (BCC) structure, as highlighted in the comprehensive review by Kong *et al.*<sup>37</sup> on BCC-structured HEAs designed for hydrogen storage. However, a key drawback associated with the arc melting technique is the risk of low temperature-melting elements evaporating during the melting process.<sup>162,243</sup> This can result in mass loss and remarkable changes in the concentration of components, potentially deviating from the desired composition. As reported in some works, this issue can be overcome by adding an excess amount of elements like Mg, Al, Mn, and V to compensate the vapor loss during melting.<sup>164,244</sup> Additionally, the crucible and uncontrolled cooling water temperature limit the ingots' size, shape, and crystal growth, which in turn affects their mechanical properties, constituting a notable disadvantage of the AM technique.<sup>237</sup> These restrictions become especially prominent when working on a smaller scale.

## 6.2. Laser engineered net shaping (LENS)

Laser Engineered Net Shaping (LENS) is an additive manufacturing technology designed to produce metal parts directly from a computer-aided design (CAD) solid model.<sup>245</sup> It involves injecting metal powder into a molten pool formed by a focused,



high-powered laser beam. Fig. 9b depicts a schematic illustration of the apparatus used for the LENS technique.<sup>241</sup> Unlike processes utilizing powder beds, such as selective laser melting (SLM), objects manufactured through LENS can be considerably larger, reaching lengths of several feet.<sup>245</sup> Researchers have shown interest in applying this method to manufacture HEAs towards energy conversion applications due to the rapid cooling rate ( $10^3$ – $10^6$  K s<sup>-1</sup>) during solidification, which is expected to prevent the occurrence of phase segregation and contribute to the formation of a single-phase structure.<sup>39,246</sup>

LENS has been employed to synthesize HEAs multiple times for different applications. For instance, Kuncce *et al.*<sup>215</sup> have effectively employed the LENS method to synthesize the ZrTiVCrFeNi-based C14-Laves phase HEA for hydrogen storage. The chemical composition was initially good after laser deposition and was further enhanced through high-temperature annealing. The alloy displayed a two-phase structure, having a predominant C14 Laves phase matrix and a minor portion of the  $\alpha$ -Ti solid-solution. The multicomponent ZrTiVCrFeNi alloy exhibited the capability to both absorb and desorb 1.81 wt% of hydrogen at low temperatures. Furthermore, other authors<sup>247</sup> used the LENS technique in a series of attempts to fabricate single phase HEAs for hydrogen storage. In their initial trial, a high laser power was essential in the process to achieve complete interdiffusion of elemental powders and to produce a chemically homogeneous TiZrNbMoV HEA. Repeatedly remelting the alloy through three cycles after its deposition using a 1 kW laser power led to the formation of a TiZrNbMoV alloy with high microstructural stability. While this alloy exhibited a high mixing entropy and induced lattice distortion, it resulted in minimal hydrogen absorption. These results could be attributed to the fact that the alloy possesses multiple dendritic phases as well as other precipitates, which play a significant role in reducing the hydrogen storage performance of the alloy. Hence, the authors emphasized that higher powder quality and LENS processing parameter optimization are required to produce more chemically homogeneous alloys. In another study by the same author, Kuncce *et al.*,<sup>248</sup> LENS technology was utilized to fabricate the LaNi-FeVMn multicomponent alloys, and their microstructures were investigated. The alloys contained second phases that are hard to prevent due to the processing parameters and the metallurgical tendency of these phases to form. The authors concluded that there was no direct correlation between the phase compositions and PCT isotherms.

In summary, the LENS technique remains an effective technique for the synthesis of HEAs for hydrogen storage applications. However, it can lead to some deviations between the predetermined composition and the actual composition of the final alloy, so further optimization is still needed. Arc melting is the main technique dedicated to produce most HEAs and especially those with single C14-Laves phase as given in Table 5. However, the effectiveness of research and development of new HEAs for hydrogen storage still relies on high throughput synthesis methods.

## 7. Hydrogen storage properties of C14-Laves phase-structured HEAs

The major challenge of C14-Laves phase HEAs is their limited hydrogen storage capacity. Nevertheless, they are known for their low-operation temperature and pressure conditions, fast kinetics, simple activation, reversibility, and cycling stability as reported in many studies.<sup>20,57,94,162</sup> In this section, the latest investigations focusing on different aspects of hydrogen storage performance of C14-Laves phase HEAs are discussed. Table 5 summarizes the hydrogen storage properties of most existing HEAs with C14-Laves phase together with their mean of synthesis.

### 7.1. Activation energy

For certain alloys, the activation energy may be more significant than for others. Clean HEAs' surfaces allow hydrogen to be readily absorbed, leading to the formation of a solid-solution known as the  $\alpha$ -phase.<sup>250–252</sup> From a practical viewpoint, some C14-HEAs can readily absorb hydrogen without applying any pre-activation treatment which makes them advantageous for hydrogen storage applications as demonstrated in several studies.<sup>40,42,157</sup> However, it is not always the case, and an activation step is often needed either before or during the hydrogenation process. C14 alloys can be activated in several ways, including evacuation under vacuum for long periods,<sup>78</sup> and heating,<sup>156</sup> using an extra step of mechanical milling to reduce the particle size,<sup>230</sup> or even by simply performing some preliminary hydrogenation/dehydrogenation cycles,<sup>253</sup> which may be sufficient to effectively activate the material.

Andrade *et al.*<sup>78</sup> reported that their novel equiatomic TiZrNbCrFeNi alloy was able to absorb 1.5 wt% of hydrogen at room temperature by only pumping the alloy at 303 K for 2 h and without conducting any thermal activation process. Differently, Kuncce *et al.*<sup>215</sup> activated their ZrTiVCrFeNi samples before PCT measurements by heating up to 500 °C under high vacuum for 2 hours. Under these conditions, they obtained a maximum hydrogen capacity of 1.81 wt% at 50 °C under 10 MPa. The authors emphasized that the high activation temperature helps to promote hydrogen absorption at lower temperature. Ma *et al.*<sup>136</sup> combined three activation processes: mechanical milling using HEBM, pre-heating, and applying three de-/hydrogenation cycles at 200 °C under 1 MPa hydrogen pressure. Interestingly, the ZrTiVFe alloy could reversibly absorb 1.58 wt% of hydrogen under 1 MPa H<sub>2</sub> at room temperature. In addition, small particle size played a crucial role in reducing the activation energy as fine particles have higher surface area, allowing for an important decrease of the initial barrier for hydrogen absorption while supplying the minimum amount of energy to activate the alloy.<sup>188,254,255</sup> Dangwal *et al.*<sup>256</sup> investigated the significant role of grain orientation and the presence of incoherent interphases on the activation of six dual-alloys in the TiVZrCrMnFeNi system for hydrogen storage, reporting that higher fraction of incoherent interphases can activate the material more easily and hence facilitate the hydrogen absorption. Furthermore, it was reported that the composition substitution may further improve the



Table 5 Summary of some comparative results of hydrogen storage properties reported for C14-Laves phase based HEAs

HEA composition	Processing method	Observed phase(s)	Activation	Absorption/desorption temperatures (°C)	Absorption pressure (MPa)	Hydrogen absorption capacity (wt%)	Hydrogen desorption capacity (wt%)	Ref.
(Ti <sub>0.5</sub> Zr <sub>0.5</sub> ) <sub>1</sub> (Fe <sub>0.33</sub> -Mn <sub>0.33</sub> Cr <sub>0.33</sub> ) <sub>2</sub>	AM (Ar)	C14-Laves phase	390 °C for 12 hours	30/30	5.2	1.7	1.7	156
TiZrNbCrFeNi	AM (Ar)	Two C14-Laves phases	Without any activation	30/30	—	1.5	0.9	78
TiZrVCrNi	AM (Ar)	C14-Laves phase	Five de/hydrogenation cycles at 32 °C under 10 MPa H <sub>2</sub>	32/300	4	1.53	1.51	71
	RF melting + melt-spun ribbon	C14-Laves phase	Easily activated	32/350	10	1.92	1.92	213
(Ti <sub>1.3</sub> Zr <sub>0.7</sub> ) <sub>1.1</sub> Cr <sub>1.1</sub> -Mn <sub>1.8</sub> Fe <sub>0.3</sub> Co <sub>0.4</sub> V <sub>0.4</sub> ZrTiVFe	AM (Ar)	C14-Laves phase	Two de/hydrogenation cycles at 25 °C under 5 MPa H <sub>2</sub>	15/15	5	1.84	1.84	164
	AM (Ar)	C14-Laves phase + HCP	Three de/hydrogenation cycles at 200 °C under 1 MPa H <sub>2</sub>	RT/400	1	1.58	1.58	136
TiZrCrFeMnNi	AM (Ar)	C14-Laves phase	450 °C for two hours	24/550	2	2.48	2.32	99
	AM (Ar)	C14-Laves phase + B2	Five de/hydrogenation cycles for one hour under 6.4 MPa H <sub>2</sub>	20/300	4	1.54	1.54	246
TiV <sub>2</sub> ZrCrMnFeNi	AM (vacuum)	C14-Laves phase + BCC	Without any activation	30/30	3.5	1.6	1.6	40
(Ti <sub>0.85</sub> Zr <sub>0.15</sub> ) <sub>1.1</sub> Cr <sub>0.95</sub> -Mo <sub>0.05</sub> Mn	AM (Ar)	C14-Laves phase	300 °C for 3 hours under 6 MPa H <sub>2</sub> , 3 de/hydrogenation cycles	30/30	6	1.76	1.53	79
TiZrNbFeNi	AM (Ar)	C14-Laves phase + BCC + B2	Without any activation	32/32	—	1.64	~1.4	157
ZrTiV MnCrFe <sub>0.5</sub>	AM (vacuum)	C14-Laves phase	400 °C for two hours	25/25	2.25	1.93	1.67	249
Ti <sub>0.24</sub> V <sub>0.17</sub> Zr <sub>0.17</sub> -Mn <sub>0.17</sub> Co <sub>0.17</sub> Fe <sub>0.08</sub>	RF induction melting (Ar)	C14-Laves phase	400 °C under 10 <sup>-4</sup> MPa	410/410	6	0.72	~0.32	224
TiZrNbCrFe	AM (Ar)	C14-Laves phase + BCC	Without any activation	200/200	—	1.9	1.9	163
Zr <sub>33</sub> Cr <sub>22</sub> Mn <sub>15</sub> -Fe <sub>25</sub> Ni <sub>5</sub>	AM (Ar)	C14-Laves phase + NiZr	450 °C for 3 hours under dynamic vacuum	RT/RT	5	1.8	1.6	162
TiZrCrMnFeNi	AM	C14-Laves phase + Cubic phase	Without any activation	30/30	3.9	1.7	1.7	42
Zr <sub>2</sub> MgVFeCrNi	AM + mechanical milling	C14-Laves phase	350 °C under 3.5 MPa H <sub>2</sub> for one hour, 3 de/hydrogenation cycles	30/30	4	0.9	~0.6	244
ZrTiVCrFeNi	LENS	C14-Laves phase + α-Ti	500 °C for two hours under high vacuum	50/50	10	1.81	~1.2	215
(ZrTiVFe) <sub>90</sub> Al <sub>10</sub>	AM (Ar)	C14-Laves phase + HCP + tetragonal	200 °C for two hours	200/200	1	1.4	0.22	230
TiVZrNbFe	AM (Ar)	C14-Laves phase + Nb-SS	Without any activation	200/200	1	1.36	0.46	188
TiZrFeMnCrV	AM + mechanical milling	C14-Laves phase	350 °C for 3 hours under dynamic vacuum + 7 MPa H <sub>2</sub> for 3 hours	30/500	7	1.8	1.8	242
TiVZrCoFeMn	AM (Ar)	C14-Laves phase	400 °C under vacuum + 3 de/hydrogenation cycles	25/25	5	1.7	0.5	221
Ti <sub>0.8</sub> Zr <sub>0.2</sub> Cr <sub>0.75</sub> -Mn <sub>1.25</sub> Ce <sub>0.02</sub>	AM (Ar)	C14-Laves phase + CeO <sub>2</sub>	One cycle: hydrogenation at 25 °C under 9 MPa of H <sub>2</sub> + dehydrogenation under vacuum at 100 °C	25/25	10	1.98	1.79	69
Ti <sub>x</sub> Zr <sub>1-x</sub> (VNiCr-MnCoAl) <sub>2</sub>	Induction melting	C14-Laves phase	Two cycles: hydrogenation at 300 °C under 2.5 MPa of H <sub>2</sub> for 2 hours + dehydrogenation at 30 °C	30/30	10	~1.7	~0.8	223

activation energy. Zhao *et al.*<sup>257</sup> investigated their alloy's activation behavior through the elemental substitution of Fe, Co, Ni, and Cu with Mn in the ZrMn<sub>0.5</sub>Cr<sub>0.5</sub>V<sub>0.5</sub>Fe<sub>0.5</sub> composition. The authors demonstrated better activation performance as the alloys were able to rapidly absorb hydrogen at above 100 °C.

## 7.2. Hydrogen storage capacity

Hydrogen capacity refers to the amount of hydrogen that a material can host under specific conditions. It can typically be

assessed either by the hydrogen-to-metal ratio (H/M) or the standard unit of weight percent (wt%).<sup>258</sup> Numerous key factors influence the ability of C14-HEAs to absorb hydrogen efficiently. These factors fall into two main categories: those intrinsic to the alloy itself, including crystal structure, composition, atomic size, particle size, surface morphology, and topography, and those associated with the hydrogen storage conditions, such as activation energy, operating temperature and H<sub>2</sub> pressure conditions, and structural stability upon



cycling.<sup>33,259,260</sup> Thus, it is essential to consider the above factors when evaluating the hydrogen-storage capacity of C14-HEAs. In the existing literature, the majority of the studies on C14-HEAs have used weight percent (wt%) as the standard unit of hydrogen capacity.<sup>42,65,78,162,164,261</sup> Additionally, most reported C14-HEAs thus far have exhibited hydrogen-to-metal ratios below 2.<sup>42,162,261</sup> It is worth mentioning that the highest values of hydrogen storage capacities achieved to date for all types of HEAs are observed in BCC-multi-principal alloys. Such examples include  $\text{Ti}_{27.5}\text{V}_{27.5}\text{Nb}_{20}\text{Cr}_{12.5}\text{Mn}_{12.5}$  (3.38 wt%),<sup>240</sup>  $(\text{VFe})_4(\text{TiCrCo})_{40-x}\text{Zr}_x$  (3.5 wt%),<sup>262</sup>  $\text{V}_{30}\text{Ti}_{35}\text{Cr}_{25}\text{Fe}_{10}$  (3.6 wt%),<sup>104</sup> and  $\text{Ti}_4\text{V}_3\text{NbCr}_2$  with a hydrogen absorption capacity of 3.7 wt%.<sup>37</sup> While these values are promising, they are often achieved under conditions of high activation energy.<sup>37</sup>

In 2023 Aranda *et al.*<sup>99</sup> successfully synthesized the TiVFeZr multi-concentrated element alloy with C14-type Laves phase structure for hydrogen storage. This alloy demonstrates an impressive hydrogen absorbing capacity of 2.48 wt% ( $\text{H/M} \approx 1.5$ ) as shown in Fig. 10a, which is believed to be the highest reported hydrogen capacity among all C14-Laves HEAs to date. This high capacity was directly attributed to the alloy's composition as it comprises high content of A-type elements, *i.e.*, Ti, Zr, and V, which absorb large amounts of hydrogen and provide a more negative enthalpy of absorption ( $-43.4 \text{ kJ mol}^{-1} \text{ H}_2$ ). Following a similar approach, Chen *et al.*<sup>249</sup> discussed the effect of the compositional combinations of Ti, V, Zr, Mn, Fe, and Cr on the hydrogen storage behavior of  $\text{Cr}_t\text{Fe}_y\text{Mn}_w\text{Ti}_x\text{V}_y\text{Zr}_z$  alloys and observed that the maximum hydrogen storage capacity increases with higher fraction of Ti and Zr and, conversely, decreases with elevated contents of B-type elements (Mn, Fe, and Cr). The alloy with the highest hydrogen storage capacity, identified as the Fe-free ( $\text{Fe}_0$ ) CrMnTiVZr alloy, reached 2.23 wt%. Additionally, the authors reported that Cr has a double role in this composition, as it shows a more favorable impact on hydrogen absorption capacity compared to the Fe and Mn. In contrast with earlier findings, Kao *et al.*<sup>65</sup> found that any increase of Zr and Ti content can lead to a decrease in the maximum absorption capacity of the  $\text{CoFeMn-Ti}_x\text{V}_y\text{Zr}_z$  alloys due to the severe segregation of these elements within the alloys, which is thought to reduce the overall size of the effective region where hydrogen absorption occurs. Therefore, a careful optimization of the design and proper selection of the constituent elements with optimum stoichiometries prior to experiments is crucial to promote higher hydrogen storage capacities.

It is well known that most HEAs display lower practical hydrogen capacities than what is predicted theoretically due to several limitations, as discussed in Section 3. Among those practical limitations, phase impurities, site blocking due to the geometry and energy of the site, chemical composition variations, and surface oxidation are the main ones. Andrade *et al.*<sup>162</sup> studied the role of the C14-Laves phase predominance in increasing the hydrogen uptake of two multi-component alloys within the ZrCrMnFeNi system. The  $\text{Zr}_{33}\text{Cr}_{22}\text{Mn}_{15}\text{Fe}_{25}\text{Ni}_5$  alloy exhibits a hydrogen absorption capacity of 1.8 wt% ( $\text{H/M} = 1.2$ ) as depicted in Fig. 10b, while the  $\text{Zr}_{33}(\text{CrMnFeNi})_{67}$  alloy

could absorb 1.6 wt% ( $\text{H/M} = 1$ ) of hydrogen (Fig. 10c). The superior performance of  $\text{Zr}_{33}\text{Cr}_{22}\text{Mn}_{15}\text{Fe}_{25}\text{Ni}_5$  was attributed to the higher predominance (98.4%) of C14-Laves phase, which fully transforms into C14-Laves hydride, compared to the  $\text{Zr}_{33}(\text{CrMnFeNi})_{67}$  alloy that contains a higher content of the second intermetallic NiZr phase (8.8%) as an unwanted phase impurity leading to a decrease of the optimal hydrogen capacity. The same results have been seen in other investigations.<sup>80,230</sup> Alternatively, the same author in a different investigation,<sup>77</sup> reported the discrepancy between the theoretical (1.61 wt%) and maximum experimental (1.4 wt%) capacities to the incomplete accessibility of all interstitial sites to hydrogen due to the chemical composition variation in the  $\text{Ti}_{21}\text{Zr}_{21}\text{Fe}_{41}\text{Ni}_{17}$  alloy's structure. Surface oxidation was also reported to be a pronounced issue that reduces the hydrogen storage capacity of HEAs and especially the absorption capacity. Raud *et al.*<sup>263</sup> evaluated the hydrogen behavior and corrosion resistance of their alloys and found that surface oxidation decreases hydrogen uptake, from 2.4 wt% to 1.8 wt%, and limits sorption kinetics.

Remarkably, Ponsoni *et al.*<sup>156</sup> pointed out a hydrogen storage capacity of 1.67 wt% that is very close to the theoretical uptake of the  $(\text{Ti}_{0.5}\text{Zr}_{0.5})_1(\text{Fe}_{0.33}\text{Mn}_{0.33}\text{Cr}_{0.33})_2$  alloy (1.7 wt%). Additionally, Edalati *et al.*<sup>42</sup> synthesized a 95 wt% C14-Laves TiZrCrMnFeNi multi-principal alloy and reported a hydrogen capacity of 1.7 wt% ( $\text{H/M} = 1$ ) that is quite close to the theoretical value, as seen in Fig. 10d. It was concluded that this hydrogen storage capacity is similar to that of other room temperature hydrogen storage materials like  $\text{LaNi}_5$ <sup>264</sup> and  $\text{TiFe}$ ,<sup>56,265</sup> suggesting its suitability for stationary hydrogen storage applications. Moreover, Liang *et al.*<sup>204</sup> reported that the hydrogen capacity can be well enhanced to reach its theoretical value by promoting more hydrogen absorption sites with lower activation energy (*i.e.*  $\text{A}_2\text{B}_2$ ) through increasing the number of grains and grain boundaries.

To understand the challenges related to the hydrogen storage capacity, the criteria set by the US Department of Energy (DOE) can be used as a reference. These targets aim for a gravimetric density of  $1.8 \text{ kWh kg}^{-1}$  (equivalent to 5.5 wt% hydrogen) and a volumetric density of  $1.3 \text{ kWh L}^{-1}$  by 2025, ultimately reaching  $2.2 \text{ kWh kg}^{-1}$  (6.5 wt% hydrogen) and  $1.7 \text{ kWh L}^{-1}$ .<sup>266,267</sup> Until now, none of the hydrides reported, nor the primary commercial methods for storing hydrogen in gaseous or liquid states, have met the DOE targets.

### 7.3. Hydrogenation kinetics

Hydrogenation kinetics is a significant factor evaluating the hydrogen storage performance efficiency of HEAs.<sup>268</sup> It is typically described as the time required for a material to absorb 90% of its maximum hydrogen storage capacity ( $t_{0.9}$ ),<sup>37,39,65</sup> indicating the rate at which it reaches its full storage potential (Fig. 10a). The " $t_{0.9}$ " parameter serves as a useful tool for estimating the hydrogen absorption kinetics of alloys. It is noteworthy to mention that hydrogen storage kinetics are influenced by diverse factors including activation energy, temperature, chemical composition, particle size, atomic sizes of the components, and the microstructure of the alloys.<sup>20,269</sup>



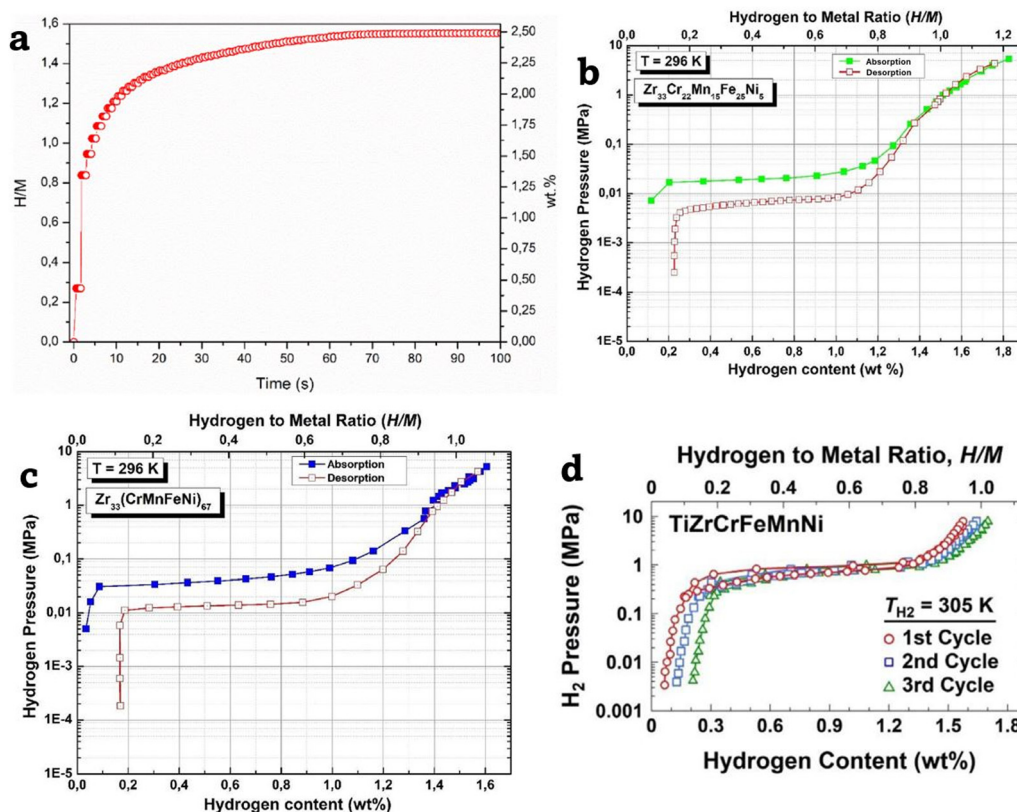


Fig. 10 (a) Kinetic curve of hydrogen absorption of the TiVFeZr HEA under 20 bar of initial  $H_2$  pressure at room temperature.<sup>99</sup> Reproduced with permission from ref. 99. Copyright © 2023, Elsevier Ltd. (b) PCT isotherms of hydrogen absorption/desorption for the  $Zr_{33}Cr_{22}Mn_{15}Fe_{25}Ni_5$  alloy at room temperature.<sup>162</sup> Reproduced with permission from ref. 162. Copyright © 2023, Elsevier Ltd. (c) PCT diagrams of hydrogen absorption/desorption for the  $Zr_{33}(CrMnFeNi)_{67}$  alloy at room temperature.<sup>162</sup> Reproduced with permission from ref. 162. Copyright © 2023, Elsevier Ltd. (d) PCT curves of absorption/desorption at 303 K of the TiZrCrFeMnNi HEA.<sup>42</sup> Reproduced with permission from ref. 42. Copyright © 2019, Elsevier Ltd.

Kao *et al.*<sup>65</sup> investigated the kinetics of hydrogen absorption of the C14-CoFeMnTi<sub>x</sub>V<sub>y</sub>Zr<sub>z</sub> alloys with varying temperatures and concentrations of Ti, V, and Zr following activation. Their results confirmed the presence of a correlation between the “ $t_{0.9}$ ” parameter and  $x$  in the CoFeMnTi<sub>x</sub>VZr alloys and  $z$  in the CoFeMnTiVZr<sub>z</sub> alloys at either 25 or 80 °C, as shown in Fig. 11a and c, respectively. The rate of hydrogen absorption in the case of CoFeMnTi<sub>x</sub>VZr decreases as the Ti content in the alloys rises from 0.5 to 2, which is attributed to lattice volume expansion and the resulting enlargement of interstitial sites, as evidenced by the XRD peaks. This investigation highlights the direct relationship between  $t_{0.9}$  and interstitial site size. Similar trends are observed for the CoFeMnTiVZr<sub>z</sub> alloys, and the values of  $t_{0.9}$  decrease as  $z$  increases due to the large atomic size of Zr and its effect on the lattice volume expansion. However, no relationship was observed between “ $t_{0.9}$ ” and  $y$  in the CoFeMnTiV<sub>y</sub>Zr alloys at both 25 and 80 °C because of the similar radius of V compared to the average radius of Co, Fe, Mn, Ti, V, and Zr in the alloy as depicted in Fig. 11b. Moreover, there was no significant influence on the interstitial sites of the alloys CoFeMnTiV<sub>y</sub>Zr. Furthermore, the influence of temperature on the kinetics was evident for all the series, which has a complex aspect as a function of the varying composition. Random behavior was observed in the case of the

CoFeMnTi<sub>x</sub>VZr and CoFeMnTiV<sub>y</sub>Zr alloys. Besides, at lower temperatures, the kinetics are faster in the case of the CoFeMnTiVZr<sub>z</sub> alloys due to the low diffusion barriers of hydrogen within the lattice.

Zhao *et al.*<sup>257</sup> also investigated the impact of temperature and compositional variations on the hydrogen storage kinetics of the  $ZrMn_{0.5}Cr_{0.5}V_{0.5}M_{0.5}$  alloys (where  $M = Fe, Co, Ni, \text{ and } Cu$ ) derived from the initial  $AB_2$ -type  $ZrMnCr_{0.5}V_{0.5}$  system. They found that all the investigated alloys have rapid hydrogen absorption rates at temperatures above 100 °C, typically around 120 seconds. However, reducing the operating temperature to room temperature significantly decreases the hydrogen absorption rate of the alloys. Thus, diffusion is faster at higher temperatures. In addition, the  $ZrMn_{0.5}Cr_{0.5}V_{0.5}Fe_{0.5}$  alloy demonstrates the most favorable hydrogen absorption kinetics at lower temperatures. This indicates that substituting Fe and Ni by Mn enhances the hydrogen absorption kinetics of the  $ZrMn_{0.5}Cr_{0.5}V_{0.5}M_{0.5}$  alloy at lower temperatures. Zhou *et al.*<sup>69</sup> explored the impact of Ce-doping on the hydrogen uptake kinetics of the TiZrCrMn alloy. The authors compared the absorption kinetics of Ce-doped and undoped  $Ti_{0.8}Zr_{0.2}Cr_{0.75}Mn_{1.25}$  and  $Ti_{0.8}Zr_{0.2}Cr_{0.75}Mn_{1.25}Ce_{0.02}$  alloys, respectively, as shown in Fig. 11d. With no pre-activation process, the undoped alloy highlights poor kinetics and limited absorption capacity



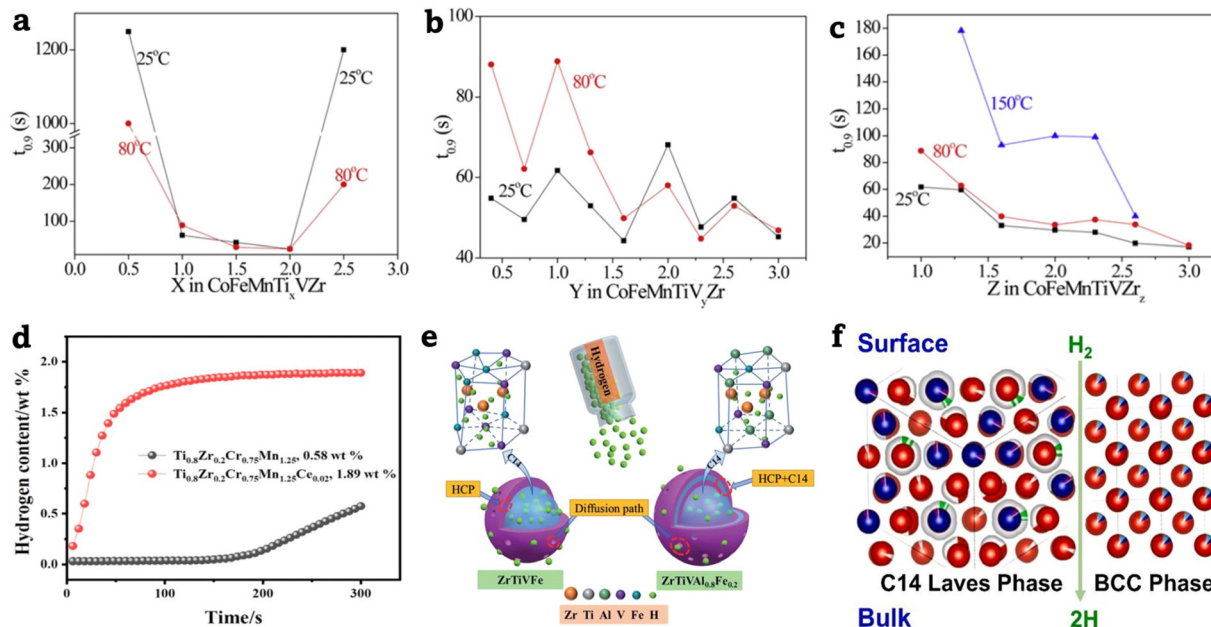


Fig. 11 The “ $t_{0.9}$ ” parameter as a function of composition at 25 °C, 80 °C, and 150 °C of (a) CoFeMnTi<sub>x</sub>VZr, (b) CoFeMnTiV<sub>y</sub>Zr, and (c) CoFeMnTiVZr<sub>z</sub>.<sup>65</sup> (a–c) are reproduced with permission from ref. 65. Copyright © 2010, Elsevier Ltd. (d) Comparison of the hydrogen absorption kinetic curves between the Ti<sub>0.8</sub>Zr<sub>0.2</sub>Cr<sub>0.75</sub>Mn<sub>1.25</sub> and Ti<sub>0.8</sub>Zr<sub>0.2</sub>Cr<sub>0.75</sub>Mn<sub>1.25</sub>Ce<sub>0.02</sub> HEAs.<sup>69</sup> Reproduced with permission from ref. 69. Copyright © 2022, American Chemical Society. (e) Schematic illustration showing the diffusion path of H atoms in the ZrTiVFe and ZrTiVAl<sub>1-x</sub>Fe<sub>x</sub> alloys.<sup>136</sup> Reproduced from ref. 136 under the CC BY-NC 3.0 license with permission from the Royal Society of Chemistry. Copyright © 2022. (f) Schematic illustration of the C14-BCC interface and its significance on hydrogen kinetics.<sup>270</sup> Reproduced with permission from ref. 270. Copyright © 2023, Elsevier Ltd.

as it started absorbing H<sub>2</sub> after 150 s and reaches 0.58 wt% of the total capacity at 300 s. Meanwhile, the Ce-doped alloy began the absorption directly upon exposure to H<sub>2</sub> and achieved a maximum capacity of 1.89 wt% after only 150 s. These results are believed to be the consequence of the lattice expansion induced by Ce-addition.

In a notable work, Ma *et al.*<sup>136</sup> investigated the effect of microstructure on the hydrogenation kinetics of ZrTiVAl<sub>1-x</sub>Fe<sub>x</sub> HEAs. The authors found that the alloys exhibit fast hydrogenation kinetics at room temperature. It was reported that the observed rapid hydrogen chemisorption kinetics at room temperature are attributed to the presence of the HCP phase. Although brittle, this phase acts as an effective diffusion pathway, promoting hydrogen atom mobility, as evidenced in Fig. 11e. Moreover, Dangwal *et al.*<sup>270</sup> studied the effect of the C14-Laves/BCC interface on the hydrogen kinetics of the TiV<sub>1.5</sub>ZrCr<sub>0.5</sub>MnFeNi alloy. The results show an outstanding effect of the interface by providing additional diffusion channels for hydrogen and thereby faster kinetics and increased hydrogen absorption capacity as illustrated in Fig. 11f. The hydrogenation kinetics can further be affected by the pre-activation treatment of the alloys, as demonstrated by Ponsoni *et al.*<sup>43</sup> in their study. They investigated the effect of the prior activation treatment on the kinetics of absorption of the (Ti<sub>0.5</sub>Zr<sub>0.5</sub>)<sub>1</sub>(Mn<sub>0.5</sub>Cr<sub>0.5</sub>)<sub>2</sub> alloy. It was discovered that, despite its rapid absorption, the inactivated alloy showed an incubation time of approximately 1 minute, followed by 5 minutes to reach its total absorption capacity of 1.90 wt%. In contrast, the activated alloy at 390 °C under dynamic vacuum for 2 hours

showed excellent rate of absorption as it achieved its total capacity in just a few seconds.

Sleiman *et al.*<sup>255</sup> investigated the particle size effect on the hydrogenation kinetics of the TiVZrHfNb HEA. Three ranges of particle sizes were selected: less than 0.5 mm, between 0.5 mm and 1 mm, and between 1 mm and 2 mm. It was concluded that particles with a diameter of less than 0.5 mm activate rapidly (Fig. 12a), as they possess higher surface area, therefore, hydrogen atoms can diffuse into the material more quickly, improving the kinetics of hydrogen absorption and reducing the incubation time. However, extremely small particles may become thermodynamically unstable or prone to oxidation, which can reduce their efficiency. Ha *et al.*<sup>253</sup> showed an opposite effect of particle size on hydrogenation kinetics. Two powders of the TiZrCr-FeMnNi alloy were prepared by hand grinding and categorized into two groups: S53 μm (fine particles) and S200 μm (coarse particles). According to the study, it was found that during the first hydrogenation, the S53 sample had a larger specific surface area, which caused a thicker or more reactive oxide layer to form. This oxide layer served as a barrier, resulting in slowing down hydrogen absorption compared to the coarser powder as seen in Fig. 12b. Therefore, controlling and optimizing particle size is important for achieving fast, stable, and reversible hydrogen storage in HEA systems.

#### 7.4. Reversibility and cycling properties

One of the main challenges in investigating the hydrogen storage performance of HEAs is to minimize the loss of effective hydrogen capacity over repeated absorption and desorption



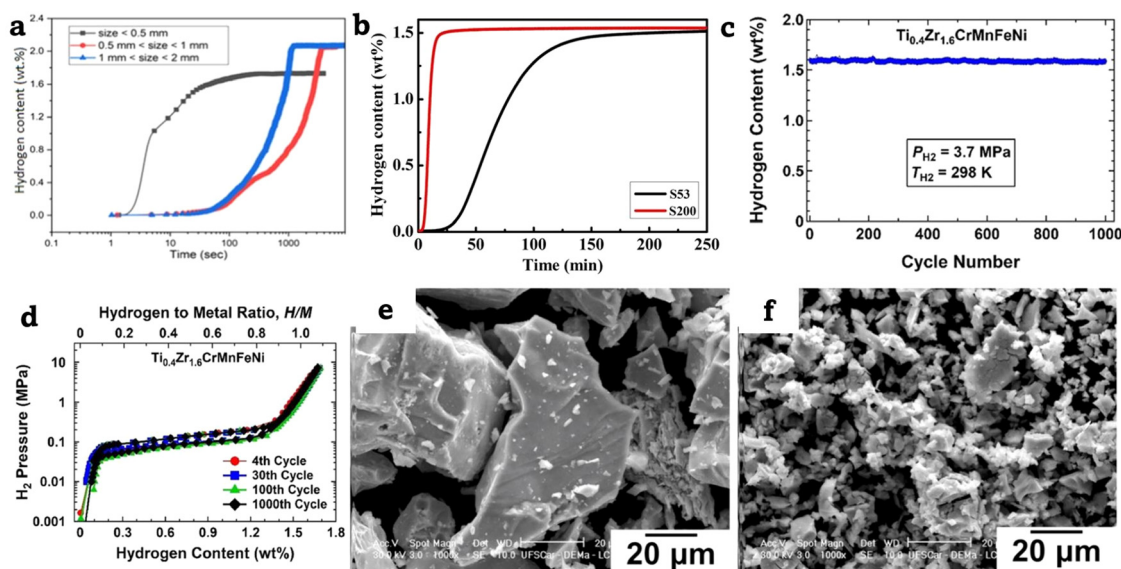


**Fig. 12** (a) Activation curves of the TiZrCrFeMnNi alloy at 300 °C for various particle sizes.<sup>255</sup> Reproduced with permission from ref. 255. Copyright © 2021, Elsevier B.V. (b) First hydrogenation kinetics of the S53  $\mu\text{m}$  and S200  $\mu\text{m}$  samples of the TiZrCrFeMnNi HEA at 20 °C under 6.4 MPa.<sup>253</sup> Reproduced with permission from ref. 253. Copyright © 2024, Elsevier Ltd. (c) Cycling performance of the  $\text{Ti}_{0.4}\text{Zr}_{1.6}\text{CrMnFeNi}$  HEA at room temperature<sup>177</sup> and (d) PCT absorption/desorption isotherms for cycles 4, 30, 100, and 1000 of the  $\text{Ti}_{0.4}\text{Zr}_{1.6}\text{CrMnFeNi}$  HEA.<sup>177</sup> (c and d) are reproduced with permission from ref. 177. Copyright © 2022, Elsevier Ltd. (e) SEM images of the  $(\text{Ti}_{0.33}\text{Zr}_{0.33}\text{Nb}_{0.33})_1(\text{Mn}_{0.5}\text{Cr}_{0.5})_2$  alloy prior to de-/hydrogenation tests<sup>43</sup> and (f) after the 50th cycle of de-/hydrogenation.<sup>43</sup> (e and f) are reproduced from ref. 43 under the CC BY 4.0 license with permission from the American Chemical Society. Copyright © 2025.

cycles. Furthermore, some researchers suggest that excellent cycling stability could be the key to scaling up certain alloys, even those having moderate hydrogen absorption capacity.<sup>271</sup> Mohammadi *et al.*<sup>177</sup> prepared the  $\text{Ti}_{0.4}\text{Zr}_{1.6}\text{CrMnFeNi}$  alloy and studied its hydrogen storage properties. The authors reported an impressive cycling stability as the alloy keeps a reversible hydrogen capacity of 1.7 wt% even after 1000 cycles as shown in Fig. 12c and d. These results confirm the excellent cycling performance and steady reversibility of this HEA, which is important for future up-scaling. Similarly, Chen *et al.*<sup>242</sup> observed the same trends in their study on the hydrogenation cycling properties of the TiZrFeMnCrV alloy. After 50 cycles, the alloy exhibited excellent absorption/desorption cyclability, with the capacity still remaining stable around 1.76 wt%. The authors noted that the alloy is supposed to be used for low powered fuel cells or stationary hydrogen energy storage applications. In contrast, Kumar *et al.*,<sup>213</sup> on the other hand, reported a slight reduction in hydrogen storage capacity of the equiatomic TiZrVCrNi system across ten cycles of hydrogen absorption and desorption, from 1.92 to 1.89 wt%. The authors ascribed this capacity decay to the thermodynamic characteristics of the alloying elements. Additional research came to the same conclusion, indicating that the loss of hydrogen capacity during cycling is a dynamic process, mainly influenced by the stoichiometry of the alloy.<sup>272</sup> Aranda *et al.*<sup>99</sup> cycled the TiVFeZr alloy 10 times at room temperature under 20 bar. The hydrogen capacity drops from 2.32 wt% in the first cycle to 1.92 wt% in the 2nd cycle. The authors believe that this reduction is mainly a consequence of the applied lower desorption temperature. Nonetheless, the alloy maintained the hydrogen capacity seen

in the 2nd cycle until the 10th cycle. Moreover, only a few alloys, as previously cited, can reversibly cycle hydrogen. Yet, many alloys tend to keep a fraction of the effective absorbed capacity, despite the applied heating to release all of it.<sup>99</sup> Therefore, with a quick inspection of the PCT diagrams, it can be seen how the material will behave in terms of cycling properties depending on its equilibrium plateau pressure.<sup>157,215</sup>

It is important to mention that cycling has a significant effect on the alloys' particle size. As reported by Ponsoni *et al.*<sup>43</sup> the particle size of the  $(\text{Ti}_{0.33}\text{Zr}_{0.33}\text{Nb}_{0.33})_1(\text{Mn}_{0.5}\text{Cr}_{0.5})_2$  alloy was decreased from 200  $\mu\text{m}$  to a range of 10 to 100  $\mu\text{m}$  after 50 cycles of hydrogen absorption/desorption. This noticeable reduction in particle size, as seen in Fig. 12e and f, is accompanied by the development of surface cracks due to the lattice expansion upon repeated hydrogenation cycles. The same results were observed in the work of Pan *et al.*<sup>273</sup> It was found that the particle size decreased from 22.56  $\mu\text{m}$  in the 10th cycle to 9.12  $\mu\text{m}$  after 500 cycles. The authors stated that this reduction results from the pulverization of the alloy particles due to microcracking caused by lattice stress upon hydrogen absorption and desorption.

## 8. Possible applications for C14-Laves phase HEAs

Despite there currently being many potential applications for hydrogen storage alloys, their practical application is still restricted to a few particular fields such as biomedical and power industry areas,<sup>274,275</sup> in which their applicability strongly



depends on the specific properties of each material. Based on the abovementioned hydrogen storage properties of the C14-Laves phase structured HEAs, these alloys may be suitable for the following possible application scenarios:

### 8.1. Large stationary hydrogen storage

It is evident that the current hydrogen absorption capacity of C14-Laves phase HEAs is still low compared to other alloys, such as BCC alloys and Mg-based hydrides.<sup>276</sup> Yet, C14-HEAs remain suitable for stationary hydrogen storage applications, where weight and volume are not significant constraints.<sup>22</sup> Hydrogen storage alloys have a great chance of meeting future energy demands across various sectors through stationary applications. Renewable energies, for instance, are now representing an important share of the global energy supply. However, its intermittent nature and technical issues make large-scale use challenging.<sup>4</sup> Given this, C14-Laves phase HEAs could play a crucial role by storing large amounts of energy, especially when converting excess electricity into hydrogen for later use. In addition, solid-state hydrogen storage employing these materials is a secure and reliable method for long-term energy storage, as most of the hydrides formed are stable at room temperature.<sup>213</sup> They can therefore serve as important backup power sources for critical infrastructure, assisting in maintaining uninterrupted operations during power outages in locations such as hospitals, data centers, and telecommunication facilities.<sup>10</sup> Moreover, it has been reported that many C14-type intermetallics can absorb hydrogen at low pressures and do not require high activation energy.<sup>42,162</sup> Due to their low energy input and lack of complex maintenance requirements, these alloys are also promising candidates for stationary hydrogen storage applications. From a raw materials cost point of view, the cost of the TiZrCrMnFeNi alloy, for instance, is approximated to 5.30 US\$ per mol, which is quite comparable to the price of the traditional LaNi<sub>5</sub>'s raw materials (5.18 US\$ per mol).<sup>277,278</sup> Both alloys possess roughly the same hydrogen capacity (1.7 wt%) with the advantage of room temperature reversibility and fast kinetics of the C14-Laves phase TiZrCrMnFeNi alloy while relying on more sustainable constituent elements than rare-earth elements.<sup>42</sup> Interestingly, Zhu *et al.*<sup>164</sup> succeeded to produce on a large scale 25 kg of their alloy after achieving remarkable hydrogen storage properties at laboratory scale, which will open doors in the future for implanting in real storage applications.

### 8.2. Energy applications

Beyond hydrogen storage, C14-Laves phase alloys have additional energy applications, such as battery electrodes. Metal-hydride batteries, for example, show promising potential to deliver higher energy densities and operate over a wide temperature range, up to 70 °C. Thanks to the structural stability of the C14-Laves phase lattice, these alloys can help overcome some of the limitations found in traditional cathode materials.<sup>279</sup> In terms of anode materials, Ti/Zr-based Laves-type alloys show significantly higher electrochemical discharge capacities (400–495 mAh g<sup>-1</sup>) compared to traditional Co-based

AB<sub>5</sub>-type alloys (around 320 mAh g<sup>-1</sup>).<sup>280,281</sup> Additionally, rare earth elements, which are frequently found in conventional anodes, can be substituted with Mg in the new alloys. By adjusting the composition, it is feasible to attain even greater performance while reducing costs and reliance on critical materials.<sup>282</sup>

Furthermore, HEAs are known for their unique four core effects (Section 2.3), which promotes outstanding characteristics such as catalytic activity, selectivity, and durability towards energy conversion-related catalytic support applications including Proton Exchange Membrane Fuel Cells (PEMFCs).<sup>106,283–285</sup> C14-Laves phase alloys as well can play potential role in such applications. Due to their durability and unique crystal structure with numerous active metal sites, they are effective in promoting chemical reactions.<sup>286</sup> In addition to the presence of a mixture of hydride-forming and non-forming components, they are able to dissociate hydrogen molecules selectively and facilitate electron transfer, which makes them promising candidates for water splitting applications, contributing to the development of efficient and sustainable energy systems.<sup>137</sup>

### 8.3. Structural materials

The structure of HEAs is the source of any differences as compared to standard alloys. They have excellent application prospects in metallurgy, corrosion resistance, the chemical industry, aerospace, equipment production, and nuclear industries owing to their distinct microstructure and compositional mixture.<sup>287</sup> Felten *et al.*<sup>288</sup> reported the substantial effect of Laves phases and nano-precipitates on the electrochemical corrosion resistance of Mg–Al–Ca alloys. The presence of Laves structures in these alloys helps to promote a stable passive layer under alkaline conditions and thereby enhances the inhibition of corrosion kinetics. Zr-based C14-Laves phases are of big interest due to corrosion resistance and neutron absorption properties, which makes them substantial materials for nuclear reactors.<sup>289</sup> Furthermore, HEAs can be used in aerospace components, turbine parts and engines as reported in several works.<sup>274,275,290,291</sup>

## 9. Potential challenges and perspectives

The commercialization of C14-Laves multi-principal alloys for hydrogen storage is blocked by several obstacles. This study draws attention to the following key challenges:

### 9.1. Compositional control

Designing a composition that satisfies all the requirements is the first step in developing suitable alloys for hydrogen storage applications. In most cases, C14-Laves intermetallics are designed using only parametric approaches or the CALPHAD method before experiments. However, these methods alone are not always sufficient to fully predict the alloy's behavior. In this situation, controlling the composition can be enhanced by using advanced computational tools like DFT and machine



learning. These techniques can greatly lower experimental expenses while also improving design. It is also important to carefully select and substitute elements, as well as to adjust their ratios, in order to achieve a better balance in the final alloy composition.

### 9.2. Processing difficulties

It is necessary to overcome some inherent problems in processing methods like arc melting, such as uncontrolled cooling rates, limited water temperature, and crucible geometry constraints. It is possible to use sophisticated tools that can be remotely controlled by software. This could improve control over crystal growth during solidification and make the process more effective and manageable. In addition, heat treatment after post-manufacturing can be a useful tool to stabilize the desired microstructure.<sup>215</sup> However, as highlighted by Cheng *et al.*,<sup>292</sup> annealing may have a negative effect on the hydrogen storage performance. Therefore, careful optimization of the heat treatment should be made to achieve favorable properties. From a different angle, thin film deposition can provide greater control over the factors influencing the production of alloys, making it a useful approach before moving on to bulk synthesis.<sup>293</sup> Furthermore, green and sustainable processing methods, such as additive manufacturing (3D printing), can be helpful due to its great degree of flexibility, use of less energy, and improvement in resource efficiency.<sup>294</sup>

### 9.3. Thermodynamics and kinetics

Kinetics and thermodynamics are key factors that govern the absorption and desorption of hydrogen, so they constitute yet another significant challenge for C14-Laves phase alloys. It is advantageous for HEAs to be able to release hydrogen at low temperatures, even at room temperature. Others, however, require high temperatures for dehydrogenation,<sup>224</sup> making them less practical for most applications, especially in the industry and transportation sectors. As previously stated, the perfect hydrogen storage material should be able to absorb and release hydrogen in a reversible way under conditions close to room temperature and atmospheric pressure. Reaching this balance is challenging though, because of the complex mechanism of H absorption within the alloy and the slow kinetics of hydrogen intake and release in some alloys despite their high capacity.<sup>22</sup>

### 9.4. Hydrogen capacity

Hydrogen capacity is a key factor in evaluating the feasibility of materials for hydrogen storage.<sup>295,296</sup> In general, C14-Laves phase HEAs show low to moderate hydrogen capacities, which is another limitation affecting their potential use in practical applications. In this essence, multiple actions can be made to help increase the H capacity of these alloys including tailoring their microstructure by adding elements, like Mg, that have a strong affinity to absorb hydrogen and hence can improve their H uptake.<sup>297</sup> According to Liang *et al.*'s work,<sup>203</sup> hybrid systems like dual phases (C14-BCC) have been shown to be useful in boosting H uptake. They reported that the combination of

C14-Laves and BCC phases is beneficial for the enhancement of hydrogen storage performance. This is attributed to the synergistic effect of the excellent diffusion properties provided by the fraction of C14-Laves phase and the strong hydrogen absorption capacity of BCC phases. Furthermore, surface engineering such as applying catalytic layer coatings, for instance, that act as hydrogen activation sites improving absorption rates and possibly increasing hydrogen capacity by trapping H atoms towards the appropriate site within the lattice, is a promising approach. Furthermore, chemical short-range order (CSRO) was found to be a crucial strategy that stabilizes locally an ordered arrangement of atoms leading to an increase in lattice strain and distortion, which could be beneficial for improving hydrogen capacity and reversibility through hydrogen binding enthalpy and creation of more void spaces to host H.<sup>298,299</sup>

### 9.5. Limited ductility

It is well known that C14-Laves phase alloys tend to be brittle and fragile, and the inclusion of some metals, like Ti, can make this brittleness more pronounced.<sup>300,301</sup> Improving the limited ductility of these alloys remains therefore a major challenge, especially for structural and hydrogen storage applications. Adding more ductile elements, like Nb, Al, or Ni, could be one way to improve the alloy's overall ductility and change the bonding properties.<sup>302</sup> Based on several studies,<sup>303,304</sup> annealing may assist in microstructure refinement and internal stress relief, enhancing ductility.

## 10. Summary and conclusions

Herein, we comprehensively and critically discussed the concept of HEAs with C14-Laves phase structures and their unique features in offering countless opportunities for the design and the development of solid-state hydrogen storage materials in many potential application fields, including stationary hydrogen storage. Based on this investigation, the following conclusions are drawn:

- Empirical parameters represent a basic and quick tool to predict whether a multicomponent alloy can form a stable solid-solution phase. However, they are time consuming when handling a large number of compositions and are not all the time reliable due to the lack of phase diagrams.

- Advanced theoretical strategies such as CALPHAD and DFT computations will progressively play a crucial role in guiding the composition design of HEAs possessing a C14-Laves single-phase and shortlisting the promising candidates for hydrogen storage as demonstrated by previous studies. For the sake of reliability, future investigations should also consider the combination of CALPHAD or DFT with machine learning, which will improve the thermodynamic modeling and give more insights about solidification paths, segregations, and diffusion phenomena, leading to a more efficient design of HEAs with reduced computational cost.

- PCT models, that estimate the alloy's thermodynamics through the Van't Hoff equation by evaluating the enthalpy and



entropy of hydrogen absorption, should also be calculated in some cases when the hydrogen storage properties are the last consideration in the design. Deeper studies that include interstitial site type and distribution, defects, and interfaces are needed for more realistic predictions.

– Large temperature gradients and quick solidification rates, which often produce fine-grained microstructures with exceptional qualities, have demonstrated that the AM process is a reliable synthesis technique for HEAs. Still, a more stable C14-Laves single phase structure that is preferred for examining its hydrogen storage capabilities can be obtained by using post heat treatment after synthesis or by finding a suitable manufacturing process with controlled parameters to avoid having segregation and second phases in the final microstructure. This issue might be handled by controlling the cooling rate depending on phase stability.

– Most C14-Laves phase based HEAs absorb hydrogen at low plateau pressure and at lower temperatures, which makes them great candidates for large stationary hydrogen storage. Nevertheless, the challenge of achieving high capacity remains present to date as well as the need for the activation of some alloys prior to cycling. Therefore, the main goal of future investigations would be the improvement of the hydrogen capacity and the decrease of the activation energy of these alloys. Future work should explore the effect of Mg and Al doping on the hydrogen absorption capacity; in addition to surface engineering by applying catalytic coating (Ni, Co) on C14-Laves phase HEAs to facilitate H trapping as well as microstructure control such as creating more local interfaces in the bulk.

– So far, the current HEAs with C14-Laves phase are still under research investigation, but with the enhancements indicated above, they might be potentially competitive in a variety of applications scenarios, including structural materials and energy applications.

## List of terms and symbols

### A. Terms and abbreviations

Term/abbreviation	Description
HEAs	High entropy alloys
MOFs	Metal–organic frameworks
COFs	Covalent–organic frameworks
MCH	Methylcyclohexane
wt%	Weight percent
at%	Atomic percent
FCC	Face-centered cubic
BCC	Body-centered cubic
CALPHAD	CALCulation of PHase Diagrams
DFT	Density functional theory
MPEAs	Multi-principal element alloys
MCAs	Multi-component alloys
CCAs	Complex concentrated alloys
HCP	Hexagonal close packing
eqn	Equation

TRIP	Transformation induced plasticity
PCT	Pressure–composition–temperature
C14	Hexagonal-type structure
C15	Cubic MgCu <sub>2</sub> -type structure
C36	Hexagonal MgNi <sub>2</sub> -type structure
A	Hydride forming element
B	Non-hydride forming element
AB <sub>2</sub>	General formula of Laves phase structures
A <sub>2</sub> B <sub>2</sub> , AB <sub>3</sub> , B <sub>4</sub>	Common tetrahedral interstitial sites in the AB <sub>2</sub> -C14 formula
VEC	Valence electron concentration
XRD	X-ray diffraction
ML	Machine learning
H	Hydrogen
M	MgZn <sub>2</sub> metal
MH <sub>x</sub>	Metal hydride
PE	<i>para</i> -Equilibrium
VAM	Vacuum arc melting
VIM	Vacuum induction melting
RF	Radio-frequency
RFIM	Radio-frequency induction melting
LC	Laser cladding
MM	Mechanical milling
BM	Ball milling
HEBM	High-energy ball milling
MS	Magnetron sputtering
AM	Arc melting
LENS	Laser engineered net shaping
USPD	Ultra-severe plastic deformation
IM	Induction melting
CAD	Computer-aided design
SLM	Selective laser melting
RT	Room temperature
DOE	Department of energy
SEM	Scanning electron microscope
PEMFC	Proton exchange membrane fuel cell
CSRO	Chemical short-range order

### B. Symbols

Symbol	Description	Unit
$R$	Universal gas constant	J mol <sup>-1</sup> K <sup>-1</sup>
$T$	Absolute temperature	K
$\Delta G_{\text{mix}}$	Gibbs free energy of mixing	kJ mol <sup>-1</sup>
$\Delta H_{\text{mix}}$	Mixing enthalpy	kJ mol <sup>-1</sup>
$\Delta S_{\text{mix}}$	Mixing entropy	kJ mol <sup>-1</sup> K <sup>-1</sup>
$\Delta G_{\text{f}}$	Gibbs free energy of formation	kJ mol <sup>-1</sup>
$\Delta G_{\text{f}}$	Formation enthalpy	kJ mol <sup>-1</sup>
$\Delta S_{\text{f}}$	Formation entropy	kJ mol <sup>-1</sup> K <sup>-1</sup>
$n$	Number of equimolar elements	—
$\varepsilon_{\text{A-H}}, \varepsilon_{\text{B-H}}$	A–H and B–H bond energies	eV



$\delta$	Atomic size mismatch	%
$r_A/r_B$	Atomic radius ratio	—
$\Delta\chi$	Electronegativity difference	%
$N$	Number of constituent elements	—
$c_i, c_j$	Atomic fractions of elements $i$ and $j$	—
$\Delta H_{ij}^{\text{mix}}$	Binary mixing enthalpy for $i$ - $j$ pair in the liquid phase with subregular solution	$\text{kJ mol}^{-1}$
$T_{\text{mix}}$	Absolute temperature of mixing	K
$\Omega$	Thermodynamic ratio between mixing entropic and mixing enthalpic contributions	—
$\text{VEC}_i$	Valence electron concentration of element $i$	—
$r_i$	Atomic radius of element $i$	$\text{\AA}$
$\bar{r}$	Average atomic radius	$\text{\AA}$
$c_i^A, c_i^B$	Atomic fractions of the element $i$ in the A and B sublattices	—
$\chi_i$	Electronegativity of element $i$	—
$\bar{\chi}$	Average electronegativity	—
$\Delta\chi_{\text{Pauling}}$	Pauling electronegativity difference	%
$\Delta\chi_{\text{Allen}}$	Allen electronegativity difference	%
$[\text{H}/\text{M}]$	Hydrogen-to-metal ratio	—
$Q$	Reaction heat	$\text{kJ mol}^{-1}$
$\alpha$	Solid-solution phase	—
$\beta$	Hydride phase	—
$P_d$	Equilibrium dissociation pressure	bar
$\gamma\text{-ZrH}$	Zr-hydride with tetragonal structure	—
$\zeta\text{-Zr}_2\text{H}$	Zr-hydride with tetragonal structure	—
$\delta\text{-ZrH}_{1.5}$	Zr-hydride with FCC structure	—
$\varepsilon\text{-ZrH}_2$	Zr-hydride with tetragonal structure	—
$\mu_{\text{H}}^{\text{gas}}, \mu_{\text{H}}^{\text{metal}}$	Chemical potentials of hydrogen in the gas phase and in the metal phase	$\text{kJ mol}^{-1}$
$P^0$	Reference pressure (1 bar)	Bar
$P_{\text{H}_2}$	Hydrogen pressure	Bar
$c_{\text{H}}$	Amount of hydrogen	—
$n_{\text{H}}, n_{\text{M}}$	Number of moles of hydrogen and metal atoms	mol
$t_{0.9}$	Time required to reach 90% of maximum capacity	s

## Author contributions

Badr El Aalami: conceptualization, methodology, investigation, visualization, writing – original draft, writing – review and editing. Hosni Idrissi: supervision, validation, funding acquisition, project administration, and writing – review and editing. Vera Trabadelo: supervision, validation, resources, funding acquisition, project administration, and writing – review and editing.

## Conflicts of interest

There are no conflicts to declare.

## Data availability

No primary research results, software or code have been included and no new data were generated or analysed as part of this review.

## Acknowledgements

The authors would like to thank the OCP Foundation for the financial support. H. Idrissi is mandated by the Belgian National Fund for Scientific Research (FSR-FNRS).

## References

- 1 Y. K. Yadav, M. A. Shaz and T. P. Yadav, Solid-State Hydrogen Storage Properties of Al–Cu–Fe–Ni–Ti High Entropy Alloy, *Int. J. Hydrogen Energy*, 2025, **99**, 985–995, DOI: [10.1016/j.ijhydene.2024.12.254](https://doi.org/10.1016/j.ijhydene.2024.12.254).
- 2 A. Aslan, O. Ilhan, A.-M. Usama, B. Savranlar, M. A. Polat, N. Metawa and A. Raboshuk, Effect of Economic Policy Uncertainty on CO<sub>2</sub> with the Discrimination of Renewable and Non Renewable Energy Consumption, *Energy*, 2024, **291**, 130382, DOI: [10.1016/j.energy.2024.130382](https://doi.org/10.1016/j.energy.2024.130382).
- 3 C. Gunathilake, I. Soliman, D. Panthi, P. Tandler, O. Fatani, N. A. Ghulamullah, D. Marasinghe, M. Farhath, T. Madhujith, K. Conrad, Y. Du and M. Jaroniec, A Comprehensive Review on Hydrogen Production, Storage, and Applications, *Chem. Soc. Rev.*, 2024, **53**(22), 10900–10969, DOI: [10.1039/D3CS00731F](https://doi.org/10.1039/D3CS00731F).
- 4 R. Radmehr, S. R. Henneberry and S. Shayanmehr, Renewable Energy Consumption, CO<sub>2</sub> Emissions, and Economic Growth Nexus: A Simultaneity Spatial Modeling Analysis of EU Countries, *Struct. Change Econ. Dyn.*, 2021, **57**, 13–27, DOI: [10.1016/j.strueco.2021.01.006](https://doi.org/10.1016/j.strueco.2021.01.006).
- 5 M. Filonchyk, M. P. Peterson, L. Zhang, V. Hurynovich and Y. He, Greenhouse Gases Emissions and Global Climate Change: Examining the Influence of CO<sub>2</sub>, CH<sub>4</sub>, and N<sub>2</sub>O, *Sci. Total Environ.*, 2024, **935**, 173359, DOI: [10.1016/j.scitotenv.2024.173359](https://doi.org/10.1016/j.scitotenv.2024.173359).
- 6 A. Mahesh and K. S. Sandhu, Hybrid Wind/Photovoltaic Energy System Developments: Critical Review and Findings, *Renewable Sustainable Energy Rev.*, 2015, **52**, 1135–1147, DOI: [10.1016/j.rser.2015.08.008](https://doi.org/10.1016/j.rser.2015.08.008).
- 7 A. Q. Al-Shetwi, Sustainable Development of Renewable Energy Integrated Power Sector: Trends, Environmental Impacts, and Recent Challenges, *Sci. Total Environ.*, 2022, **822**, 153645, DOI: [10.1016/j.scitotenv.2022.153645](https://doi.org/10.1016/j.scitotenv.2022.153645).
- 8 T. He, P. Pachfule, H. Wu, Q. Xu and P. Chen, Hydrogen Carriers, *Nat. Rev. Mater.*, 2016, **1**(12), 16059, DOI: [10.1038/natrevmats.2016.59](https://doi.org/10.1038/natrevmats.2016.59).
- 9 D. Erdemir and I. Dincer, A Perspective on the Use of Ammonia as a Clean Fuel: Challenges and Solutions, *Int. J. Energy Res.*, 2021, **45**(4), 4827–4834, DOI: [10.1002/er.6232](https://doi.org/10.1002/er.6232).
- 10 M. G. Rasul, M. A. Hazrat, M. A. Sattar, M. I. Jahirul and M. J. Shearer, The Future of Hydrogen: Challenges on



- Production, Storage and Applications, *Energy Convers. Manage.*, 2022, 272, 116326, DOI: [10.1016/j.enconman.2022.116326](https://doi.org/10.1016/j.enconman.2022.116326).
- 11 J. Chi and H. Yu, Water Electrolysis Based on Renewable Energy for Hydrogen Production, *Chin. J. Catal.*, 2018, 39(3), 390–394, DOI: [10.1016/S1872-2067\(17\)62949-8](https://doi.org/10.1016/S1872-2067(17)62949-8).
  - 12 *Energy Density of Hydrogen – The Physics Factbook*, <https://hypertextbook.com/facts/2005/MichelleFung.shtml> (accessed 2025-07-17).
  - 13 *paitonenergy*, *Hydrogen Energy: An Innovation for Zero Emissions*, PT Paiton Energy, <https://paitonenergy.com/hydrogen-energy-an-innovation-for-zero-emissions/> (accessed 2025-07-16).
  - 14 L. Ge, B. Zhang, W. Huang, Y. Li, L. Hou, J. Xiao, Z. Mao and X. Li, A Review of Hydrogen Generation, Storage, and Applications in Power System, *J. Energy Storage*, 2024, 75, 109307, DOI: [10.1016/j.est.2023.109307](https://doi.org/10.1016/j.est.2023.109307).
  - 15 B. E. Lebrouhi, J. J. Djoupo, B. Lamrani, K. Benabdelaziz and T. Kousksou, Global Hydrogen Development – A Technological and Geopolitical Overview, *Int. J. Hydrogen Energy*, 2022, 47(11), 7016–7048, DOI: [10.1016/j.ijhydene.2021.12.076](https://doi.org/10.1016/j.ijhydene.2021.12.076).
  - 16 T. Capurso, M. Stefanizzi, M. Torresi and S. M. Camporeale, Perspective of the Role of Hydrogen in the 21st Century Energy Transition, *Energy Convers. Manage.*, 2022, 251, 114898, DOI: [10.1016/j.enconman.2021.114898](https://doi.org/10.1016/j.enconman.2021.114898).
  - 17 A. Kovač, M. Paranos and D. Marciuš, Hydrogen in Energy Transition: A Review, *Int. J. Hydrogen Energy*, 2021, 46(16), 10016–10035, DOI: [10.1016/j.ijhydene.2020.11.256](https://doi.org/10.1016/j.ijhydene.2020.11.256).
  - 18 L. Schlapbach and A. Züttel, Hydrogen-Storage Materials for Mobile Applications, *Nature*, 2001, 414(6861), 353–358, DOI: [10.1038/35104634](https://doi.org/10.1038/35104634).
  - 19 *Basic Hydrogen Properties Chart/H2tools/Hydrogen Tools*, <https://h2tools.org/basic-hydrogen-properties-chart> (accessed 2024-08-14).
  - 20 L. Luo, L. Chen, L. Li, S. Liu, Y. Li, C. Li, L. Li, J. Cui and Y. Li, High-Entropy Alloys for Solid Hydrogen Storage: A Review, *Int. J. Hydrogen Energy*, 2024, 50, 406–430, DOI: [10.1016/j.ijhydene.2023.07.146](https://doi.org/10.1016/j.ijhydene.2023.07.146).
  - 21 *Hydrogen Storage*, Energy.gov, <https://www.energy.gov/eere/fuelcells/hydrogen-storage> (accessed 2025-07-17).
  - 22 E. Nemukula, C. B. Mtshali and F. Nemangwele, Metal Hydrides for Sustainable Hydrogen Storage: A Review, *Int. J. Energy Res.*, 2025, 2025(1), 6300225, DOI: [10.1155/er/6300225](https://doi.org/10.1155/er/6300225).
  - 23 M. Fu, X. Ma, K. Zhao, X. Li and D. Su, High-Entropy Materials for Energy-Related Applications, *iScience*, 2021, 24(3), 102177, DOI: [10.1016/j.isci.2021.102177](https://doi.org/10.1016/j.isci.2021.102177).
  - 24 G. Rohit, M. S. Santosh, M. N. Kumar and K. Raghavendra, Numerical Investigation on Structural Stability and Explicit Performance of High-Pressure Hydrogen Storage Cylinders, *Int. J. Hydrogen Energy*, 2023, 48(14), 5565–5575, DOI: [10.1016/j.ijhydene.2022.11.154](https://doi.org/10.1016/j.ijhydene.2022.11.154).
  - 25 P. Martin, I. B. Ocko, S. Esquivel-Elizondo, R. Kupers, D. Cebon, T. Baxter and S. P. Hamburg, A Review of Challenges with Using the Natural Gas System for Hydrogen, *Energy Sci. Eng.*, 2024, 12(10), 3995–4009, DOI: [10.1002/ese3.1861](https://doi.org/10.1002/ese3.1861).
  - 26 M. R. Usman, Hydrogen Storage Methods: Review and Current Status, *Renewable Sustainable Energy Rev.*, 2022, 167, 112743, DOI: [10.1016/j.rser.2022.112743](https://doi.org/10.1016/j.rser.2022.112743).
  - 27 M. S. Salman, N. Rambhujun, C. Prathana, K. Srivastava and K.-F. Aguey-Zinsou, Catalysis in Liquid Organic Hydrogen Storage: Recent Advances, Challenges, and Perspectives, *Ind. Eng. Chem. Res.*, 2022, 61(18), 6067–6105, DOI: [10.1021/acs.iecr.1c03970](https://doi.org/10.1021/acs.iecr.1c03970).
  - 28 P. M. Modisha, C. N. M. Ouma, R. Garidzirai, P. Wasserscheid and D. Bessarabov, The Prospect of Hydrogen Storage Using Liquid Organic Hydrogen Carriers, *Energy Fuels*, 2019, 33(4), 2778–2796, DOI: [10.1021/acs.energyfuels.9b00296](https://doi.org/10.1021/acs.energyfuels.9b00296).
  - 29 A. Bourane, M. Elanany, T. V. Pham and S. P. Katikaneni, An Overview of Organic Liquid Phase Hydrogen Carriers, *Int. J. Hydrogen Energy*, 2016, 41(48), 23075–23091, DOI: [10.1016/j.ijhydene.2016.07.167](https://doi.org/10.1016/j.ijhydene.2016.07.167).
  - 30 K. M. Thomas, Hydrogen Adsorption and Storage on Porous Materials, *Catal. Today*, 2007, 120(3), 389–398, DOI: [10.1016/j.cattod.2006.09.015](https://doi.org/10.1016/j.cattod.2006.09.015).
  - 31 N. Jasminská, T. Brestovič, M. Puškár, R. Grega, J. Rajzinger and J. Korba, Evaluation of Hydrogen Storage Capacities on Individual Adsorbents, *Measurement*, 2014, 56, 219–230, DOI: [10.1016/j.measurement.2014.07.002](https://doi.org/10.1016/j.measurement.2014.07.002).
  - 32 S. Meduri and J. Nandanavanam, Materials for Hydrogen Storage at Room Temperature – An Overview, *Mater. Today: Proc.*, 2023, 72, 1–8, DOI: [10.1016/j.matpr.2022.05.059](https://doi.org/10.1016/j.matpr.2022.05.059).
  - 33 M. Sahlberg, D. Karlsson, C. Zlotea and U. Jansson, Superior Hydrogen Storage in High Entropy Alloys, *Sci. Rep.*, 2016, 6(1), 36770, DOI: [10.1038/srep36770](https://doi.org/10.1038/srep36770).
  - 34 A. Kumar, P. Muthukumar, P. Sharma and E. A. Kumar, Absorption Based Solid State Hydrogen Storage System: A Review, *Sustainable Energy Technol. Assess.*, 2022, 52, 102204, DOI: [10.1016/j.seta.2022.102204](https://doi.org/10.1016/j.seta.2022.102204).
  - 35 M. R. Kalibek, A. D. Ospanova, B. Suleimenova, R. Soltan, T. Orazbek, A. M. Makhmet, Kh. S. Rafikova and N. Nuraje, Solid-State Hydrogen Storage Materials, *Discover Nano*, 2024, 19(1), 195, DOI: [10.1186/s11671-024-04137-y](https://doi.org/10.1186/s11671-024-04137-y).
  - 36 E. H. Abdechafik, H. A. Ousaleh, S. Mehmood, Y. F. Baba, I. Bürger, M. Linder and A. Faik, An Analytical Review of Recent Advancements on Solid-State Hydrogen Storage, *Int. J. Hydrogen Energy*, 2024, 52, 1182–1193, DOI: [10.1016/j.ijhydene.2023.10.218](https://doi.org/10.1016/j.ijhydene.2023.10.218).
  - 37 L. Kong, B. Cheng, D. Wan and Y. Xue, A Review on BCC-Structured High-Entropy Alloys for Hydrogen Storage, *Front. Mater.*, 2023, 10, 1135864, DOI: [10.3389/fmats.2023.1135864](https://doi.org/10.3389/fmats.2023.1135864).
  - 38 N. A. A. Rusman and M. Dahari, A Review on the Current Progress of Metal Hydrides Material for Solid-State Hydrogen Storage Applications, *Int. J. Hydrogen Energy*, 2016, 41(28), 12108–12126, DOI: [10.1016/j.ijhydene.2016.05.244](https://doi.org/10.1016/j.ijhydene.2016.05.244).
  - 39 F. Yang, J. Wang, Y. Zhang, Z. Wu, Z. Zhang, F. Zhao, J. Huot, J. Grobivč Novaković and N. Novaković, Recent Progress on the Development of High Entropy Alloys (HEAs) for Solid Hydrogen Storage: A Review, *Int. J. Hydrogen Energy*, 2022, 47(21), 11236–11249, DOI: [10.1016/j.ijhydene.2022.01.141](https://doi.org/10.1016/j.ijhydene.2022.01.141).



- 40 S. Dangwal and K. Edalati, High-Entropy Alloy TiV<sub>2</sub>ZrCrMnFeNi for Hydrogen Storage at Room Temperature with Full Reversibility and Good Activation, *Scr. Mater.*, 2024, **238**, 115774, DOI: [10.1016/j.scriptamat.2023.115774](https://doi.org/10.1016/j.scriptamat.2023.115774).
- 41 P. Edalati, G. Andrade, R. B. Strozi, S. Dangwal, K. Edalati and R. Floriano, Room Temperature Hydrogen Storage Properties of Ti-Zr-Mn-Fe-Co High-Entropy Alloys Designed by Semi-Empirical Descriptors, Thermodynamic Calculations and Machine Learning, *J. Alloys Compd.*, 2025, **1022**, 180051, DOI: [10.1016/j.jallcom.2025.180051](https://doi.org/10.1016/j.jallcom.2025.180051).
- 42 P. Edalati, R. Floriano, A. Mohammadi, Y. Li, G. Zepon, H.-W. Li and K. Edalati, Reversible Room Temperature Hydrogen Storage in High-Entropy Alloy TiZrCrMnFeNi, *Scr. Mater.*, 2020, **178**, 387–390, DOI: [10.1016/j.scriptamat.2019.12.009](https://doi.org/10.1016/j.scriptamat.2019.12.009).
- 43 J. B. Ponsoni, V. Aranda, W. J. Botta and G. Zepon, Reversible Hydrogen Storage at Moderate Pressure–Temperature Conditions of C14 Laves Phase Alloys of the (Ti<sub>0.5–x</sub>Zr<sub>0.5–x</sub>Nb<sub>2x</sub>)<sub>1</sub>(Mn<sub>0.5</sub>Cr<sub>0.5</sub>)<sub>2</sub> System, *ACS Appl. Energy Mater.*, 2025, **8**(12), 8351–8364, DOI: [10.1021/acsaem.5c00876](https://doi.org/10.1021/acsaem.5c00876).
- 44 N. Klopčič, I. Grimmer, F. Winkler, M. Sartory and A. Trattner, A Review on Metal Hydride Materials for Hydrogen Storage, *J. Energy Storage*, 2023, **72**, 108456, DOI: [10.1016/j.est.2023.108456](https://doi.org/10.1016/j.est.2023.108456).
- 45 J. Bellosta Von Colbe, J.-R. Ares, J. Barale, M. Baricco, C. Buckley, G. Capurso, N. Gallandat, D. M. Grant, M. N. Guzik, I. Jacob, E. H. Jensen, T. Jensen, J. Jepsen, T. Klassen, M. V. Lototsky, K. Manickam, A. Montone, J. Puzkiel, S. Sartori, D. A. Sheppard, A. Stuart, G. Walker, C. J. Webb, H. Yang, V. Yartys, A. Züttel and M. Dornheim, Application of Hydrides in Hydrogen Storage and Compression: Achievements, Outlook and Perspectives, *Int. J. Hydrogen Energy*, 2019, **44**(15), 7780–7808, DOI: [10.1016/j.ijhydene.2019.01.104](https://doi.org/10.1016/j.ijhydene.2019.01.104).
- 46 B. P. Tarasov, P. V. Fursikov, A. A. Volodin, M. S. Bocharnikov, Y. Y. Shimkus, A. M. Kashin, V. A. Yartys, S. Chidziva, S. Pasupathi and M. V. Lototsky, Metal Hydride Hydrogen Storage and Compression Systems for Energy Storage Technologies, *Int. J. Hydrogen Energy*, 2021, **46**(25), 13647–13657, DOI: [10.1016/j.ijhydene.2020.07.085](https://doi.org/10.1016/j.ijhydene.2020.07.085).
- 47 Y. Yin, B. Li, Z. Yuan, Y. Qi and Y. Zhang, Microstructure and Hydrogen Storage Properties of Mg-Based Mg<sub>85</sub>Zn<sub>5</sub>Ni<sub>10</sub> Alloy Powders, *J. Iron Steel Res. Int.*, 2018, **25**(11), 1172–1178, DOI: [10.1007/s42243-018-0177-1](https://doi.org/10.1007/s42243-018-0177-1).
- 48 S. Kurko, I. Milanović, J. Grbović Novaković, N. Ivanović and N. Novaković, Investigation of Surface and Near-Surface Effects on Hydrogen Desorption Kinetics of MgH<sub>2</sub>, *Int. J. Hydrogen Energy*, 2014, **39**(2), 862–867, DOI: [10.1016/j.ijhydene.2013.10.107](https://doi.org/10.1016/j.ijhydene.2013.10.107).
- 49 T. Sato, H. Saitoh, R. Utsumi, J. Ito, Y. Nakahira, K. Obana, S. Takagi and S. Orimo, Hydrogen Absorption Reactions of Hydrogen Storage Alloy LaNi<sub>5</sub> under High Pressure, *Molecules*, 2023, **28**(3), 1256, DOI: [10.3390/molecules28031256](https://doi.org/10.3390/molecules28031256).
- 50 N. A. A. Rusman and M. Dahari, A Review on the Current Progress of Metal Hydrides Material for Solid-State Hydrogen Storage Applications, *Int. J. Hydrogen Energy*, 2016, **41**(28), 12108–12126, DOI: [10.1016/j.ijhydene.2016.05.244](https://doi.org/10.1016/j.ijhydene.2016.05.244).
- 51 *Thermodynamic analysis of a metal hydride hydrogen compressor with aluminium substituted LaNi<sub>5</sub> hydrides* – *ScienceDirect*, <https://www.sciencedirect.com/science/article/abs/pii/S0360319922042331?via%3Dihub> (accessed 2024-08-15).
- 52 A. N. Kazakov, V. I. Borzenko, D. O. Dunikov, I. A. Romanov and D. V. Blinov, Efficient LaNi<sub>5</sub>-Based Hydride-Forming Materials for Energy Storage Systems, *Nanobiotechnol. Rep.*, 2021, **16**(2), 188–194, DOI: [10.1134/S2635167621020087](https://doi.org/10.1134/S2635167621020087).
- 53 R. L. Cohen, K. W. West and J. H. Wernick, Degradation of LaNi<sub>5</sub> by Temperature-Induced Cycling, *J. Common Met.*, 1980, **73**(2), 273–279, DOI: [10.1016/0022-5088\(80\)90315-X](https://doi.org/10.1016/0022-5088(80)90315-X).
- 54 *Overview of hydrogen compression materials based on a three-stage metal hydride hydrogen compressor* – *ScienceDirect*, <https://www.sciencedirect.com/science/article/abs/pii/S0925838821038755?via%3Dihub> (accessed 2024-08-15).
- 55 K. Edalati, E. Akiba and Z. Horita, High-Pressure Torsion for New Hydrogen Storage Materials, *Sci. Technol. Adv. Mater.*, 2018, **19**(1), 185–193, DOI: [10.1080/14686996.2018.1435131](https://doi.org/10.1080/14686996.2018.1435131).
- 56 G. K. Sujan, Z. Pan, H. Li, D. Liang and N. Alam, An Overview on TiFe Intermetallic for Solid-State Hydrogen Storage: Microstructure, Hydrogenation and Fabrication Processes, *Crit. Rev. Solid State Mater. Sci.*, 2020, **45**(5), 410–427, DOI: [10.1080/10408436.2019.1652143](https://doi.org/10.1080/10408436.2019.1652143).
- 57 R. R. Shahi, A. K. Gupta and P. Kumari, Perspectives of High Entropy Alloys as Hydrogen Storage Materials, *Int. J. Hydrogen Energy*, 2023, **48**(56), 21412–21428, DOI: [10.1016/j.ijhydene.2022.02.113](https://doi.org/10.1016/j.ijhydene.2022.02.113).
- 58 H.-J. Lin, Y.-S. Lu, L.-T. Zhang, H.-Z. Liu, K. Edalati and Á. Révész, Recent Advances in Metastable Alloys for Hydrogen Storage: A Review, *Rare Met.*, 2022, **41**(6), 1797–1817, DOI: [10.1007/s12598-021-01917-8](https://doi.org/10.1007/s12598-021-01917-8).
- 59 D. B. Miracle and O. N. Senkov, A Critical Review of High Entropy Alloys and Related Concepts, *Acta Mater.*, 2017, **122**, 448–511, DOI: [10.1016/j.actamat.2016.08.081](https://doi.org/10.1016/j.actamat.2016.08.081).
- 60 Y. Zhang, *High-Entropy Materials: A Brief Introduction*, Springer, Singapore, 2019, DOI: [10.1007/978-981-13-8526-1](https://doi.org/10.1007/978-981-13-8526-1).
- 61 B. Cantor, I. T. H. Chang, P. Knight and A. J. B. Vincent, Microstructural Development in Equiatomic Multicomponent Alloys, *Mater. Sci. Eng., A*, 2004, **375–377**, 213–218, DOI: [10.1016/j.msea.2003.10.257](https://doi.org/10.1016/j.msea.2003.10.257).
- 62 J.-W. Yeh, S.-K. Chen, S.-J. Lin, J.-Y. Gan, T.-S. Chin, T.-T. Shun, C.-H. Tsau and S.-Y. Chang, Nanostructured High-Entropy Alloys with Multiple Principal Elements: Novel Alloy Design Concepts and Outcomes, *Adv. Eng. Mater.*, 2004, **6**(5), 299–303, DOI: [10.1002/adem.200300567](https://doi.org/10.1002/adem.200300567).
- 63 *High-Entropy Alloys*, ed. M. C. Gao, J.-W. Yeh, P. K. Liaw and Y. Zhang, Springer International Publishing, Cham, 2016, DOI: [10.1007/978-3-319-27013-5](https://doi.org/10.1007/978-3-319-27013-5).
- 64 V. E. Gromov, S. V. Kononov, Y. F. Ivanov and K. A. Osintsev, *Structure and Properties of High-Entropy Alloys, Advanced Structured Materials*, Springer International



- Publishing, Cham, 2021, vol. 107, DOI: [10.1007/978-3-030-78364-8](https://doi.org/10.1007/978-3-030-78364-8).
- 65 Y.-F. Kao, S.-K. Chen, J.-H. Sheu, J.-T. Lin, W.-E. Lin, J.-W. Yeh, S.-J. Lin, T.-H. Liou and C.-W. Wang, Hydrogen Storage Properties of Multi-Principal-Component CoFeMn-Ti<sub>x</sub>V<sub>y</sub>Zr<sub>z</sub> Alloys, *Int. J. Hydrogen Energy*, 2010, 35(17), 9046–9059, DOI: [10.1016/j.ijhydene.2010.06.012](https://doi.org/10.1016/j.ijhydene.2010.06.012).
- 66 W. Chen, A. Hilhorst, G. Bokas, S. Gorsse, P. J. Jacques and G. Hautier, A Map of Single-Phase High-Entropy Alloys, *Nat. Commun.*, 2023, 14(1), 2856, DOI: [10.1038/s41467-023-38423-7](https://doi.org/10.1038/s41467-023-38423-7).
- 67 H. Shen, J. Zhang, J. Hu, J. Zhang, Y. Mao, H. Xiao, X. Zhou and X. Zu, A Novel TiZrHfMoNb High-Entropy Alloy for Solar Thermal Energy Storage, *Nanomaterials*, 2019, 9(2), 248, DOI: [10.3390/nano9020248](https://doi.org/10.3390/nano9020248).
- 68 C. Zlotea, M. A. Sow, G. Ek, J.-P. Couzinié, L. Perrière, I. Guillot, J. Bourgon, K. T. Møller, T. R. Jensen, E. Akiba and M. Sahlberg, Hydrogen Sorption in TiZrNbHfTa High Entropy Alloy, *J. Alloys Compd.*, 2019, 775, 667–674, DOI: [10.1016/j.jallcom.2018.10.108](https://doi.org/10.1016/j.jallcom.2018.10.108).
- 69 L. Zhou, W. Li, H. Hu, H. Zeng and Q. Chen, Ce-Doped TiZrCrMn Alloys for Enhanced Hydrogen Storage, *Energy Fuels*, 2022, 36(7), 3997–4005, DOI: [10.1021/acs.energyfuels.2c00011](https://doi.org/10.1021/acs.energyfuels.2c00011).
- 70 N. Yurchenko, N. Stepanov and G. Salishchev, Laves-Phase Formation Criterion for High-Entropy Alloys, *Mater. Sci. Technol.*, 2017, 33(1), 17–22, DOI: [10.1080/02670836.2016.1153277](https://doi.org/10.1080/02670836.2016.1153277).
- 71 A. Kumar, T. P. Yadav and N. K. Mukhopadhyay, Notable Hydrogen Storage in Ti–Zr–V–Cr–Ni High Entropy Alloy, *Int. J. Hydrogen Energy*, 2022, 47(54), 22893–22900, DOI: [10.1016/j.ijhydene.2022.05.107](https://doi.org/10.1016/j.ijhydene.2022.05.107).
- 72 J. B. Ponsoni, V. Aranda, T. D. S. Nascimento, R. B. Strozi, W. J. Botta and G. Zepon, Design of Multicomponent Alloys with C14 Laves Phase Structure for Hydrogen Storage Assisted by Computational Thermodynamic, *Acta Mater.*, 2022, 240, 118317, DOI: [10.1016/j.actamat.2022.118317](https://doi.org/10.1016/j.actamat.2022.118317).
- 73 J. B. Ponsoni, V. Aranda, W. J. Botta and G. Zepon, Reversible Hydrogen Storage at Moderate Pressure–Temperature Conditions of C14 Laves Phase Alloys of the (Ti<sub>0.5–x</sub>Zr<sub>0.5–x</sub>Nb<sub>2x</sub>)<sub>1</sub>(Mn<sub>0.5</sub>Cr<sub>0.5</sub>)<sub>2</sub> System, *ACS Appl. Energy Mater.*, 2025, 8(12), 8351–8364, DOI: [10.1021/acsaem.5c00876](https://doi.org/10.1021/acsaem.5c00876).
- 74 J. Ren, V. Y. Kumkale, H. Hou, V. S. Kadam, C. V. Jagtap, P. E. Lokhande, H. M. Pathan, A. Pereira, H. Lei and T. X. Liu, A Review of High-Entropy Materials with Their Unique Applications, *Adv. Compos. Hybrid Mater.*, 2025, 8(2), 195, DOI: [10.1007/s42114-025-01275-4](https://doi.org/10.1007/s42114-025-01275-4).
- 75 H. Kamaruddin, Z. Jianghong, L. Yu, W. Yuefan and H. Yizhong, A Review of Noble Metal-Free High Entropy Alloys for Water Splitting Applications, *J. Mater. Chem. A*, 2024, 12(17), 9933–9961, DOI: [10.1039/D4TA00690A](https://doi.org/10.1039/D4TA00690A).
- 76 T. R. Somo, M. V. Lototsky, V. A. Yartys, M. W. Davids and S. N. Nyamsi, Hydrogen Storage Behaviours of High Entropy Alloys: A Review, *J. Energy Storage*, 2023, 73, 108969, DOI: [10.1016/j.est.2023.108969](https://doi.org/10.1016/j.est.2023.108969).
- 77 G. Andrade, P. Edalati, S. Dangwal, K. Edalati and R. Floriano, Microstructural Characterization and Hydrogen Storage Properties at Room Temperature of Ti<sub>21</sub>Zr<sub>21</sub>-Fe<sub>41</sub>Ni<sub>17</sub> Medium Entropy Alloy, *ACS Appl. Energy Mater.*, 2025, 8(4), 2033–2042, DOI: [10.1021/acsaem.4c02468](https://doi.org/10.1021/acsaem.4c02468).
- 78 G. Andrade, G. Zepon, K. Edalati, A. Mohammadi, Z. Ma, H.-W. Li and R. Floriano, Crystal Structure and Hydrogen Storage Properties of AB-Type TiZrNbCrFeNi High-Entropy Alloy, *Int. J. Hydrogen Energy*, 2023, 48(36), 13555–13565, DOI: [10.1016/j.ijhydene.2022.12.134](https://doi.org/10.1016/j.ijhydene.2022.12.134).
- 79 Y. Yan, Z. Li, Y. Wu and S. Zhou, Hydrogen Absorption-Desorption Characteristic of (Ti<sub>0.85</sub>Zr<sub>0.15</sub>)<sub>1.1</sub>Cr<sub>1–x</sub>Mo<sub>x</sub>Mn Based Alloys with C14 Laves Phase, *Prog. Nat. Sci. Mater. Int.*, 2022, 32(2), 143–149, DOI: [10.1016/j.pnsc.2022.03.001](https://doi.org/10.1016/j.pnsc.2022.03.001).
- 80 X. Ma, X. Ding, R. Chen, J. Zhang, Q. Song and H. Cui, Microstructural Features and Improved Reversible Hydrogen Storage Properties of ZrTiVFe High-Entropy Alloy via Cu Alloying, *Int. J. Hydrogen Energy*, 2023, 48(7), 2718–2730, DOI: [10.1016/j.ijhydene.2022.10.130](https://doi.org/10.1016/j.ijhydene.2022.10.130).
- 81 B. S. Murty, J. W. Yeh, S. Ranganathan and P. P. Bhattacharjee, *1 – A Brief History of Alloys and the Birth of High-Entropy Alloys*, Butterworth-Heinemann, Boston, 2019, pp. 1–12, DOI: [10.1016/B978-0-12-816067-1.00001-1](https://doi.org/10.1016/B978-0-12-816067-1.00001-1).
- 82 I. Müller, *A History of Thermodynamics: The Doctrine of Energy and Entropy*, Springer, Berlin, Heidelberg, 2007, DOI: [10.1007/978-3-540-46227-9](https://doi.org/10.1007/978-3-540-46227-9).
- 83 S. Gorsse, J.-P. Couzinié and D. B. Miracle, From High-Entropy Alloys to Complex Concentrated Alloys, *Comptes Rendus Phys.*, 2018, 19(8), 721–736, DOI: [10.1016/j.crhy.2018.09.004](https://doi.org/10.1016/j.crhy.2018.09.004).
- 84 C. Oses, C. Toher and S. Curtarolo, High-Entropy Ceramics, *Nat. Rev. Mater.*, 2020, 5(4), 295–309, DOI: [10.1038/s41578-019-0170-8](https://doi.org/10.1038/s41578-019-0170-8).
- 85 S. Guo, Q. Hu, C. Ng and C. T. Liu, More than Entropy in High-Entropy Alloys: Forming Solid Solutions or Amorphous Phase, *Intermetallics*, 2013, 41, 96–103, DOI: [10.1016/j.intermet.2013.05.002](https://doi.org/10.1016/j.intermet.2013.05.002).
- 86 J. Liu, X. Wang, A. Singh, H. Xu, F. Kong and F. Yang, The Evolution of Intermetallic Compounds in High-Entropy Alloys: From the Secondary Phase to the Main Phase, *Metals*, 2021, 11(12), 2054, DOI: [10.3390/met11122054](https://doi.org/10.3390/met11122054).
- 87 O. Maulik, D. Kumar, S. Kumar, S. K. Dewangan and V. Kumar, Structure and Properties of Lightweight High Entropy Alloys: A Brief Review, *Mater. Res. Express*, 2018, 5(5), 052001, DOI: [10.1088/2053-1591/aabbca](https://doi.org/10.1088/2053-1591/aabbca).
- 88 W. Zhu, X. Gao, Y. Yao, S. Hu, Z. Li, Y. Teng, H. Wang, H. Gong, Z. Chen and Y. Yang, Nanostructured High Entropy Alloys as Structural and Functional Materials, *ACS Nano*, 2024, 18(20), 12672–12706, DOI: [10.1021/acsnano.4c03435](https://doi.org/10.1021/acsnano.4c03435).
- 89 F. Marques, M. Balcerzak, F. Winkelmann, G. Zepon and M. Felderhoff, Review and Outlook on High-Entropy Alloys for Hydrogen Storage, *Energy Environ. Sci.*, 2021, 14(10), 5191–5227, DOI: [10.1039/D1EE01543E](https://doi.org/10.1039/D1EE01543E).
- 90 A. Amiri and R. Shahbazian-Yassar, Recent Progress of High-Entropy Materials for Energy Storage and Conversion,



- J. Mater. Chem. A*, 2021, **9**(2), 782–823, DOI: [10.1039/D0TA09578H](https://doi.org/10.1039/D0TA09578H).
- 91 X. Yan and Y. Zhang, Functional Properties and Promising Applications of High Entropy Alloys, *Scr. Mater.*, 2020, **187**, 188–193, DOI: [10.1016/j.scriptamat.2020.06.017](https://doi.org/10.1016/j.scriptamat.2020.06.017).
- 92 J. Kim, A. Wakai and A. Moridi, Materials and Manufacturing Renaissance: Additive Manufacturing of High-Entropy Alloys, *J. Mater. Res.*, 2020, **35**(15), 1963–1983, DOI: [10.1557/jmr.2020.140](https://doi.org/10.1557/jmr.2020.140).
- 93 E. P. George, D. Raabe and R. O. Ritchie, High-Entropy Alloys, *Nat. Rev. Mater.*, 2019, **4**(8), 515–534, DOI: [10.1038/s41578-019-0121-4](https://doi.org/10.1038/s41578-019-0121-4).
- 94 Y. F. Ye, Q. Wang, J. Lu, C. T. Liu and Y. Yang, High-Entropy Alloy: Challenges and Prospects, *Mater. Today*, 2016, **19**(6), 349–362, DOI: [10.1016/j.mattod.2015.11.026](https://doi.org/10.1016/j.mattod.2015.11.026).
- 95 M.-H. Tsai and J.-W. Yeh, High-Entropy Alloys: A Critical Review, *Mater. Res. Lett.*, 2014, **2**(3), 107–123, DOI: [10.1080/21663831.2014.912690](https://doi.org/10.1080/21663831.2014.912690).
- 96 F. Marques, H. C. Pinto, S. J. A. Figueroa, F. Winkelmann, M. Felderhoff, W. J. Botta and G. Zepon, Mg-Containing Multi-Principal Element Alloys for Hydrogen Storage: A Study of the MgTiNbCr<sub>0.5</sub>Mn<sub>0.5</sub>Ni<sub>0.5</sub> and Mg<sub>0.68</sub>TiNbNi<sub>0.55</sub> Compositions, *Int. J. Hydrogen Energy*, 2020, **45**(38), 19539–19552, DOI: [10.1016/j.ijhydene.2020.05.069](https://doi.org/10.1016/j.ijhydene.2020.05.069).
- 97 J. Cermak, L. Kral and P. Roupčova, A New Light-Element Multi-Principal-Elements Alloy AlMg<sub>2</sub>TiZn and Its Potential for Hydrogen Storage, *Renewable Energy*, 2022, **198**, 1186–1192, DOI: [10.1016/j.renene.2022.08.108](https://doi.org/10.1016/j.renene.2022.08.108).
- 98 B. H. Silva, C. Zlotea, Y. Champion, W. J. Botta and G. Zepon, Design of TiVNb-(Cr, Ni or Co) Multicomponent Alloys with the Same Valence Electron Concentration for Hydrogen Storage, *J. Alloys Compd.*, 2021, **865**, 158767, DOI: [10.1016/j.jallcom.2021.158767](https://doi.org/10.1016/j.jallcom.2021.158767).
- 99 V. Aranda, D. R. Leiva, J. Huot, W. J. Botta and G. Zepon, Hydrogen Storage Properties of the TiVFeZr Multicomponent Alloy with C14-Type Laves Phase Structure, *Intermetallics*, 2023, **162**, 108020, DOI: [10.1016/j.intermet.2023.108020](https://doi.org/10.1016/j.intermet.2023.108020).
- 100 S. Gorsse, D. B. Miracle and O. N. Senkov, Mapping the World of Complex Concentrated Alloys, *Acta Mater.*, 2017, **135**, 177–187, DOI: [10.1016/j.actamat.2017.06.027](https://doi.org/10.1016/j.actamat.2017.06.027).
- 101 Y. Zhang and Q. Xing, *High Entropy Alloys: Manufacturing Routes*, 2022, 327–338, DOI: [10.1016/B978-0-12-803581-8.12123-X](https://doi.org/10.1016/B978-0-12-803581-8.12123-X).
- 102 D. Kumar, Recent Advances in Tribology of High Entropy Alloys: A Critical Review, *Prog. Mater. Sci.*, 2023, **136**, 101106, DOI: [10.1016/j.pmatsci.2023.101106](https://doi.org/10.1016/j.pmatsci.2023.101106).
- 103 B. S. Murty, J. W. Yeh, S. Ranganathan and P. P. Bhattacharjee, 2 – High-Entropy Alloys, *Basic Concepts*, 2019, 13–30, DOI: [10.1016/B978-0-12-816067-1.00002-3](https://doi.org/10.1016/B978-0-12-816067-1.00002-3).
- 104 Y. Yan, Y. Chen, H. Liang, C. Wu, M. Tao and T. Mingjing, Effect of Al on Hydrogen Storage Properties of V<sub>30</sub>Ti<sub>35</sub>-Cr<sub>25</sub>Fe<sub>10</sub> Alloy, *J. Alloys Compd.*, 2006, **426**(1–2), 253–255, DOI: [10.1016/j.jallcom.2005.12.122](https://doi.org/10.1016/j.jallcom.2005.12.122).
- 105 B. S. Murty, J. W. Yeh, S. Ranganathan and P. P. Bhattacharjee, 4 – Alloy Design and Phase Selection Rules in High-Entropy Alloys, 2019, 51–79, DOI: [10.1016/B978-0-12-816067-1.00004-7](https://doi.org/10.1016/B978-0-12-816067-1.00004-7).
- 106 K. Li and W. Chen, Recent Progress in High-Entropy Alloys for Catalysts: Synthesis, Applications, and Prospects, *Mater. Today Energy*, 2021, **20**, 100638, DOI: [10.1016/j.mtener.2021.100638](https://doi.org/10.1016/j.mtener.2021.100638).
- 107 R. B. Strozi, D. R. Leiva, J. Huot, W. J. Botta and G. Zepon, An Approach to Design Single BCC Mg-Containing High Entropy Alloys for Hydrogen Storage Applications, *Int. J. Hydrogen Energy*, 2021, **46**(50), 25555–25561, DOI: [10.1016/j.ijhydene.2021.05.087](https://doi.org/10.1016/j.ijhydene.2021.05.087).
- 108 J. Montero, G. Ek, L. Laversenne, V. Nassif, G. Zepon, M. Sahlberg and C. Zlotea, Hydrogen Storage Properties of the Refractory Ti–V–Zr–Nb–Ta Multi-Principal Element Alloy, *J. Alloys Compd.*, 2020, **835**, 155376, DOI: [10.1016/j.jallcom.2020.155376](https://doi.org/10.1016/j.jallcom.2020.155376).
- 109 K. Ito, L. T. Zhang, V. K. Vasudevan and M. Yamaguchi, Multiphase and Microstructure Effects on the Hydrogen Absorption/Desorption Behavior of a Ti–22Al–27Nb Alloy, *Acta Mater.*, 2001, **49**(6), 963–972, DOI: [10.1016/S1359-6454\(00\)00402-X](https://doi.org/10.1016/S1359-6454(00)00402-X).
- 110 F. Otto, A. Dlouhý, C. Somsen, H. Bei, G. Eggeler and E. P. George, The Influences of Temperature and Microstructure on the Tensile Properties of a CoCrFeMnNi High-Entropy Alloy, *Acta Mater.*, 2013, **61**(15), 5743–5755, DOI: [10.1016/j.actamat.2013.06.018](https://doi.org/10.1016/j.actamat.2013.06.018).
- 111 W. Li, G. Wang, S. Wu and P. K. Liaw, Creep, Fatigue, and Fracture Behavior of High-Entropy Alloys, *J. Mater. Res.*, 2018, **33**(19), 3011–3034, DOI: [10.1557/jmr.2018.191](https://doi.org/10.1557/jmr.2018.191).
- 112 Y. Lu, H. Jiang, S. Guo, T. Wang, Z. Cao and T. Li, A New Strategy to Design Eutectic High-Entropy Alloys Using Mixing Enthalpy, *Intermetallics*, 2017, **91**, 124–128, DOI: [10.1016/j.intermet.2017.09.001](https://doi.org/10.1016/j.intermet.2017.09.001).
- 113 Z. Li, K. G. Pradeep, Y. Deng, D. Raabe and C. C. Tasan, Metastable High-Entropy Dual-Phase Alloys Overcome the Strength–Ductility Trade-Off, *Nature*, 2016, **534**(7606), 227–230, DOI: [10.1038/nature17981](https://doi.org/10.1038/nature17981).
- 114 B. S. Murty, J. W. Yeh, S. Ranganathan and P. P. Bhattacharjee, 7 – Solid Solution Phases and Their Microstructures in HEAs, in *High-Entropy Alloys (Second Edition)*, ed. B. S. Murty, J. W. Yeh, S. Ranganathan and P. P. Bhattacharjee, Elsevier, 2019, pp. 119–144, DOI: [10.1016/B978-0-12-816067-1.00007-2](https://doi.org/10.1016/B978-0-12-816067-1.00007-2).
- 115 J.-W. Yeh, Recent Progress in High-Entropy Alloys, *Annales de Chimie Science des Matériaux*, 2006, **31**, 633–648, DOI: [10.3166/acsm.31.633-648](https://doi.org/10.3166/acsm.31.633-648).
- 116 S. S. Nene, S. Sinha, D. K. Yadav and A. Dutta, Metallurgical Aspects of High Entropy Alloys, *J. Alloys Compd.*, 2024, **1005**, 175849, DOI: [10.1016/j.jallcom.2024.175849](https://doi.org/10.1016/j.jallcom.2024.175849).
- 117 T. P. Yadav, A. Kumar, S. K. Verma and N. K. Mukhopadhyay, High-Entropy Alloys for Solid Hydrogen Storage: Potentials and Prospects, *Trans. Indian Natl. Acad. Eng.*, 2022, **7**(1), 147–156, DOI: [10.1007/s41403-021-00316-w](https://doi.org/10.1007/s41403-021-00316-w).
- 118 G. H. Vineyard, Theory of Order-Disorder Kinetics, *Phys. Rev.*, 1956, **102**(4), 981–992, DOI: [10.1103/PhysRev.102.981](https://doi.org/10.1103/PhysRev.102.981).



- 119 K.-Y. Tsai, M.-H. Tsai and J.-W. Yeh, Sluggish Diffusion in Co–Cr–Fe–Mn–Ni High-Entropy Alloys, *Acta Mater.*, 2013, **61**(13), 4887–4897, DOI: [10.1016/j.actamat.2013.04.058](https://doi.org/10.1016/j.actamat.2013.04.058).
- 120 *Nanoscale Science and Technology, Reprinted*, ed. R. W. Kelsall, I. W. Hamley and M. Geoghegan, Wiley, Chichester, 2006.
- 121 C. Yang, Q.-S. Xia, C.-H. Yin and D.-P. Hua, Atomistic Study of Inverse Size Effect Induced by Interfacial Plasticity in Pearlitic Multi-Principal Element Alloy, *Rare Met.*, 2024, **43**(7), 3341–3355, DOI: [10.1007/s12598-024-02664-2](https://doi.org/10.1007/s12598-024-02664-2).
- 122 *High Entropy Alloys: Innovations, Advances, and Applications*, ed. T. S. Srivatsan and M. Gupta, CRC Press, Boca Raton, 2020, DOI: [10.1201/9780367374426](https://doi.org/10.1201/9780367374426).
- 123 W. Cao, M. Zheng, W. Ding, X. Mao, C. Wang, W. Wang and J. Xin, Large Relrod Extension Induced by Lattice Distortion in High Entropy Alloy, *Mater. Res. Express*, 2019, **6**(6), 066558, DOI: [10.1088/2053-1591/ab0f4b](https://doi.org/10.1088/2053-1591/ab0f4b).
- 124 B. Wu, Y. Zhao, H. Ali, R. Chen, H. Chen, J. Wen, Y. Liu, L. Liu, K. Yang, L. Zhang, Z. He, Q. Yao, H. Zhang, B. Sa, C. Wen, Y. Qiu, H. Xiong, M. Lin, Y. Liu, C. Wang and H. Su, A Reasonable Approach to Describe the Atom Distributions and Configurational Entropy in High Entropy Alloys Based on Site Preference, *Intermetallics*, 2022, **144**, 107489, DOI: [10.1016/j.intermet.2022.107489](https://doi.org/10.1016/j.intermet.2022.107489).
- 125 L. R. Owen and N. G. Jones, Lattice Distortions in High-Entropy Alloys, *J. Mater. Res.*, 2018, **33**(19), 2954–2969, DOI: [10.1557/jmr.2018.322](https://doi.org/10.1557/jmr.2018.322).
- 126 C. Tandoc, Y.-J. Hu, L. Qi and P. K. Liaw, Mining of Lattice Distortion, Strength, and Intrinsic Ductility of Refractory High Entropy Alloys, *Npj Comput. Mater.*, 2023, **9**(1), 53, DOI: [10.1038/s41524-023-00993-x](https://doi.org/10.1038/s41524-023-00993-x).
- 127 J. Kumar, A. Linda and K. Biswas, Lattice Distortion in FCC HEAs and Its Effect on Mechanical Properties: Critical Analysis and Way Forward, *J. Appl. Phys.*, 2023, **133**(15), 155102, DOI: [10.1063/5.0144456](https://doi.org/10.1063/5.0144456).
- 128 S. C. Cao, A. X. Guo, Z. Lin, W. Xiong and S. Zhan, Strengthening and Toughening of 3D Printing High Entropy Alloy, *J. Mater. Sci. Eng.*, 2022, **11**, 3, DOI: [10.37421/2169-0022.2022.11.13](https://doi.org/10.37421/2169-0022.2022.11.13).
- 129 Y. Lu, X. Wu, Z. Fu, Q. Yang, Y. Zhang, Q. Liu, T. Li, Y. Tian, H. Tan, Z. Li, T. Wang and T. Li, Ductile and Ultrahigh-Strength Eutectic High-Entropy Alloys by Large-Volume 3D Printing, *J. Mater. Sci. Technol.*, 2022, **126**, 15–21, DOI: [10.1016/j.jmst.2022.04.004](https://doi.org/10.1016/j.jmst.2022.04.004).
- 130 S. Dangwal and K. Edalati, Significance of Interphase Boundaries on Activation of High-Entropy Alloys for Room-Temperature Hydrogen Storage, *Int. J. Hydrogen Energy*, 2024, **50**, 626–636, DOI: [10.1016/j.ijhydene.2023.07.327](https://doi.org/10.1016/j.ijhydene.2023.07.327).
- 131 M. Sahlberg, D. Karlsson, C. Zlotea and U. Jansson, Superior Hydrogen Storage in High Entropy Alloys, *Sci. Rep.*, 2016, **6**(1), 36770, DOI: [10.1038/srep36770](https://doi.org/10.1038/srep36770).
- 132 E. J. Pickering and N. G. Jones, High-Entropy Alloys: A Critical Assessment of Their Founding Principles and Future Prospects, *Int. Mater. Rev.*, 2016, **61**(3), 183–202, DOI: [10.1080/09506608.2016.1180020](https://doi.org/10.1080/09506608.2016.1180020).
- 133 A. Hobhaydar, X. Wang, Y. Wang, H. Li, N. Van Tran and H. Zhu, Effect of Tungsten Doping on the Irradiation Resistance of FeCrV-Based Refractory Medium Entropy Alloy for Potential Nuclear Applications, *J. Alloys Compd.*, 2023, **966**, 171635, DOI: [10.1016/j.jallcom.2023.171635](https://doi.org/10.1016/j.jallcom.2023.171635).
- 134 S. Ranganathan, Alloyed Pleasures: Multimetalllic Cocktails, *Curr. Sci. Bangalore*, 2003, **85**(10), 1404–1406.
- 135 C.-J. Tong, M.-R. Chen, J.-W. Yeh, S.-J. Lin, S.-K. Chen, T.-T. Shun and S.-Y. Chang, Mechanical Performance of the Al<sub>x</sub>CoCrCuFeNi High-Entropy Alloy System with Multi-principal Elements, *Metall. Mater. Trans. A*, 2005, **36**(5), 1263–1271, DOI: [10.1007/s11661-005-0218-9](https://doi.org/10.1007/s11661-005-0218-9).
- 136 X. Ma, X. Ding, R. Chen, X. Gao, Y. Su and H. Cui, Enhanced Hydrogen Storage Properties of ZrTiVAl<sub>1-x</sub>Fe<sub>x</sub> High-Entropy Alloys by Modifying the Fe Content, *RSC Adv.*, 2022, **12**(18), 11272–11281, DOI: [10.1039/D2RA01064J](https://doi.org/10.1039/D2RA01064J).
- 137 F. Stein and A. Leineweber, Laves Phases: A Review of Their Functional and Structural Applications and an Improved Fundamental Understanding of Stability and Properties, *J. Mater. Sci.*, 2021, **56**(9), 5321–5427, DOI: [10.1007/s10853-020-05509-2](https://doi.org/10.1007/s10853-020-05509-2).
- 138 V. A. Yartys and M. V. Lototsky, Laves Type Intermetallic Compounds as Hydrogen Storage Materials: A Review, *J. Alloys Compd.*, 2022, **916**, 165219, DOI: [10.1016/j.jallcom.2022.165219](https://doi.org/10.1016/j.jallcom.2022.165219).
- 139 J. Nei, K. Young, S. O. Salley and K. Y. S. Ng, Determination of C14/C15 Phase Abundance in Laves Phase Alloys, *Mater. Chem. Phys.*, 2012, **136**(2), 520–527, DOI: [10.1016/j.matchemphys.2012.07.020](https://doi.org/10.1016/j.matchemphys.2012.07.020).
- 140 J. B. Ponsoni, V. Aranda, T. Da Silva Nascimento, R. Belli Strozi, W. J. Botta and G. Zepon, Design of Multicomponent Alloys with Single C14 Laves Phase for Hydrogen Storage Assisted by Computational Thermodynamic, 2021, DOI: [10.26434/chemrxiv-2021-s9nsp](https://doi.org/10.26434/chemrxiv-2021-s9nsp).
- 141 D. Grüner, F. Stein, M. Palm, J. Konrad, A. Ormeci, W. Schnelle, Y. Grin and G. Kreiner, Preparation, Phase Stability and Structure of the C36 Laves Phase Nb<sub>1-x</sub>Co<sub>2+x</sub>, *Z. Für Krist. – Cryst. Mater.*, 2006, **221**(5–7), 319–333, DOI: [10.1524/zkri.2006.221.5-7.319](https://doi.org/10.1524/zkri.2006.221.5-7.319).
- 142 R. Ryltsev, V. Gaviko, S. Estemirova, E. Sterkhov, L. Cherepanova, D. Yagodin, N. Chtchelkatchev, N. Dubinin and S. Uporov, Laves Phase Formation in High Entropy Alloys, *Metals*, 2021, **11**(12), 1962, DOI: [10.3390/met11121962](https://doi.org/10.3390/met11121962).
- 143 R. Nagar, S. Srivastava, S. L. Hudson, S. L. Amaya, A. Tanna, M. Sharma, R. Achayalingam, S. Sonkaria, V. Khare and S. S. Srinivasan, Recent Developments in State-of-the-Art Hydrogen Energy Technologies – Review of Hydrogen Storage Materials, *Sol. Compass*, 2023, **5**, 100033, DOI: [10.1016/j.solcom.2023.100033](https://doi.org/10.1016/j.solcom.2023.100033).
- 144 A. R. Merlino, C. R. Luna, A. Juan and M. E. Pronsato, A DFT Study of Hydrogen Storage in Zr(Cr<sub>0.5</sub>Ni<sub>0.5</sub>)<sub>2</sub> Laves Phase, *Int. J. Hydrogen Energy*, 2016, **41**(4), 2700–2710, DOI: [10.1016/j.ijhydene.2015.10.077](https://doi.org/10.1016/j.ijhydene.2015.10.077).
- 145 M. E. Dematteis, N. Berti, F. Cuevas, M. Latroche and M. Baricco, Substitutional Effects in TiFe for Hydrogen



- Storage: A Comprehensive Review, *Mater. Adv.*, 2021, 2(8), 2524–2560, DOI: [10.1039/D1MA00101A](https://doi.org/10.1039/D1MA00101A).
- 146 R. Li, L. Xie, W. Y. Wang, P. K. Liaw and Y. Zhang, High-Throughput Calculations for High-Entropy Alloys: A Brief Review, *Front. Mater.*, 2020, 7, 290, DOI: [10.3389/fmats.2020.00290](https://doi.org/10.3389/fmats.2020.00290).
- 147 Y. Zhang, Y. J. Zhou, J. P. Lin, G. L. Chen and P. K. Liaw, Solid-Solution Phase Formation Rules for Multi-component Alloys, *Adv. Eng. Mater.*, 2008, 10(6), 534–538, DOI: [10.1002/adem.200700240](https://doi.org/10.1002/adem.200700240).
- 148 R. Griessen and T. Riesterer, Heat of Formation Models, in *Hydrogen in Intermetallic Compounds I: Electronic, Thermodynamic, and Crystallographic Properties, Preparation*, ed. L. Schlapbach, Springer, Berlin, Heidelberg, 1988, pp. 219–284, DOI: [10.1007/3540183337\\_13](https://doi.org/10.1007/3540183337_13).
- 149 A. Takeuchi and A. Inoue, Mixing Enthalpy of Liquid Phase Calculated by Miedema's Scheme and Approximated with Sub-Regular Solution Model for Assessing Forming Ability of Amorphous and Glassy Alloys, *Intermetallics*, 2010, 18(9), 1779–1789, DOI: [10.1016/j.intermet.2010.06.003](https://doi.org/10.1016/j.intermet.2010.06.003).
- 150 S. Guo, Phase Selection Rules for Cast High Entropy Alloys: An Overview, *Mater. Sci. Technol.*, 2015, 31(10), 1223–1230, DOI: [10.1179/1743284715Y.0000000018](https://doi.org/10.1179/1743284715Y.0000000018).
- 151 S. S. Mishra, T. P. Yadav, O. N. Srivastava, N. K. Mukhopadhyay and K. Biswas, Formation and Stability of C14 Type Laves Phase in Multi Component High-Entropy Alloys, *J. Alloys Compd.*, 2020, 832, 153764, DOI: [10.1016/j.jallcom.2020.153764](https://doi.org/10.1016/j.jallcom.2020.153764).
- 152 X. Yang and Y. Zhang, Prediction of High-Entropy Stabilized Solid-Solution in Multi-Component Alloys, *Mater. Chem. Phys.*, 2012, 132(2), 233–238, DOI: [10.1016/j.matchemphys.2011.11.021](https://doi.org/10.1016/j.matchemphys.2011.11.021).
- 153 *Pauling Electronegativity*, Chemistry LibreTexts. [https://chem.libretexts.org/Bookshelves/Physical\\_and\\_Theoretical\\_Chemistry\\_Textbook\\_Maps/Supplemental\\_Modules\\_\(Physical\\_and\\_Theoretical\\_Chemistry\)/Physical\\_Properties\\_of\\_Matter/Atomic\\_and\\_Molecular\\_Properties/Electronegativity/Pauling\\_Electronegativity](https://chem.libretexts.org/Bookshelves/Physical_and_Theoretical_Chemistry_Textbook_Maps/Supplemental_Modules_(Physical_and_Theoretical_Chemistry)/Physical_Properties_of_Matter/Atomic_and_Molecular_Properties/Electronegativity/Pauling_Electronegativity) (accessed 2025-01-03).
- 154 M. M. Nygård, G. Ek, D. Karlsson, M. H. Sørby, M. Sahlberg and B. C. Hauback, Counting Electrons – A New Approach to Tailor the Hydrogen Sorption Properties of High-Entropy Alloys, *Acta Mater.*, 2019, 175, 121–129, DOI: [10.1016/j.actamat.2019.06.002](https://doi.org/10.1016/j.actamat.2019.06.002).
- 155 V. F. Gorban', N. A. Krapivka and S. A. Firstov, High-Entropy Alloys: Interrelations between Electron Concentration, Phase Composition, Lattice Parameter, and Properties, *Phys. Met. Metallogr.*, 2017, 118(10), 970–981, DOI: [10.1134/S0031918X17080051](https://doi.org/10.1134/S0031918X17080051).
- 156 J. B. Ponsoni, M. Balcerzak, W. J. Botta, M. Felderhoff and G. Zepon, A Comprehensive Investigation of the  $(\text{Ti}_{0.5}\text{Zr}_{0.5})_1(\text{Fe}_{0.33}\text{Mn}_{0.33}\text{Cr}_{0.33})_2$  Multicomponent Alloy for Room-Temperature Hydrogen Storage Designed by Computational Thermodynamic Tools, *J. Mater. Chem. A*, 2023, 11(26), 14108–14118, DOI: [10.1039/D3TA02197A](https://doi.org/10.1039/D3TA02197A).
- 157 R. Floriano, G. Zepon, K. Edalati, G. L. B. G. Fontana, A. Mohammadi, Z. Ma, H.-W. Li and R. J. Contieri, Hydrogen Storage in TiZrNbFeNi High Entropy Alloys, Designed by Thermodynamic Calculations, *Int. J. Hydrogen Energy*, 2020, 45(58), 33759–33770, DOI: [10.1016/j.ijhydene.2020.09.047](https://doi.org/10.1016/j.ijhydene.2020.09.047).
- 158 S. Guo and C. T. Liu, Phase Stability in High Entropy Alloys: Formation of Solid-Solution Phase or Amorphous Phase, *Prog. Nat. Sci.*, 2011, 21(6), 433–446, DOI: [10.1016/S1002-0071\(12\)60080-X](https://doi.org/10.1016/S1002-0071(12)60080-X).
- 159 *WebElements Periodic Table » Periodicity » Electronegativity (Allen) » Periodic table gallery*. [https://winter.group.shef.ac.uk/webelements/periodicity/eneg\\_allen/](https://winter.group.shef.ac.uk/webelements/periodicity/eneg_allen/) (accessed 2025-01-03).
- 160 M.-H. Tsai, Three Strategies for the Design of Advanced High-Entropy Alloys, *Entropy*, 2016, 18(7), 252, DOI: [10.3390/e18070252](https://doi.org/10.3390/e18070252).
- 161 Y. Dong, Y. Lu, L. Jiang, T. Wang and T. Li, Effects of Electro-Negativity on the Stability of Topologically Close-Packed Phase in High Entropy Alloys, *Intermetallics*, 2014, 52, 105.
- 162 G. Andrade, B. H. Silva, G. Zepon and R. Floriano, Hydrogen Storage Properties of Zr-Based Multicomponent Alloys with C14-Laves Phase Structure Derived from the Zr–Cr–Mn–Fe–Ni System, *Int. J. Hydrogen Energy*, 2024, 51, 246–254, DOI: [10.1016/j.ijhydene.2023.11.111](https://doi.org/10.1016/j.ijhydene.2023.11.111).
- 163 R. Floriano, G. Zepon, K. Edalati, G. L. B. G. Fontana, A. Mohammadi, Z. Ma, H.-W. Li and R. J. Contieri, Hydrogen Storage Properties of New A3B2-Type TiZrNbCrFe High-Entropy Alloy, *Int. J. Hydrogen Energy*, 2021, 46(46), 23757–23766, DOI: [10.1016/j.ijhydene.2021.04.181](https://doi.org/10.1016/j.ijhydene.2021.04.181).
- 164 Y. Zhu, X.-S. Yang, Z.-L. Xu, G. C.-P. Tsui, Q. Zhou, R. Tang, F. Xiao and K. Chan, Development of AB2-Type TiZrCrMn-FeCoV Intermetallic High-Entropy Alloy for Reversible Room-Temperature Hydrogen Storage, *J. Energy Storage*, 2024, 75, 109553, DOI: [10.1016/j.est.2023.109553](https://doi.org/10.1016/j.est.2023.109553).
- 165 D. Jiang, L. Xie and L. Wang, Current Application Status of Multi-Scale Simulation and Machine Learning in Research on High-Entropy Alloys, *J. Mater. Res. Technol.*, 2023, 26, 1341–1374, DOI: [10.1016/j.jmrt.2023.07.233](https://doi.org/10.1016/j.jmrt.2023.07.233).
- 166 *CALPHAD Methodology*, Thermo-Calc Software, <https://thermo-calc.com/about-us/methodology/the-calphad-methodology/> (accessed 2025-01-06).
- 167 Q. Luo, C. Zhai, D. Sun, W. Chen and Q. Li, Interpolation and Extrapolation with the CALPHAD Method, *J. Mater. Sci. Technol.*, 2019, 35(9), 2115–2120, DOI: [10.1016/j.jmst.2019.05.016](https://doi.org/10.1016/j.jmst.2019.05.016).
- 168 U. R. Kattner, The calphad method and its role in material and process development, *Tecnol. Metal., Mater. Min.*, 2016, 13(1), 3–15, DOI: [10.4322/2176-1523.1059](https://doi.org/10.4322/2176-1523.1059).
- 169 *Thermo-Calc Getting Started Guide*, Thermo-Calc Software, <https://thermo-calc.com/support/getting-started-guides/thermo-calc-guide/> (accessed 2025-03-16).
- 170 X. Chang, M. Zeng, K. Liu and L. Fu, Phase Engineering of High-Entropy Alloys, *Adv. Mater.*, 2020, 32(14), 1907226, DOI: [10.1002/adma.201907226](https://doi.org/10.1002/adma.201907226).
- 171 Z.-K. Liu, Thermodynamics and Its Prediction and CALPHAD Modeling: Review, State of the Art, and Perspectives,



- Calphad*, 2023, **82**, 102580, DOI: [10.1016/j.calphad.2023.102580](https://doi.org/10.1016/j.calphad.2023.102580).
- 172 Accelerating CALPHAD-based Phase Diagram Predictions in Complex Alloys Using Universal Machine Learning Potentials: Opportunities and Challenges, <https://arxiv.org/html/2411.15351v1> (accessed 2025-03-25).
- 173 A. Verma, N. Wilson and K. Joshi, Solid State Hydrogen Storage: Decoding the Path through Machine Learning, *Int. J. Hydrogen Energy*, 2024, **50**, 1518–1528, DOI: [10.1016/j.ijhydene.2023.10.056](https://doi.org/10.1016/j.ijhydene.2023.10.056).
- 174 I. Peivaste, E. Jossou and A. A. Tiamiyu, Data-Driven Analysis and Prediction of Stable Phases for High-Entropy Alloy Design, *Sci. Rep.*, 2023, **13**(1), 22556, DOI: [10.1038/s41598-023-50044-0](https://doi.org/10.1038/s41598-023-50044-0).
- 175 Y. Zeng, M. Man, K. Bai and Y.-W. Zhang, Revealing High-Fidelity Phase Selection Rules for High Entropy Alloys: A Combined CALPHAD and Machine Learning Study, *Mater. Des.*, 2021, **202**, 109532, DOI: [10.1016/j.matdes.2021.109532](https://doi.org/10.1016/j.matdes.2021.109532).
- 176 Z. Ding, Y. Li, H. Jiang, Y. Zhou, H. Wan, J. Qiu, F. Jiang, J. Tan, W. Du, Y. Chen, L. L. Shaw and F. Pan, The Integral Role of High-Entropy Alloys in Advancing Solid-State Hydrogen Storage, *Interdiscip. Mater.*, 2025, **4**(1), 75–108, DOI: [10.1002/idm2.12216](https://doi.org/10.1002/idm2.12216).
- 177 A. Mohammadi, Y. Ikeda, P. Edalati, M. Mito, B. Grabowski, H.-W. Li and K. Edalati, High-Entropy Hydrides for Fast and Reversible Hydrogen Storage at Room Temperature: Binding-Energy Engineering via First-Principles Calculations and Experiments, *Acta Mater.*, 2022, **236**, 118117, DOI: [10.1016/j.actamat.2022.118117](https://doi.org/10.1016/j.actamat.2022.118117).
- 178 J. Hu, J. Zhang, H. Xiao, L. Xie, G. Sun, H. Shen, P. Li, J. Zhang and X. Zu, A First-Principles Study of Hydrogen Storage of High Entropy Alloy TiZrVMoNb, *Int. J. Hydrogen Energy*, 2021, **46**(40), 21050–21058, DOI: [10.1016/j.ijhydene.2021.03.200](https://doi.org/10.1016/j.ijhydene.2021.03.200).
- 179 S. Kurko, I. Milanović, J. Grbović Novaković, N. Ivanović and N. Novaković, Investigation of Surface and Near-Surface Effects on Hydrogen Desorption Kinetics of MgH<sub>2</sub>, *Int. J. Hydrogen Energy*, 2014, **39**(2), 862–867, DOI: [10.1016/j.ijhydene.2013.10.107](https://doi.org/10.1016/j.ijhydene.2013.10.107).
- 180 A. Verma and K. Joshi, MH-PCTpro: A Machine Learning Model for Rapid Prediction of Pressure-Composition-Temperature (PCT) Isotherms, *iScience*, 2025, **28**(4), 112251, DOI: [10.1016/j.isci.2025.112251](https://doi.org/10.1016/j.isci.2025.112251).
- 181 S. Li, S. Tang, Y. Liu, S. Peng and J. Cui, Synthesis of Nanostructured Mg<sub>2</sub>FeH<sub>6</sub> Hydride and Hydrogen Sorption Properties of Complex, *Trans. Nonferrous Met. Soc. China*, 2010, **20**(12), 2281–2288, DOI: [10.1016/S1003-6326\(10\)60641-3](https://doi.org/10.1016/S1003-6326(10)60641-3).
- 182 I. Dovgaliuk, D. A. Safin, N. A. Tumanov, F. Morelle, A. Moulai, R. Černý, Z. Łodziana, M. Devillers and Y. Filinchuk, Solid Aluminum Borohydrides for Prospective Hydrogen Storage, *ChemSusChem*, 2017, **10**(23), 4725–4734, DOI: [10.1002/cssc.201701629](https://doi.org/10.1002/cssc.201701629).
- 183 A. Züttel, Materials for Hydrogen Storage, *Mater. Today*, 2003, **6**(9), 24–33, DOI: [10.1016/S1369-7021\(03\)00922-2](https://doi.org/10.1016/S1369-7021(03)00922-2).
- 184 A. Boretti, A Narrative Review of Metal and Complex Hydride Hydrogen Storage, *Next Research*, 2025, **2**(2), 100226, DOI: [10.1016/j.nexres.2025.100226](https://doi.org/10.1016/j.nexres.2025.100226).
- 185 *Energy Carriers and Conversion Systems – Hydrogen (eBook)*, <https://www.eolss.net/ebooklib/bookinfo/energy-carriers-conversion-systems-with-emphasis-hydrogen.aspx> (accessed 2025-07-24).
- 186 S. K. Dubey, K. R. Kumar, V. Tiwari and U. Srivastva, Characterization and Performance Analysis of Metal Hydride Based Thermochemical Energy Storage System: A Comparative Study of Single and Dual Metal Hydride System, *Int. J. Hydrogen Energy*, 2025, **157**, 150408, DOI: [10.1016/j.ijhydene.2025.150408](https://doi.org/10.1016/j.ijhydene.2025.150408).
- 187 M. Dornheim, Thermodynamics of Metal Hydrides: Tailoring Reaction Enthalpies of Hydrogen Storage Materials, in *Thermodynamics – Interaction Studies – Solids, Liquids and Gases*, ed. J. C. Moreno Piraján, InTech, 2011, DOI: [10.5772/21662](https://doi.org/10.5772/21662).
- 188 X. Ma, X. Ding, R. Chen, X. Chen, Q. Song and H. Cui, Study on Microstructure and the Hydrogen Storage Behavior of a TiVZrNbFe High-Entropy Alloy, *Intermetallics*, 2023, **157**, 107885, DOI: [10.1016/j.intermet.2023.107885](https://doi.org/10.1016/j.intermet.2023.107885).
- 189 M. Wirmas, M. H. Mahyuddin, M. K. Agusta and H. K. Dipojono, DFT Study of H<sub>2</sub> Adsorption and Dissociation on Supported PdZn Clusters, *J. Phys. Conf. Ser.*, 2025, **2980**(1), 012035, DOI: [10.1088/1742-6596/2980/1/012035](https://doi.org/10.1088/1742-6596/2980/1/012035).
- 190 Y. Fukai, Metal-Hydrogen System Under Extended p, T Conditions, in *The Metal-Hydrogen System: Basic Bulk Properties*, ed. Y. Fukai, Springer, Berlin, Heidelberg, 1993, pp. 71–119, DOI: [10.1007/978-3-662-02801-8\\_3](https://doi.org/10.1007/978-3-662-02801-8_3).
- 191 A. Pshenichnikov, J. Stuckert, M. Walter and D. Litvinov, Hydrides and fracture of pure zirconium and zircaloy-4 hydrogenated at temperatures typical for loss-of-coolant accident conditions, 2015.
- 192 J. She, Y. Zhan, C. Li, Y. Du, H. Xu and Y. He, Phase Equilibria of the Al–Pr–Zr Ternary System at 773 K, *J. Alloys Compd.*, 2010, **503**(1), 57–60, DOI: [10.1016/j.jallcom.2010.05.004](https://doi.org/10.1016/j.jallcom.2010.05.004).
- 193 D. J. Sprouster, M. Ouyang, N. Cetiner, P. Negi, A. Sharma, D. Bhardwaj, Y. Huang, X. Hu, K. Shirvan and L. L. Snead, Low Temperature Neutron Irradiation Stability of Zirconium Hydride and Yttrium Hydride, *J. Nucl. Mater.*, 2025, **609**, 155770, DOI: [10.1016/j.jnucmat.2025.155770](https://doi.org/10.1016/j.jnucmat.2025.155770).
- 194 S. C. Lumley, R. W. Grimes, S. T. Murphy, P. A. Burr, A. Chroneos, P. R. Chard-Tuckey and M. R. Wenman, The Thermodynamics of Hydride Precipitation: The Importance of Entropy, Enthalpy and Disorder, *Acta Mater.*, 2014, **79**, 351–362, DOI: [10.1016/j.actamat.2014.07.019](https://doi.org/10.1016/j.actamat.2014.07.019).
- 195 M. Liyanage, D. Reith, V. Eyert and W. A. Curtin, Neural Network Potential for Zr–H, *J. Nucl. Mater.*, 2024, **602**, 155341, DOI: [10.1016/j.jnucmat.2024.155341](https://doi.org/10.1016/j.jnucmat.2024.155341).
- 196 A. Szoka, G. Gajowiec, A. Zieliński, W. Serbiński, J.-M. Olive and A. Ossowska, Hydrogen Degradation of Pre-Oxidized Zirconium Alloys, *Adv. Mater. Sci.*, 2017, **17**(1), 5–21, DOI: [10.1515/adms-2017-0001](https://doi.org/10.1515/adms-2017-0001).
- 197 D. O. Northwood and U. Kosasih, Hydrides and Delayed Hydrogen Cracking in Zirconium and Its Alloys, *Int. Met. Rev.*, 1983, **28**(1), 92–121, DOI: [10.1179/imtr.1983.28.1.92](https://doi.org/10.1179/imtr.1983.28.1.92).



- 198 V. Perovic, G. C. Weatherly and C. J. Simpson, Hydride Precipitation in  $\alpha/\beta$  Zirconium Alloys, *Acta Metall.*, 1983, **31**(9), 1381–1391, DOI: [10.1016/0001-6160\(83\)90008-1](https://doi.org/10.1016/0001-6160(83)90008-1).
- 199 K. B. Colas, A. T. Motta, J. D. Almer, M. R. Daymond, M. Kerr, A. D. Banchik, P. Vizcaino and J. R. Santisteban, *In Situ* Study of Hydride Precipitation Kinetics and Re-Orientation in Zircaloy Using Synchrotron Radiation, *Acta Mater.*, 2010, **58**(20), 6575–6583, DOI: [10.1016/j.actamat.2010.07.018](https://doi.org/10.1016/j.actamat.2010.07.018).
- 200 J. Blomqvist, J. Olofsson, A.-M. Alvarez and C. Bjerkén, Structure and Thermodynamical Properties of Zirconium Hydrides from First-Principle, in *Proceedings of the 15th International Conference on Environmental Degradation of Materials in Nuclear Power Systems—Water Reactors*, ed. J. T. Busby, G. Ilevbare and P. L. Andresen, Springer International Publishing, Cham, 2016, pp. 671–681, DOI: [10.1007/978-3-319-48760-1\\_42](https://doi.org/10.1007/978-3-319-48760-1_42).
- 201 *Zirconium Hydrides – an overview | ScienceDirect Topics*, <https://www.sciencedirect.com/topics/physics-and-astronomy/zirconium-hydrides> (accessed 2025-04-04).
- 202 M. D. B. Ferraz, W. J. Botta and G. Zepon, Synthesis, Characterization and First Hydrogen Absorption/Desorption of the  $\text{Mg}_{35}\text{Al}_{15}\text{Ti}_{25}\text{V}_{10}\text{Zn}_{15}$  High Entropy Alloy, *Int. J. Hydrogen Energy*, 2022, **47**(54), 22881–22892, DOI: [10.1016/j.ijhydene.2022.05.098](https://doi.org/10.1016/j.ijhydene.2022.05.098).
- 203 J. Liang, G. Li, X. Ding, Y. Li, Z. Wen, T. Zhang and Y. Qu, Effect of C14 Laves/BCC on Microstructure and Hydrogen Storage Properties of  $(\text{Ti}_{32.5}\text{V}_{27.5}\text{Zr}_{7.5}\text{Nb}_{32.5})_{1-x}\text{Fe}_x$  ( $x = 0.03, 0.06, 0.09$ ) High Entropy Hydrogen Storage Alloys, *J. Energy Storage*, 2023, **73**, 108852, DOI: [10.1016/j.est.2023.108852](https://doi.org/10.1016/j.est.2023.108852).
- 204 J. Liang, G. Li, X. Ding, Y. Li, Z. Wen, T. Zhang and Y. Qu, The Synergistic Effect of Ni and C14 Laves Phase on the Hydrogen Storage Properties of TiVZrNbNi High Entropy Hydrogen Storage Alloy, *Intermetallics*, 2024, **164**, 108102, DOI: [10.1016/j.intermet.2023.108102](https://doi.org/10.1016/j.intermet.2023.108102).
- 205 L. F. Chanchetti, B. Hessel Silva, J. Montero, C. Zlotea, Y. Champion, W. J. Botta and G. Zepon, Structural Characterization and Hydrogen Storage Properties of the  $\text{Ti}_{31}\text{V}_{26}\text{Nb}_{26}\text{Zr}_{12}\text{M}_5$  ( $\text{M} = \text{Fe}, \text{Co}, \text{or Ni}$ ) Multi-Phase Multi-component Alloys, *Int. J. Hydrogen Energy*, 2023, **48**(6), 2247–2255, DOI: [10.1016/j.ijhydene.2022.10.060](https://doi.org/10.1016/j.ijhydene.2022.10.060).
- 206 V. A. Yartys, O. Isnard, A. B. Riabov and L. G. Akselrud, Unusual Effects on Hydrogenation: Anomalous Expansion and Volume Contraction, *J. Alloys Compd.*, 2003, **356–357**, 109–113, DOI: [10.1016/S0925-8388\(03\)00106-3](https://doi.org/10.1016/S0925-8388(03)00106-3).
- 207 B. Y. Ao, X. L. Wang, P. Shi, P. H. Chen, X. Q. Ye, X. C. Lai, J. J. Ai and T. Gao, Lattice Contraction of Cerium Hydrides from First-Principles LDA +  $U$  Calculations, *Int. J. Hydrogen Energy*, 2012, **37**(6), 5108–5113, DOI: [10.1016/j.ijhydene.2011.12.095](https://doi.org/10.1016/j.ijhydene.2011.12.095).
- 208 H. Senoh, T. Kiyobayashi, N. Takeichi, H. Tanaka, Q. xu, H. Takeshita, M. Toyouchi, T. Oishi and N. Kuriyama, Hydrogenation and Dehydrogenation Properties of RHNi5 (RH = Heavy Rare Earth) Binary Intermetallic Compounds, *Mater. Trans.*, 2004, **45**, 292–295, DOI: [10.2320/matertrans.45.292](https://doi.org/10.2320/matertrans.45.292).
- 209 A. Züttel, Hydrogen Storage Methods, *Naturwissenschaften*, 2004, **91**(4), 157–172, DOI: [10.1007/s00114-004-0516-x](https://doi.org/10.1007/s00114-004-0516-x).
- 210 G. Zepon, B. H. Silva, C. Zlotea, W. J. Botta and Y. Champion, Thermodynamic Modelling of Hydrogen-Multicomponent Alloy Systems: Calculating Pressure-Composition-Temperature Diagrams, *Acta Mater.*, 2021, **215**, 117070, DOI: [10.1016/j.actamat.2021.117070](https://doi.org/10.1016/j.actamat.2021.117070).
- 211 T. B. Flanagan and W. A. Oates, Some Thermodynamic Aspects of Metal Hydrogen Systems, *J. Alloys Compd.*, 2005, **404–406**, 16–23, DOI: [10.1016/j.jallcom.2004.11.108](https://doi.org/10.1016/j.jallcom.2004.11.108).
- 212 T. B. Flanagan and W. A. Oates, Thermodynamics of Inter-metallic Compound-Hydrogen Systems, in *Hydrogen in Inter-metallic Compounds I: Electronic, Thermodynamic, and Crystallographic Properties, Preparation*, ed. L. Schlapbach, Springer, Berlin, Heidelberg, 1988, pp. 49–85, DOI: [10.1007/3540183337\\_10](https://doi.org/10.1007/3540183337_10).
- 213 A. Kumar, T. P. Yadav, M. A. Shaz and N. K. Mukhopadhyay, Hydrogen Storage Properties in Rapidly Solidified TiZrVCrNi High-entropy Alloys, *Energy Storage*, 2024, **6**(1), e532, DOI: [10.1002/est2.532](https://doi.org/10.1002/est2.532).
- 214 E. Akiba and H. Iba, Hydrogen Absorption by Laves Phase Related BCC Solid Solution, *Intermetallics*, 1998, **6**(6), 461–470, DOI: [10.1016/S0966-9795\(97\)00088-5](https://doi.org/10.1016/S0966-9795(97)00088-5).
- 215 I. Kuncce, M. Polanski and J. Bystrzycki, Structure and Hydrogen Storage Properties of a High Entropy ZrTiVCrFeNi Alloy Synthesized Using Laser Engineered Net Shaping (LENS), *Int. J. Hydrogen Energy*, 2013, **38**(27), 12180–12189, DOI: [10.1016/j.ijhydene.2013.05.071](https://doi.org/10.1016/j.ijhydene.2013.05.071).
- 216 D. P. Broom and M. Hirscher, Improving Reproducibility in Hydrogen Storage Material Research, *Chem-PhysChem*, 2021, **22**(21), 2141–2157, DOI: [10.1002/cphc.202100508](https://doi.org/10.1002/cphc.202100508).
- 217 J. Barale, Hydrogen Storage and Compression Based on Metal Hydrides, 2022.
- 218 *Advances in High-Entropy Alloy Research: Unraveling Fabrication Techniques, Microstructural Transformations, and Mechanical Properties*/Journal of Bio- and Tribo-Corrosion, <https://link.springer.com/article/10.1007/s40735-025-00999-6> (accessed 2025-07-21).
- 219 All about Alloys, *Nat. Synth.*, 2022, **1**(2), 97, DOI: [10.1038/s44160-022-00036-1](https://doi.org/10.1038/s44160-022-00036-1).
- 220 S. Yang, F. Yang, C. Wu, Y. Chen, Y. Mao and L. Luo, Hydrogen Storage and Cyclic Properties of  $(\text{VFe})_{60}(\text{TiCrCo})_{40-x}\text{Zr}_x$  ( $0 \leq x \leq 2$ ) Alloys, *J. Alloys Compd.*, 2016, **663**, 460–465, DOI: [10.1016/j.jallcom.2015.12.125](https://doi.org/10.1016/j.jallcom.2015.12.125).
- 221 B. Sarac, V. Zadorozhnyy, E. Berdonosova, Y. P. Ivanov, S. Klyamkin, S. Gumrukcu, A. S. Sarac, A. Korol, D. Semenov, M. Zadorozhnyy, A. Sharma, A. L. Greer and J. Eckert, Hydrogen Storage Performance of the Multi-Principal-Component CoFeMnTiVZr Alloy in Electrochemical and Gas–Solid Reactions, *RSC Adv.*, 2020, **10**(41), 24613–24623, DOI: [10.1039/D0RA04089D](https://doi.org/10.1039/D0RA04089D).
- 222 F. Aouaini, N. Bouazizi, M. M. Almoneef, H. Al-Ghamdi and A. B. Lamine, Absorption and Desorption of Hydrogen in  $\text{Ti}_{1.02}\text{Cr}_{1.1}\text{Mn}_{0.3}\text{Fe}_{0.6}\text{RE}_{0.03}$ : Experiments, Characterization and Analytical Interpretation Using Statistical Physics



- Treatment, *RSC Adv.*, 2021, **11**(26), 15905–15920, DOI: [10.1039/D1RA00999K](https://doi.org/10.1039/D1RA00999K).
- 223 K. Young, M. A. Fetcenko, F. Li and T. Ouchi, Structural, Thermodynamic, and Electrochemical Properties of  $Ti_xZr_{1-x}(VNiCrMnCoAl)_2$  C14 Laves Phase Alloys, *J. Alloys Compd.*, 2008, **464**(1), 238–247, DOI: [10.1016/j.jallcom.2007.09.096](https://doi.org/10.1016/j.jallcom.2007.09.096).
- 224 A. Kumar, T. P. Yadav, M. A. Shaz and N. K. Mukhopadhyay, Hydrogen Storage Performance of C14 Type  $Ti_{0.24}V_{0.17}Zr_{0.17}Mn_{0.17}Co_{0.17}Fe_{0.08}$  High Entropy Intermetallics, *Trans. Indian Natl. Acad. Eng.*, 2024, **9**(3), 585–593, DOI: [10.1007/s41403-023-00390-2](https://doi.org/10.1007/s41403-023-00390-2).
- 225 K. X. Zheng, D. T. Yu, J. L. Liu, C. L. Wu, S. Zhang, C. H. Zhang, Q. Wang and D. Zhang, Laser Cladding of FeCoCrNiTi High-Entropy Alloy Coatings to Modulate the Microstructure and Enhance the Tribo-Corrosion Behavior on 304 Stainless Steel, *Surf. Coat. Technol.*, 2025, **505**, 132114, DOI: [10.1016/j.surfcoat.2025.132114](https://doi.org/10.1016/j.surfcoat.2025.132114).
- 226 L. F. Mosinoiu, I.-C. Badea, A. E. Sobetkii, I. Anasiei, M. Petriceanu, D. Mitrica and R.-R. Piticescu, High Entropy Alloys and Methods for Synthesis, *MATEC Web Conf.*, 2024, **401**, 14002, DOI: [10.1051/mateconf/202440114002](https://doi.org/10.1051/mateconf/202440114002).
- 227 A. Kumar, A. Singh and A. Suhane, Mechanically Alloyed High Entropy Alloys: Existing Challenges and Opportunities, *J. Mater. Res. Technol.*, 2022, **17**, 2431–2456, DOI: [10.1016/j.jmrt.2022.01.141](https://doi.org/10.1016/j.jmrt.2022.01.141).
- 228 Z. Cai, Y. Guo, J. Liu, J. Liu, J. Guo, X. Du and S. Huang, Progress in Light-Weight High Entropy Alloys, *J. Wuhan Univ. Technol., Mater. Sci. Ed.*, 2021, **36**(5), 737–753, DOI: [10.1007/s11595-021-2467-x](https://doi.org/10.1007/s11595-021-2467-x).
- 229 N. I. Muhammad Nadzri, D. S. C. Halin, M. M. Al Bakri Abdullah, S. Joseph, M. A. A. Mohd Salleh, P. Vizureanu, D.-P. Burduhos-Nergis and A. V. Sandu, High-Entropy Alloy for Thin Film Application: A Review, *Coatings*, 2022, **12**(12), 1842, DOI: [10.3390/coatings12121842](https://doi.org/10.3390/coatings12121842).
- 230 X. Ma, X. Ding, R. Chen, W. Cao and Q. Song, Study on Hydrogen Storage Property of (ZrTiVFe) Al High-Entropy Alloys by Modifying Al Content, *Int. J. Hydrogen Energy*, 2022, **47**(13), 8409–8418, DOI: [10.1016/j.ijhydene.2021.12.172](https://doi.org/10.1016/j.ijhydene.2021.12.172).
- 231 R. Z. Valiev, Y. Estrin, Z. Horita, T. G. Langdon, M. J. Zechetbauer and Y. T. Zhu, Producing Bulk Ultrafine-Grained Materials by Severe Plastic Deformation, *JOM*, 2006, **58**(4), 33–39, DOI: [10.1007/s11837-006-0213-7](https://doi.org/10.1007/s11837-006-0213-7).
- 232 arc MELTER – AMAZEMET, <https://www.amazemet.com/arc-melter/> (accessed 2025-06-27).
- 233 B. S. Murty, J. W. Yeh, S. Ranganathan and P. P. Bhattacharjee, 6 – Synthesis and Processing, in *High-Entropy Alloys (Second Edition)*, ed. B. S. Murty, J. W. Yeh, S. Ranganathan and P. P. Bhattacharjee, Elsevier, 2019, pp. 103–117, DOI: [10.1016/B978-0-12-816067-1.00006-0](https://doi.org/10.1016/B978-0-12-816067-1.00006-0).
- 234 A comparative study on Arc- and vacuum induction-melting for  $Ti_{16.6}Zr_{16.6}Hf_{16.6}Co_{10}Ni_{20}Cu_{20}$  high entropy shape memory Alloy Production | Discover Materials, <https://link.springer.com/article/10.1007/s43939-024-00134-1> (accessed 2025-06-27).
- 235 G. L. B. G. Fontana, P. Edalati, S. Dangwal, K. Edalati, R. B. Strozi and R. Floriano, Crystal Structure and Hydrogen Storage Properties of ZrNbFeCo Medium-Entropy Alloy, *Intermetallics*, 2025, **176**, 108576, DOI: [10.1016/j.intermet.2024.108576](https://doi.org/10.1016/j.intermet.2024.108576).
- 236 Y. A. Alshataif, S. Sivasankaran, F. A. Al-Mufadi, A. S. Alaboodi and H. R. Ammar, Manufacturing Methods, Microstructural and Mechanical Properties Evolutions of High-Entropy Alloys: A Review, *Met. Mater. Int.*, 2020, **26**(8), 1099–1133, DOI: [10.1007/s12540-019-00565-z](https://doi.org/10.1007/s12540-019-00565-z).
- 237 S. Salifu and P. A. Olubambi, Effects of Fabrication Techniques on the Mechanical Properties of High Entropy Alloys: A Review, *Int. J. Lightweight Mater. Manuf.*, 2024, **7**(1), 97–121, DOI: [10.1016/j.ijlmm.2023.08.001](https://doi.org/10.1016/j.ijlmm.2023.08.001).
- 238 Y. Zhang and Q. Xing, High Entropy Alloys: Manufacturing Routes, in *Encyclopedia of Materials: Metals and Alloys*, Elsevier, 2022, pp. 327–338, DOI: [10.1016/B978-0-12-803581-8.12123-X](https://doi.org/10.1016/B978-0-12-803581-8.12123-X).
- 239 H. Shen, J. Hu, P. Li, G. Huang, J. Zhang, J. Zhang, Y. Mao, H. Xiao, X. Zhou, X. Zu, X. Long and S. Peng, Compositional Dependence of Hydrogenation Performance of Ti-Zr-Hf-Mo-Nb High-Entropy Alloys for Hydrogen/Tritium Storage, *J. Mater. Sci. Technol.*, 2020, **55**, 116–125, DOI: [10.1016/j.jmst.2019.08.060](https://doi.org/10.1016/j.jmst.2019.08.060).
- 240 L. Serrano, M. Moussa, J.-Y. Yao, G. Silva, J.-L. Bobet, S. F. Santos and K. R. Cardoso, Development of Ti-V-Nb-Cr-Mn High Entropy Alloys for Hydrogen Storage, *J. Alloys Compd.*, 2023, **945**, 169289, DOI: [10.1016/j.jallcom.2023.169289](https://doi.org/10.1016/j.jallcom.2023.169289).
- 241 A. Antolak-Dudka, P. Platek, T. Durejko, P. Baranowski, J. Malachowski, M. Sarzyński and T. Czujko, Static and Dynamic Loading Behavior of  $Ti_6Al_4V$  Honeycomb Structures Manufactured by Laser Engineered Net Shaping (LENSTM) Technology, *Materials*, 2019, **12**(8), 1225, DOI: [10.3390/ma12081225](https://doi.org/10.3390/ma12081225).
- 242 J. Chen, Z. Li, H. Huang, Y. Lv, B. Liu, Y. Li, Y. Wu, J. Yuan and Y. Wang, Superior Cycle Life of TiZrFeMnCrV High Entropy Alloy for Hydrogen Storage, *Scr. Mater.*, 2022, **212**, 114548, DOI: [10.1016/j.scriptamat.2022.114548](https://doi.org/10.1016/j.scriptamat.2022.114548).
- 243 A. Percheron-Guégan and J.-M. Welter, Preparation of Intermetallics and Hydrides, in *Hydrogen in Intermetallic Compounds I: Electronic, Thermodynamic, and Crystallographic Properties, Preparation*, ed. L. Schlapbach, Springer, Berlin, Heidelberg, 1988, pp. 11–48, DOI: [10.1007/3540183337\\_9](https://doi.org/10.1007/3540183337_9).
- 244 F. Yin, Y. Chang, T. Si, J. Chen, H.-W. Li, Y. Li and Q. Zhang, Structural and Kinetic Adjustments of Zr-Based High-Entropy Alloys with Laves Phases by Substitution of Mg Element, *Energy Adv.*, 2023, **2**(9), 1409–1418, DOI: [10.1039/D3YA00243H](https://doi.org/10.1039/D3YA00243H).
- 245 M. Izadi, A. Farzaneh, M. Mohammed, I. Gibson and B. Rolfe, A Review of Laser Engineered Net Shaping (LENS) Build and Process Parameters of Metallic Parts, *Rapid Prototyp. J.*, 2020, **26**(6), 1059–1078, DOI: [10.1108/RPJ-04-2018-0088](https://doi.org/10.1108/RPJ-04-2018-0088).
- 246 O. T. Onawale, P. V. Cobbinah, R. A. Nzeukou and W. R. Matizamhuka, Synthesis Route, Microstructural Evolution,



- and Mechanical Property Relationship of High-Entropy Alloys (HEAs): A Review, *Materials*, 2021, **14**(11), 3065, DOI: [10.3390/ma14113065](https://doi.org/10.3390/ma14113065).
- 247 I. Kunce, M. Polanski and J. Bystrzycki, Microstructure and Hydrogen Storage Properties of a TiZrNbMoV High Entropy Alloy Synthesized Using Laser Engineered Net Shaping (LENS), *Int. J. Hydrogen Energy*, 2014, **39**(18), 9904–9910, DOI: [10.1016/j.ijhydene.2014.02.067](https://doi.org/10.1016/j.ijhydene.2014.02.067).
- 248 I. Kunce, M. Polański and T. Czujko, Microstructures and Hydrogen Storage Properties of LaNiFeVMn Alloys, *Int. J. Hydrogen Energy*, 2017, **42**(44), 27154–27164, DOI: [10.1016/j.ijhydene.2017.09.039](https://doi.org/10.1016/j.ijhydene.2017.09.039).
- 249 S.-K. Chen, P.-H. Lee, H. Lee and H.-T. Su, Hydrogen Storage of C14-CrFeVmnwTi<sub>x</sub>V<sub>y</sub>Zr<sub>z</sub> Alloys, *Mater. Chem. Phys.*, 2018, **210**, 336–347, DOI: [10.1016/j.matchemphys.2017.08.008](https://doi.org/10.1016/j.matchemphys.2017.08.008).
- 250 F. Zaera, The Surface Chemistry of Metal-Based Hydrogenation Catalysis, *ACS Catal.*, 2017, **7**, 4947–4967, DOI: [10.1021/acscatal.7b01368](https://doi.org/10.1021/acscatal.7b01368).
- 251 M. Jiang, Y. Yang, H. Li and B. Liang, Theoretical Study on the Surface Poisoning of High-Entropy Alloys during Hydrogen Storage Cycles: The Effect of Metal Elements and Phases, *Phys. Chem. Chem. Phys.*, 2024, **26**(37), 24384–24394, DOI: [10.1039/D4CP02831G](https://doi.org/10.1039/D4CP02831G).
- 252 H. Kim, S. Kang, J. Y. Lee, T. W. Heo, B. C. Wood, J.-H. Shim, Y. W. Cho, D. H. Kim, J.-Y. Suh and Y.-S. Lee, A New Perspective on the Initial Hydrogenation of TiFe<sub>0.9</sub>M<sub>0.1</sub> (M = V, Cr, Fe, Co, Ni) Alloys Gained from Surface Oxide Analyses and Nucleation Energetics, *Appl. Surf. Sci.*, 2023, **610**, 155443, DOI: [10.1016/j.apsusc.2022.155443](https://doi.org/10.1016/j.apsusc.2022.155443).
- 253 H. Ha, S. J. Jung, S. G. Jeong, R. E. Kim, H.-K. Park and H. S. Kim, Enhancing Hydrogen Storage Kinetics and Capacity via Particle Size Modulation in TiZrCrFeMnNi High-Entropy Alloy, *Int. J. Hydrogen Energy*, 2025, **99**, 1047–1054, DOI: [10.1016/j.ijhydene.2024.12.185](https://doi.org/10.1016/j.ijhydene.2024.12.185).
- 254 N. Z. Abd Khalim Khafidz, Z. Yaakob, K. L. Lim and S. N. Timmiati, The Kinetics of Lightweight Solid-State Hydrogen Storage Materials: A Review, *Int. J. Hydrogen Energy*, 2016, **41**(30), 13131–13151, DOI: [10.1016/j.ijhydene.2016.05.169](https://doi.org/10.1016/j.ijhydene.2016.05.169).
- 255 S. Sleiman and J. Huot, Effect of Particle Size, Pressure and Temperature on the Activation Process of Hydrogen Absorption in TiVZrHfNb High Entropy Alloy, *J. Alloys Compd.*, 2021, **861**, 158615, DOI: [10.1016/j.jallcom.2021.158615](https://doi.org/10.1016/j.jallcom.2021.158615).
- 256 S. Dangwal and K. Edalati, Influence of Interphase Boundary Coherency in High-Entropy Alloys on Their Hydrogen Storage Performance, *J. Alloys Compd.*, 2025, **1036**, 182070, DOI: [10.1016/j.jallcom.2025.182070](https://doi.org/10.1016/j.jallcom.2025.182070).
- 257 H. Zhao, P. Yao, Y. Zhao, Z. Zeng, C. Xia and T. Yang, Microstructure and Hydrogen Storage Properties of Zr-Based AB<sub>2</sub>-Type High Entropy Alloys, *J. Alloys Compd.*, 2023, **960**, 170665, DOI: [10.1016/j.jallcom.2023.170665](https://doi.org/10.1016/j.jallcom.2023.170665).
- 258 D. Pukazhselvan, V. Kumar and S. K. Singh, High Capacity Hydrogen Storage: Basic Aspects, New Developments and Milestones, *Nano Energy*, 2012, **1**(4), 566–589, DOI: [10.1016/j.nanoen.2012.05.004](https://doi.org/10.1016/j.nanoen.2012.05.004).
- 259 L. Luo, L. Chen, L. Li, S. Liu, Y. Li, C. Li, L. Li, J. Cui and Y. Li, High-Entropy Alloys for Solid Hydrogen Storage: A Review, *Int. J. Hydrogen Energy*, 2024, **50**, 406–430, DOI: [10.1016/j.ijhydene.2023.07.146](https://doi.org/10.1016/j.ijhydene.2023.07.146).
- 260 A. Züttel, Materials for Hydrogen Storage, in *Catalysis for Sustainable Energy Production*, ed. P. Barbaro and C. Bianchini, Wiley, 2009, pp. 107–169, DOI: [10.1002/9783527625413.ch5](https://doi.org/10.1002/9783527625413.ch5).
- 261 R. Floriano, G. Zepon, K. Edalati, G. L. B. G. Fontana, A. Mohammadi, Z. Ma, H.-W. Li and R. J. Contieri, Hydrogen Storage Properties of New A3B2-Type TiZrNbCrFe High-Entropy Alloy, *Int. J. Hydrogen Energy*, 2021, **46**(46), 23757–23766, DOI: [10.1016/j.ijhydene.2021.04.181](https://doi.org/10.1016/j.ijhydene.2021.04.181).
- 262 S. Yang, F. Yang, C. Wu, Y. Chen, Y. Mao and L. Luo, Hydrogen Storage and Cyclic Properties of (VFe)<sub>60</sub>(TiCrCo)<sub>40-x</sub>Zr<sub>x</sub> (0 ≤ x ≤ 2) Alloys, *J. Alloys Compd.*, 2016, **663**, 460–465, DOI: [10.1016/j.jallcom.2015.12.125](https://doi.org/10.1016/j.jallcom.2015.12.125).
- 263 V. Raud, A. Habrioux, L. Pirault-Roy and J.-L. Bobet, Development of Refractory High Entropy Alloys: Relationship between Composition, Structure, Hydrogen Absorption Properties and Corrosion Resistance Properties, *J. Alloys Compd.*, 2025, **1044**, 184380, DOI: [10.1016/j.jallcom.2025.184380](https://doi.org/10.1016/j.jallcom.2025.184380).
- 264 *Hydrogen Absorption Reactions of Hydrogen Storage Alloy LaNi5 under High Pressure – PMC*, <https://pubmed.ncbi.nlm.nih.gov/articles/PMC9919125/> (accessed 2025-06-29).
- 265 H. Liu, J. Zhang, P. Sun, C. Zhou, Y. Liu and Z. Z. Fang, An Overview of TiFe Alloys for Hydrogen Storage: Structure, Processes, Properties, and Applications, *J. Energy Storage*, 2023, **68**, 107772, DOI: [10.1016/j.est.2023.107772](https://doi.org/10.1016/j.est.2023.107772).
- 266 *DOE Technical Targets for Hydrogen Storage Systems for Material Handling Equipment*, Energy.gov, <https://www.energy.gov/eere/fuelcells/doe-technical-targets-hydrogen-storage-systems-material-handling-equipment> (accessed 2025-06-29).
- 267 *Homepage – U.S. Energy Information Administration (EIA)*, <https://www.eia.gov/> (accessed 2025-08-05).
- 268 D. Fruchart, N. Skryabina and V. N. Aptukov, Why Mechanical Texture Improves Magnesium Hydrogenation Kinetics?, *Int. J. Hydrogen Energy*, 2025, **149**, 150061, DOI: [10.1016/j.ijhydene.2025.150061](https://doi.org/10.1016/j.ijhydene.2025.150061).
- 269 F. Pineda, C. Martínez, P. Martín and C. Aguilar, High-Entropy Alloys: A Review of Their Performance as Promising Materials for Hydrogen and Molten Salt Storage, *Rev. Adv. Mater. Sci.*, 2023, **62**(1), 20230150, DOI: [10.1515/rams-2023-0150](https://doi.org/10.1515/rams-2023-0150).
- 270 S. Dangwal and K. Edalati, Significance of Interphase Boundaries on Activation of High-Entropy Alloys for Room-Temperature Hydrogen Storage, *Int. J. Hydrogen Energy*, 2024, **50**, 626–636, DOI: [10.1016/j.ijhydene.2023.07.327](https://doi.org/10.1016/j.ijhydene.2023.07.327).
- 271 P. Hájková, J. Horník, E. Čížmárová and F. Kalianko, Metallic Materials for Hydrogen Storage—A Brief Overview, *Coatings*, 2022, **12**(12), 1813, DOI: [10.3390/coatings12121813](https://doi.org/10.3390/coatings12121813).



- 272 S. Nayeboossadri and D. Book, Compositional Effects on the Hydrogen Cycling Stability of Multicomponent Ti-Mn Based Alloys, *Int. J. Hydrogen Energy*, 2019, **44**(21), 10722–10731, DOI: [10.1016/j.ijhydene.2019.02.138](https://doi.org/10.1016/j.ijhydene.2019.02.138).
- 273 Q. Pan, H. Shen, X. Han, J. Zhu, Z. Li, T. Pan, L. Xu and L. Lv, Effect of Non-Stoichiometric Mn and Cr on the Hydrogen Storage Properties of Ti–Mn–Based Alloys, *RSC Adv.*, 2025, **15**(22), 17153–17163, DOI: [10.1039/D5RA00542F](https://doi.org/10.1039/D5RA00542F).
- 274 Z. Wang and S. Zhang, Research and Application Progress of High-Entropy Alloys, *Coatings*, 2023, **13**(11), 1916, DOI: [10.3390/coatings13111916](https://doi.org/10.3390/coatings13111916).
- 275 V. E. Gromov, Y. A. Shlyarova, S. V. Kononov, S. V. Vorob'ev and O. A. Peregudov, Application of High-Entropy Alloys, *Steel Transl.*, 2021, **51**(10), 700–704, DOI: [10.3103/S096709122110003X](https://doi.org/10.3103/S096709122110003X).
- 276 F. Yang, Y. Zhang, F. Ciucci, Z. Wu, S. Wang, Y. Wang and Z. Zhang, Towards a Consistent Understanding of the Metal Hydride Reaction Kinetics: Measurement, Modeling and Data Processing, *J. Alloys Compd.*, 2018, **741**, 610–621, DOI: [10.1016/j.jallcom.2018.01.163](https://doi.org/10.1016/j.jallcom.2018.01.163).
- 277 X. Fu, C. A. Schuh and E. A. Olivetti, Materials Selection Considerations for High Entropy Alloys, *Scr. Mater.*, 2017, **138**, 145–150, DOI: [10.1016/j.scriptamat.2017.03.014](https://doi.org/10.1016/j.scriptamat.2017.03.014).
- 278 Q. Lai, Y. Sun, T. Wang, P. Modi, C. Cazorla, U. B. Demirci, J. R. Ares Fernandez, F. Leardini and K.-F. Aguey-Zinsou, How to Design Hydrogen Storage Materials? Fundamentals, Synthesis, and Storage Tanks, *Adv. Sustainable Syst.*, 2019, **3**(9), 1900043, DOI: [10.1002/adsu.201900043](https://doi.org/10.1002/adsu.201900043).
- 279 K. Young, T. Ouchi and M. A. Fetcenko, Roles of Ni, Cr, Mn, Sn, Co, and Al in C14 Laves Phase Alloys for NiMH Battery Application, *J. Alloys Compd.*, 2009, **476**(1), 774–781, DOI: [10.1016/j.jallcom.2008.09.146](https://doi.org/10.1016/j.jallcom.2008.09.146).
- 280 I. D. Wijayanti, R. Denys, S. Suwarno, A. A. Volodin, M. V. Lototskyy, M. N. Guzik, J. Nei, K. Young, H. J. Roven and V. Yartys, Hydrides of Laves Type Ti–Zr Alloys with Enhanced H Storage Capacity as Advanced Metal Hydride Battery Anodes, *J. Alloys Compd.*, 2020, **828**, 154354, DOI: [10.1016/j.jallcom.2020.154354](https://doi.org/10.1016/j.jallcom.2020.154354).
- 281 I. D. Wijayanti, H. J. Roven and V. Yartys, Effect of Mn Content in the Ti/Zr-Based AB<sub>2</sub> Laves Type Alloys on Their Electrochemical Performance, *J. Energy Storage*, 2024, **96**, 112751, DOI: [10.1016/j.est.2024.112751](https://doi.org/10.1016/j.est.2024.112751).
- 282 C. Wan, R. V. Denys and V. A. Yartys, Effects of Ti Substitution for Zr on the Electrochemical Characteristics and Structure of AB<sub>2</sub>-Type Laves-Phase Alloys as Metal Hydride Anodes, *J. Alloys Compd.*, 2021, **889**, 161655, DOI: [10.1016/j.jallcom.2021.161655](https://doi.org/10.1016/j.jallcom.2021.161655).
- 283 Z. Zhu, Z. Li, Z. Liu, C. Gu, Q. Zhang and L. Wang, Advanced Development of High-Entropy Alloys in Catalytic Applications, *Small Methods*, 2025, 2500411, DOI: [10.1002/smt.202500411](https://doi.org/10.1002/smt.202500411).
- 284 J. Chen, J. Ma, T. Huang, Q. Liu, X. Liu, R. Luo, J. Xu, X. Wang, T. Jiang, H. Liu, Z. Lv, T. Yao, G. Wang, X. Zheng, Z. Li and W. Chen, Iridium-Free High-Entropy Alloy for Acidic Water Oxidation at High Current Densities, *Angew. Chem., Int. Ed.*, 2025, **64**(21), e202503330, DOI: [10.1002/anie.202503330](https://doi.org/10.1002/anie.202503330).
- 285 S. Liu, Y. Wang, T. Jiang, S. Jin, M. Sajid, Z. Zhang, J. Xu, Y. Fan, X. Wang, J. Chen, Z. Liu, X. Zheng, K. Zhang, Q. Nian, Z. Zhu, Q. Peng, T. Ahmad, K. Li and W. Chen, Non-Noble Metal High-Entropy Alloy-Based Catalytic Electrode for Long-Life Hydrogen Gas Batteries, *ACS Nano*, 2024, **18**(5), 4229–4240, DOI: [10.1021/acsnano.3c09482](https://doi.org/10.1021/acsnano.3c09482).
- 286 K. Young, M. A. Fetcenko, F. Li and T. Ouchi, Structural, Thermodynamic, and Electrochemical Properties of Ti<sub>x</sub>Zr<sub>1-x</sub>(VNiCrMnCoAl)<sub>2</sub> C14 Laves Phase Alloys, *J. Alloys Compd.*, 2008, **464**(1), 238–247, DOI: [10.1016/j.jallcom.2007.09.096](https://doi.org/10.1016/j.jallcom.2007.09.096).
- 287 J. M. Torralba, P. Alvaredo and A. García-Junceda, Powder Metallurgy and High-Entropy Alloys: Update on New Opportunities, *Powder Metall.*, 2020, **63**(4), 227–236, DOI: [10.1080/00325899.2020.1807713](https://doi.org/10.1080/00325899.2020.1807713).
- 288 The effect of Laves phases and nano-precipitates on the electrochemical corrosion resistance of Mg–Al–Ca alloys under alkaline conditions, <https://www.sciopen.com/article/10.1016/j.jma.2024.06.011> (accessed 2025-11-06).
- 289 R. Krishnan and M. K. Asundi, Zirconium Alloys in Nuclear Technology, *Proc. – Indian Acad. Sci., Sect. C*, 1981, **4**(1), 41–56, DOI: [10.1007/BF02843474](https://doi.org/10.1007/BF02843474).
- 290 T. Sonar, M. Ivanov, E. Trofimov, A. Tingaev and I. Suleymanova, An Overview of Microstructure, Mechanical Properties and Processing of High Entropy Alloys and Its Future Perspectives in Aeroengine Applications, *Mater. Sci. Energy Technol.*, 2024, **7**, 35–60, DOI: [10.1016/j.mset.2023.07.004](https://doi.org/10.1016/j.mset.2023.07.004).
- 291 T. Sonar, M. Ivanov, E. Trofimov, A. Tingaev and I. Suleymanova, An Overview of Microstructure, Mechanical Properties and Processing of High Entropy Alloys and Its Future Perspectives in Aeroengine Applications, *Mater. Sci. Energy Technol.*, 2024, **7**, 35–60, DOI: [10.1016/j.mset.2023.07.004](https://doi.org/10.1016/j.mset.2023.07.004).
- 292 T. Cheng, J. Huang, W. Fang, L. He, X. Duan, G. Zou, X. Li and X. Ren, Effects of Annealing on Hydrogen Storage Performance in TiZrCrMnFeNi High-Entropy Alloy, *Crystals*, 2025, **15**(4), 297, DOI: [10.3390/cryst15040297](https://doi.org/10.3390/cryst15040297).
- 293 N. I. Muhammad Nadzri, D. S. C. Halin, M. M. Al Bakri Abdullah, S. Joseph, M. A. A. Mohd Salleh, P. Vizureanu, D.-P. Burduhos-Nergis and A. V. Sandu, High-Entropy Alloy for Thin Film Application: A Review, *Coatings*, 2022, **12**(12), 1842, DOI: [10.3390/coatings12121842](https://doi.org/10.3390/coatings12121842).
- 294 *Additively manufactured high-entropy alloys for hydrogen storage: Predictions: Heliyon*, [https://www.cell.com/heliyon/fulltext/S2405-8440\(24\)08746-2](https://www.cell.com/heliyon/fulltext/S2405-8440(24)08746-2) (accessed 2025-04-07).
- 295 Y. Jiang and W. Jiang, High Entropy Alloys: Emerging Materials for Advanced Hydrogen Storage, *Energy Technol.*, 2024, **12**(12), 2401061, DOI: [10.1002/ente.202401061](https://doi.org/10.1002/ente.202401061).
- 296 Y. K. Yadav, M. A. Shaz and T. P. Yadav, Solid-State Hydrogen Storage Properties of Al–Cu–Fe–Ni–Ti High Entropy Alloy, *Int. J. Hydrogen Energy*, 2025, **99**, 985–995, DOI: [10.1016/j.ijhydene.2024.12.254](https://doi.org/10.1016/j.ijhydene.2024.12.254).
- 297 R. B. Strozi, D. R. Leiva, J. Huot, W. J. Botta and G. Zepon, An Approach to Design Single BCC Mg-Containing High Entropy Alloys for Hydrogen Storage Applications, *Int.*



- J. Hydrogen Energy*, 2021, **46**(50), 25555–25561, DOI: [10.1016/j.ijhydene.2021.05.087](https://doi.org/10.1016/j.ijhydene.2021.05.087).
- 298 S. Moniri, Y. Yang, Y. Yuan, J. Zhou, L. Yang, F. Zhu, Y. Liao, Y. Yao, L. Hu, P. Ercius, J. Ding and J. Miao, Three-Dimensional Atomic Positions and Local Chemical Order of Medium- and High-Entropy Alloys, *arXiv*, 2023, preprint, arXiv:2305.14123, DOI: [10.48550/arXiv.2305.14123](https://doi.org/10.48550/arXiv.2305.14123).
- 299 Y.-J. Chen, J.-W. Zhang, C.-H. Xu, M.-H. Li, S.-L. Hu, Y.-X. Wang, X.-T. Zu, H.-Y. Xiao, X.-S. Zhou, S.-M. Peng and H.-H. Shen, Research Progress and Development Tendency on Storage Mechanism of Multi-Principal Element Alloys for Hydrogen/Tritium Storage, *Rare Met.*, 2024, **43**(11), 5549–5572, DOI: [10.1007/s12598-024-02738-1](https://doi.org/10.1007/s12598-024-02738-1).
- 300 P. K. Ojha, S. Yoshida, U. Sunkari, B. Tripathy, N. Tsuji and P. P. Bhattacharjee, Highly Deformable Laves Phase in a High Entropy Alloy, *Scr. Mater.*, 2024, **240**, 115828, DOI: [10.1016/j.scriptamat.2023.115828](https://doi.org/10.1016/j.scriptamat.2023.115828).
- 301 C. T. Liu, J. H. Zhu, M. P. Brady, C. G. McKamey and L. M. Pike, Physical Metallurgy and Mechanical Properties of Transition-Metal Laves Phase Alloys, *Intermetallics*, 2000, **8**(9), 1119–1129, DOI: [10.1016/S0966-9795\(00\)00109-6](https://doi.org/10.1016/S0966-9795(00)00109-6).
- 302 F. Xu, X. Gao, H. Cui, Q. Song and R. Chen, Lightweight and High Hardness (AlNbTiVCr)<sub>100-x</sub>Ni<sub>x</sub> High Entropy Alloys Reinforced by Laves Phase, *Vacuum*, 2023, **213**, 112115, DOI: [10.1016/j.vacuum.2023.112115](https://doi.org/10.1016/j.vacuum.2023.112115).
- 303 L. Lou, T. Chen, Z. Bi, W. Wang, Z. Cai, J. Zhou, R. Shuai, Y. Liu, H. Wang and C. Li, Effect of Annealing Temperature on the Microstructure and Mechanical Properties of Al<sub>0.2</sub>CrNbTiV Lightweight Refractory High-Entropy Alloy, *Int. J. Refract. Met. Hard Mater.*, 2024, **125**, 106903, DOI: [10.1016/j.ijrmhm.2024.106903](https://doi.org/10.1016/j.ijrmhm.2024.106903).
- 304 S. Khadka, H. K. Bilan, T. Ma and P. A. Yuya, Laves Phase and Equiaxed Grains Formation in Directed Energy Deposited AlCuFeNiTi High Entropy Alloy, *J. Alloys Compd.*, 2023, **961**, 171089, DOI: [10.1016/j.jallcom.2023.171089](https://doi.org/10.1016/j.jallcom.2023.171089).

